

The effect of oxidized guanines on DNA synthesis by DNA polymerase β

By
© 2020

Mallory Renee Smith
B.Sc., University of North Georgia, 2014

Submitted to the graduate degree program in Biochemistry and Molecular Biology and
the Graduate Faculty of the University of Kansas in partial fulfillment of the
requirements for the degree of Doctor of Philosophy.

Committee Chair: Bret Freudenthal, Ph.D.

James Calvet, Ph.D.

Liskin Swint-Kruse, Ph.D.

Kenneth Peterson, Ph.D.

Jeffrey Bose, Ph.D.

Date Defended: July 7th, 2020

The dissertation committee for Mallory Smith certifies that this
is the approved version of the following dissertation:

The effect of oxidized guanines on DNA synthesis by DNA polymerase β

Chair: Bret Freudenthal, Ph.D.

Graduate Director: Aron Fenton, Ph.D.

Date Approved: July 13th, 2020

Abstract

DNA replication is the fundamental biological task of duplicating genetic information for passing on to a daughter cell. DNA polymerases are the molecular machines that read the parent DNA strand and instruct the addition of correct corresponding nucleotides (also termed fidelity) to form a new DNA strand. DNA replication is extremely accurate to prevent deleterious alterations to the genetic code. However, DNA is damaged more than 10,000 times per cell per day. 8-oxo-7,8-dihydro-2'-guanosine (8-oxo-G) is a form of DNA oxidative damage that threatens fidelity by base pairing with both a canonical cytosine and a non-canonical adenine. Due to its dual coding potential, DNA polymerases frequently make the mistake of inserting adenine instead of cytosine during DNA replication. We hypothesized that other oxidized guanines, such as 4,6-diamino-5-formamidopyrimidine (Fapy•dG) and 7,8-dihydro-8-oxo-ribo-guanosine (r8-oxo-G), may also be error-prone during DNA polymerase processing. To evaluate the mutagenicity of Fapy•dG and r8-oxo-G, we employed a well-characterized human DNA polymerase involved in DNA repair, DNA polymerase β (pol β). This work broadly shows that pol β has similar strategies for excluding damaged nucleotide triphosphates, but unique mechanistic barriers in response to different oxidized guanines in different DNA positions. By furthering our understanding of damaged DNA processing by DNA polymerase β , this work expands the current literature of DNA polymerase discrimination mechanisms and informs on the mutagenic properties of formerly uncharacterized damaged DNA substrates.

Acknowledgements

My Ph.D. career has been full of new experiences, personal growth, and people that have truly enriched my life. In the Freudenthal Lab, the department of Biochemistry and Molecular Biology, and the University of Kansas Medical Center, I found an academic family that valued me and helped me succeed in every possible way.

To my lab family – First and foremost, Dr. Bret Freudenthal has proudly served as an academic father, providing the structure and encouragement I needed to become a great scientist and a compassionate leader. Your mentorship has shaped and provided for my academic success in more ways than I could ever detail. However, the greatest impact you have made on my life and my career is your constant faith in me to achieve more than I gave myself credit for and to push me to be the person you knew I could be. To Dr. Amy Whitaker, my academic older sister, you have both inspired and taught me so much of what I have learned, but I am especially grateful for the confidence you have instilled in me over the past five years. I will always treasure your unwavering support and friendship through the trials and triumphs of life and graduate school. I'd also like to thank my lab twin, Matthew Schaich, for making me laugh every day. Your positivity and joy for life is infectious and has made this journey unforgettably fun. To my academic baby sister, Nicole Hoitsma, I will truly miss being able to share our small day-to-day triumphs and failures with each other. To the rest of my Freudenthal Lab family for which I haven't acknowledged directly, both former and present, your constant support and the countless smiles you have put on my face will not be forgotten.

To my family and friends – you are undoubtedly my biggest cheerleaders. You have helped me stay true to my heart when my mind was focused on my academic pursuits. I thank you for your patience throughout my academic journey and all the times it was difficult for me to be as present as I would have liked to be. Regardless, you still fought to keep me grounded and connected to the world around me, and for that, I am immensely grateful.

To my committee, department, and school – I thank you all for the assistance and kindness you have given without hesitation. My voice was always met with a listening ear, and it was a pleasure to serve the broader KUMC community through the diverse leadership roles I held. Lastly, I would like to thank my dissertation committee for all the hours you have spent enhancing my training and giving me the necessary feedback to broaden the vision of my project.

Funding and Conflicts of Interest

The work contained here would not have been possible without the financial support of the National Institutes of Health and the National Institute of Environmental Health Sciences through multiple awards. Chapter 2 of this dissertation was funded by the National Institute of Environmental Health Sciences [R00ES024431]. Chapter 3 was supported by the Intramural Research Program of the National Institutes of Health [Z01-ES050158, S.H.W.], the National Institutes of Health [R01-ES027558, B.D.F.] and the National Institute of Environmental Health Sciences [Z01-ES050159, S.H.W.]. Chapter 4 was funded by the National Institutes of Health [R01-ES027558, B.D.F.], [R35-GM128562, B.D.F.] and [R01-CA080830, J.B.S.]. There are no conflicts of interest to report.

Table of Contents

Chapter 1: Introduction	1
1.1 DNA Damage	2
1.1.1. <i>Oxidative DNA damage</i>	<i>2</i>
1.1.2. <i>Ribonucleotides and deoxyribonucleotide damage</i>	<i>5</i>
1.1.3. <i>Base excision repair</i>	<i>7</i>
1.2. DNA Polymerase Beta (pol β)	10
1.2.1. <i>A structural and kinetic model for replicative DNA polymerases.....</i>	<i>10</i>
1.2.2. <i>Substrate discrimination and the nucleotidyl transferase reaction.....</i>	<i>11</i>
1.2.3. <i>DNA synthesis mechanisms that involve DNA Damage.....</i>	<i>15</i>
1.3. Guanine Adducts	15
1.3.1. <i>8-Oxo-7,8-dihydro-2'-deoxyguanosine (8-oxo-dG)</i>	<i>18</i>
1.3.2. <i>4,6-Diamino-5-formamidopyrimidine (Fapy•dG)</i>	<i>19</i>
1.3.3. <i>7,8-Dihydro-8-oxo-ribo-guanosine triphosphate (r8-oxo-GTP).....</i>	<i>23</i>
Chapter 2: Extension from the 8-oxo-dG adduct is favored opposite a mutagenic base	25
2.1 Significance and Hypothesis	26
2.2 Abstract	27
2.3 Introduction.....	28
2.4 Materials and Methods	31
2.4.1 <i>Expression and purification of DNA Polymerase β</i>	<i>31</i>

2.4.2.	<i>DNA sequences and oligonucleotide annealing</i>	31
2.4.3.	<i>Pol β/DNA complex crystallization and time-lapse crystallography.....</i>	32
2.4.4.	<i>Crystallographic data collection and refinement</i>	32
2.4.5.	<i>Kinetic characterization using steady-state kinetics.....</i>	33
2.5	Results.....	34
2.5.1.	<i>Kinetic characterization of extension from 8-oxo-dG.....</i>	34
2.5.2.	<i>8-oxodG forms stable base pairs opposite dC (anti-) and dA (syn-) in binary complexes at the primer terminus position.....</i>	39
2.4.3.	<i>8-oxodG opposite dC breaks the Arg254 and Asp256 salt bridge.....</i>	42
2.5.4.	<i>Arg254 realigns into a catalytically competent position following catalytic initiation... ..</i>	47
2.6.	Discussion.....	54
2.6.1.	<i>8-oxo-dG:C results in a clash at the phosphate backbone</i>	56
2.6.2.	<i>Pol β accommodates the mutagenic 8-oxo-dG:A base pair at the primer terminus</i>	57
2.6.3.	<i>The Asp256 and Arg254 salt bridge serves an important role during catalysis</i>	59
2.6.4.	<i>Broader implications for 8-oxo-dG at primer termini</i>	60
Chapter 3:	β-C-Fapy•dGTP insertion hinders the open-closed DNA polymerase transition.....	63
3.1	Abstract	64
3.2	Introduction.....	65

3.3	Methods	70
3.3.1.	<i>Expression and purification and crystallization of DNA Polymerase β D276G</i>	70
3.3.2.	<i>DNA sequences and oligonucleotide annealing</i>	70
3.3.4.	<i>Crystallographic data collection and refinement</i>	71
3.3.5.	<i>Kinetic characterization using single-turnover kinetics</i>	74
3.4	Results.....	76
3.4.1.	<i>β-C-Fapy•dGTP is inefficiently inserted by DNA polymerase β</i>	76
3.4.2.	<i>Fapy•dGTP adopts an altered nucleotide binding position during insertion opposite dC and dA.....</i>	78
3.4.3.	<i>Pol β active site residue (Asp276) impedes insertion by hindering polymerase closure.....</i>	83
3.5	Discussion.....	89
3.5.1.	<i>β-C-Fapy•dGTP insertion may be facilitated in the open conformation of DNA polymerase β</i>	90
3.5.2.	<i>Mechanistic insight into DNA polymerase β active-site residues.....</i>	91
3.5.3.	<i>The mechanism of Fapy•dG mutagenesis differs from 8-oxo-dG</i>	94
3.5.4.	<i>The biological significance of characterizing Fapy•dGTP insertion with pol β</i>	95
	Chapter 4: The combined effect of oxidative damage and ribonucleotide sugar on the nucleotidyl transferase reaction.	97
4.1	Abstract	99

4.2	Introduction	100
4.3.	Methods	104
4.3.1.	<i>Site-directed mutagenesis</i>	104
4.3.2.	<i>Expression and purification of DNA Polymerase β Y271G</i>	104
4.3.3.	<i>DNA sequences and oligonucleotide annealing</i>	106
4.3.4.	<i>Pol β/DNA/8-oxo-rGTP complex crystallization</i>	106
4.3.5.	<i>Crystallographic data collection and refinement</i>	106
4.3.6.	<i>Kinetic characterization using single-turnover kinetics</i>	109
4.3.7.	<i>FRET polymerase closure assay</i>	112
4.4.	Results	115
4.4.1.	<i>r8-oxo-GTP is a mutagenic substrate for DNA polymerase β</i>	115
4.4.2.	<i>FRET collaboration reveals poor enzyme closure in vitro</i>	117
4.4.3.	<i>r8-oxo-GTP base-pair interactions are similar to 8-oxo-dGTP</i>	119
4.5.	Discussion	126
4.5.1.	<i>The adducted O8 promotes mutagenic r8-oxo-GTP insertion by pol β. ...</i>	129
4.5.2.	<i>r8-oxo-GTP shares attributes from both rNTP and 8-oxodGTP discrimination</i>	130
4.5.3.	<i>Biological consequences of r8-oxo-GTP insertion</i>	132
Chapter 5:	Conclusions and Future Directions	134
5.1.	Patterns of oxidative guanine base-pairing in multiple DNA registries	135
5.2.	Mechanisms for nucleotide discrimination by DNA polymerase β	138

References..... 145

List of Figures

Figure 1.1 Common lesions generated by oxidative DNA damage for all four DNA bases.	4
Figure 1.2 Scheme of the proteins and intermediates in the base excision repair pathway.	9
Figure 1.3 N-subdomain closure of DNA polymerase β upon binding a correct incoming nucleotide.	14
Figure 1.4 Formation of 8-oxo- and formamidopyrimidine guanine lesions.	17
Figure 1.5 The different possible conformations of Fapy•dG.....	22
Figure 2.1 Kinetic characterization of extension from 8-oxo-dG by pol β	36
Figure 2.2 Construction of 8-oxo-dG terminated pol β DNA substrates.....	40
Figure 2.3 Binary complex structures with 8-oxo-dG at the primer terminus.	41
Figure 2.4 Ternary ground state structures with 8-oxo-dG:dC at the primer terminus. ..	45
Figure 2.5 Overlays of 8-oxo-dG:dC primer terminus with reference structure containing a dG:dC base pair.	46
Figure 2.6 Pol β extension from 8-oxo-dG:dC by time-lapse X-ray crystallography.	48
Figure 2.7 Ternary ground state structures with 8-oxo-dG:dA at the primer terminus. ..	50

Figure 2.8 Overall scheme demonstrating the structural insights from mutagenic and non-mutagenic extension of 8-oxo-dG that inform on their differing extension efficiencies...	55
Figure 3.1 Chemical structures of Fapy•dG α - and β -anomers and Fapy•dG Analog, β -C-Fapy•dGTP.....	68
Figure 3.2 Single-turnover analysis for gap filling insertion with β -C-Fapy•dGTP opposite cytosine.....	75
Figure 3.3 Discrimination plot for insertion of β -C-Fapy•dGTP.	77
Figure 3.4 Pre-catalytic non-mutagenic pol β :DNA: β -C-Fapy•dGTP complex.....	80
Figure 3.5 Pre-catalytic mutagenic pol β :DNA: β -C-Fapy•dGTP complex.....	82
Figure 3.6 Discrimination plot for insertion of β -C-Fapy•dGTP.	84
Figure 3.7 Pre-catalytic mutant (D276G) pol β non-mutagenic complex.	86
Figure 3.8 Pre-catalytic mutant (D276G) pol β mutagenic complex.	88
Figure 3.9 Comparison of the pol β : β -C-Fapy•dGTP complex with biologically relevant complexes.	92
Figure 4.1 The chemical structure of various guanine nucleotides.....	101
Figure 4.2 The ribonucleotide steric gate in DNA pol β	103
Figure 4.3 Single-turnover kinetics with r8-oxo-GTP, rGTP, or dGTP.	111

Figure 4.4 Diagram of the polymerase closure FRET system.....	113
Figure 4.5 Evaluating pol β subdomain closure via steady-state FRET.	114
Figure 4.6 Discrimination plot evaluating r8-oxo-GTP insertion.....	116
Figure 4.7 Calculated interprobe distances from FRET efficiencies during steady-state FRET experiments.	118
Figure 4.8 Open complex of the pol β :r8-oxo-GTP:dC asymmetric unit.	121
Figure 4.9 X-ray crystallographic structure of Y271G pol β in complex with r8-oxo-GTP opposite dC.....	123
Figure 4.10 X-ray crystallographic structure of Y271G pol β in complex with r8-oxo-GTP opposite dA.	125
Figure 4.11 Scheme of r8-oxo-GTP processing by human DNA polymerase β	128
Figure 5.1 Protein and active site changes that facilitate DNA synthesis by DNA polymerase β	140

List of Tables

Table 1. Steady-state kinetic parameters for correct dCTP insertion on 8-oxo-dG primer termini.	37
Table 2. Data collection and refinement statistics of binary and ternary polymerase β /DNA co-complexes with dCTP extending from 8-oxodGTP across from cytosine.	43
Table 3. Data collection and refinement statistics of binary and ternary polymerase β /DNA co-complexes with dCTP extending from 8-oxodGTP across from adenine.....	53
Table 4. Data collection and refinement statistics of ternary polymerase β :DNA co-complexes with incoming β -C-Fapy•dGTP.	73
Table 5. Experimental DNA substrate sequences for characterizing r8-oxo-GTP.	105
Table 6. Data collection and refinement statistics of ternary Y271G pol β :DNA co-complexes with incoming r8-oxo-GTP or rGTP.....	108

Chapter 1: Introduction

Parts of this chapter were previously published in *Frontiers in Bioscience (Landmark edition)* Whitaker AM, Schaich MA, Smith MR, Freudenthal BD; Base excision repair of oxidative DNA damage: from mechanism to disease. 2017;22:1493-1522. – and – *Cellular and Molecular Life Sciences*. Hoitsma NM, Whitaker AM, Schaich MA, Smith MR, Fairlamb M, and Freudenthal BD; Structure and function relationships in mammalian DNA polymerases., 2020;77(1):35-59. My contributions to the above reviews are presented here with major adaptations and abides by the reuse policies of Springer Nature and Frontiers in Bioscience.

1.1 DNA Damage

Genomic DNA is continually damaged, producing a variety of lesions that differ depending on the DNA-damaging source. DNA lesions must be repaired or bypassed to maintain genome stability and ensure survival of the cell. The base excision repair pathway (BER) is responsible for repairing two of the most common types of DNA damage: spontaneous hydrolysis and oxidative DNA damage. Oxidative damage alters the structure of duplex DNA and a wide variety of other nucleic acid structures, such as deoxyribonucleotide triphosphates, ribonucleotide triphosphates, and single-stranded RNA. Below, I will expand on these topics to provide essential background on my dissertation which investigates how oxidative DNA lesions are discriminated during DNA synthesis in order to minimize genomic errors using a model DNA polymerase that functions in the BER pathway.

1.1.1. Oxidative DNA damage

Oxidative DNA damage is a prevalent form of DNA damage inflicted by reactive oxygen species (ROS), such as superoxide anions ($\bullet\text{O}_2$), hydroxyl radicals ($\bullet\text{OH}$), and hydrogen peroxide (H_2O_2). ROS are chiefly produced as a by-product of mitochondrial respiration but can also result from inflammation, chemotherapy, ionizing radiation, redox-cycling, and chemical oxidants (1,2). Because ROS are constitutively produced, cells have evolved antioxidant defense systems to combat ROS damage. Antioxidants work to minimize ROS by scavenging and reducing oxygen species or chelating the metals that produce them. However, without sufficient antioxidant defenses, cells enter a state of oxidative stress. During oxidative stress, ROS will damage proteins, lipids, and, of

particular importance, genomic DNA. Oxidation of genomic DNA is closely associated with initiating and progressing aging and human diseases, including cancer and neurological disease (3). Therefore, it is imperative that cellular repair systems (*i.e.* DNA repair, proteolysis) rescue the damage done by ROS by removing and replacing damaged DNA and proteins. The base excision repair (BER) pathway is the pathway responsible for repairing small oxidative DNA lesions (*e.g.* AP sites and base damage) and is essential for cell viability (4-6). Because oxidative base damage is a unifying theme studied in this dissertation, the BER pathway and its biological significance of repairing oxidative base damage are detailed further in **Section 1.1.3**.

DNA oxidation can occur at both the DNA backbone and all four DNA bases (adenine, cytosine, thymine, and guanine) (7). Most commonly, ROS causes spontaneous loss of the DNA base by attacking the N-glycosidic linkage, resulting in an apurinic/apyrimidic site (AP site) that lacks coding potential (8). Other forms of oxidative DNA damage that occur at the DNA backbone can generate single strand breaks or even convert a deoxyribose sugar to a ribose sugar (9). Furthermore, ROS can produce more than 100 different types of base damage, including fragmented or ring-opened forms and oxidized aromatic derivatives. Several common and well-studied base lesions are displayed in Figure 1.1. Of the hundreds of oxidized bases, guanine base damage is the most common among all four DNA bases and has been the focus of most oxidative DNA damage studies (10,11). If oxidative base lesions are left unrepaired, oxidized bases can cause DNA mutations through altered base-pairing properties. Although guanine lesions are more prevalent than others, the mutagenic potential of each DNA base lesion is unique and merits individual characterization. The DNA lesions investigated in this

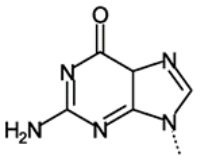
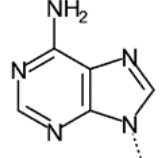
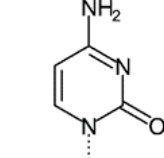
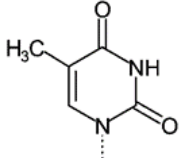
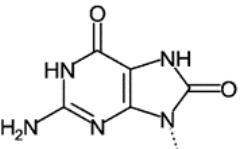
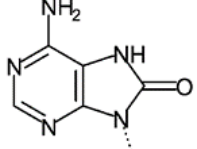
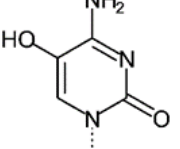
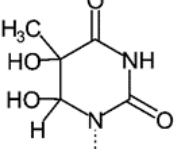
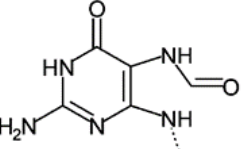
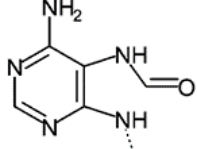
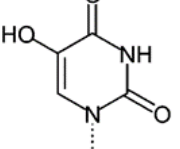
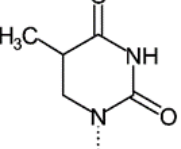
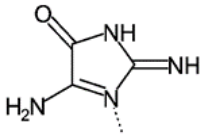
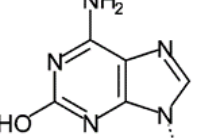
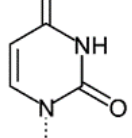
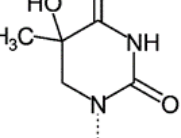
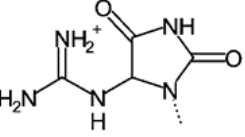
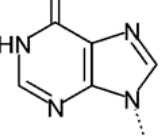
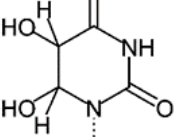
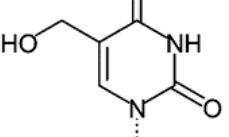
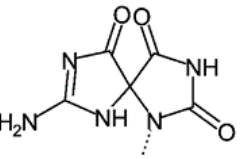
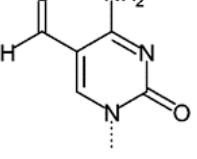
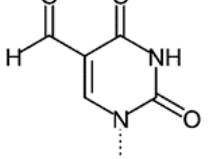
Parent DNA Base				
				
	Guanine	Adenine	Cytosine	Thymine
Products of DNA Base Damage				
	8-oxoG	8-oxoA	OH5C	Tg
				
	FapyG	FapyA	OH5U	DHT
				
Oxazolone	2OHA	Uracil	Th5	
				
Guanidino-hydantoin	Inosine	Ura-Gly	Hm5U	
				
Spiroimino-dihydantoin		5-foC	5-foU	

Figure 1.1 Common lesions generated by oxidative DNA damage for all four DNA bases.

Figure reused with permission from (4).

dissertation are different forms of oxidized guanines and are discussed in more detail in **Section 1.3.**

1.1.2. Ribonucleotides and deoxyribonucleotide damage

Although damage to duplex DNA is unavoidable, duplex DNA is partially protected by nucleosome and chromatin structures. In contrast, the building blocks of DNA, deoxyribonucleotides (dNTPs), are not shielded and are potentially more vulnerable to oxidation (12-14). To protect against dNTP oxidation, nucleotide “sanitizing” enzymes recognize and hydrolyze common oxidized nucleotides, removing them from the nucleotide pool (15). If nucleotide pools are not fully sanitized, these oxidatively damaged dNTPs can be inserted into genomic DNA and cause mutagenesis (16). One such nucleotide sanitation enzyme, MutT Homolog 1 (MTH1), specifically recognizes oxidized guanine dNTPs, particularly 8-oxo-7,8-dihydro-2'-deoxyguanosine triphosphate (8-oxo-dGTP) (17,18).

MTH1 inhibitors have been developed as a potential cancer therapeutic (19,20). MTH1 inhibitors were rationally developed to increase the amount of 8-oxo-dGTP in oxidatively stressed tissues, such as cancerous tissues, which are more sensitive to genomic stress. Therefore, the stress of 8-oxo-dGTP accumulation and insertion into the DNA of cancerous tissues was thought to have an anti-tumor effect and initiate cell death pathways. Non-cancerous cells should be less oxidatively stressed which allows for less 8-oxo-dGTP generation and insertion into the genome. Additionally, normal cells should be able to use the BER and MUTYH pathways to relieve what 8-oxo-dG does enter the genome due to MTH1 inhibition. Overall, the development of MTH1 inhibitors highlights the importance of understanding the interplay between oxidative DNA damage, genomic

stability, and human disease. However, the efficacy of anti-tumor activity by MTH1 inhibition has since shown conflicting results, possibly due to cancerous tissues having upregulated DNA repair pathways (21).

In addition to dNTPs, ribonucleotides (rNTPs) in the nucleotide pool are also subject to oxidation by ROS. Using sensitive high-performance liquid chromatography with electrochemical detection, oxidized ribonucleotides were quantified to make up 0.2 to 5% of the ribonucleotide pool under mildly oxidative conditions (12). Being the building blocks of RNA, oxidized rNTPs may have mutagenic potential during transcription or translation. However, RNA transcripts have a shorter lifetime, making the consequences of rNTP oxidation on transcription and translation more difficult to directly assess. Oxidized ribonucleotides, such as r8-oxo-GTP, have been shown capable of being utilized by RNA polymerases, albeit, at reduced rates as compared to undamaged rGTPs (22,23). Molecules of mRNA containing oxidized rNTPs can induce errors during protein translation, implicating a myriad of other biological implications that extend past the scope of this dissertation (24).

Most DNA polymerases exclude rNTP insertions into the genome by using an active site residue that clashes with the 2'-OH of the ribose oxygen, termed the steric gate (25). Although the steric gate keeps 99.9% of ribonucleotides out of genomic DNA, more than a million ribonucleotides are still inserted into the genome during DNA replication (26-28). Since rNTPs are also subject to oxidation by ROS, oxidized rNTPs may be a potential substrate for DNA polymerases. Generally, the study of oxidized ribonucleotides has lagged behind that of oxidized deoxyribonucleotides, despite its biological prevalence and potential to affect biological processes involving DNA, RNA, and NTP signaling. But,

a few studies have investigated the mutagenic potential of oxidized rNTP insertion using DNA polymerases from bacteria, yeast, and humans with varying results (29-31). The biochemical mechanism of oxidized rNTP insertion into DNA remained an unexplored question by the field until the studies described in **Chapter 4**.

Regardless of how ribose sugars enter into the genome, the reactive 2' hydroxyl group on the ribose sugar poses a threat to genome stability (28). To prevent the accumulation of ribose sugars in DNA, a specialized DNA repair pathway has evolved, ribonucleotide excision repair (RER). The importance of RER is underscored by the millions of ribonucleotides mistakenly inserted into the genome every cell division (28). RER searches genomic DNA for ribonucleotides to remove and replace them with deoxyribonucleotides (32). This repair pathway is initiated by the RNaseH2 protein which recognizes RNA/DNA hybrids and cleaves the embedded ribonucleotides. Alternative mechanisms that result in ribonucleotides in genomic DNA, such as ROS attack to ribose sugars, and insertion by RNA/DNA polymerase μ , are also important to consider given the recently revealed ribonucleotide burdens on genomic DNA. As exemplified by oxidized guanine bases in **Section 1.3**, the addition of one extra oxygen atom can significantly alter the chemical and biological properties of a molecule, necessitating entire repair pathways for preventing their accumulation into DNA.

1.1.3. Base excision repair

The base excision repair (BER) pathway is essential for repairing small DNA lesions like spontaneous depurination or base oxidation (**Section 1.1.1.**). Somewhere between one to seventy thousand lesions are produced per cell per day and subsequently require BER proteins for repair (2,3). The BER pathway broadly consists of damage recognition

proteins (glycosylases), a DNA cutting protein (nuclease), DNA replacement protein (DNA polymerase), and a sealing protein that reconnects the DNA (ligase), see [Figure 1.2](#). BER is additionally supported by scaffolding protein X-ray repair cross-complementing protein 1 (XRCC1), and recruitment/signaling protein, poly(ADP-ribose) polymerase 1 (PARP-1). DNA polymerase β (pol β) is the DNA replacement protein in the BER pathway and is a focus of this dissertation due to its role as a biochemical DNA polymerase model, as well as its upregulation during times of DNA damage.

Pol β performs two reactions during BER: a lyase reaction and DNA synthesis (33). The lyase activity catalyzes the removal of the backbone intermediate, 5'-2-deoxyribose-5-phosphate (dRP), forming a one nucleotide gap. This acts as the substrate for pol β to add a new DNA base using its DNA synthesis activity. Of these two activities, the dRP lyase activity is essential to sustain life, whereas a loss of DNA synthesis activity can be compensated by other polymerases (34). Furthermore, pol β deletion is embryonic lethal and polymorphisms in the POLB gene are associated with human disease highlighting the pivotal role by which pol β maintains genomic integrity (5,35). Because pol β was utilized for all analyses in this dissertation to characterize the effect of DNA damage on DNA synthesis, pol β is discussed in further detail in the next section.

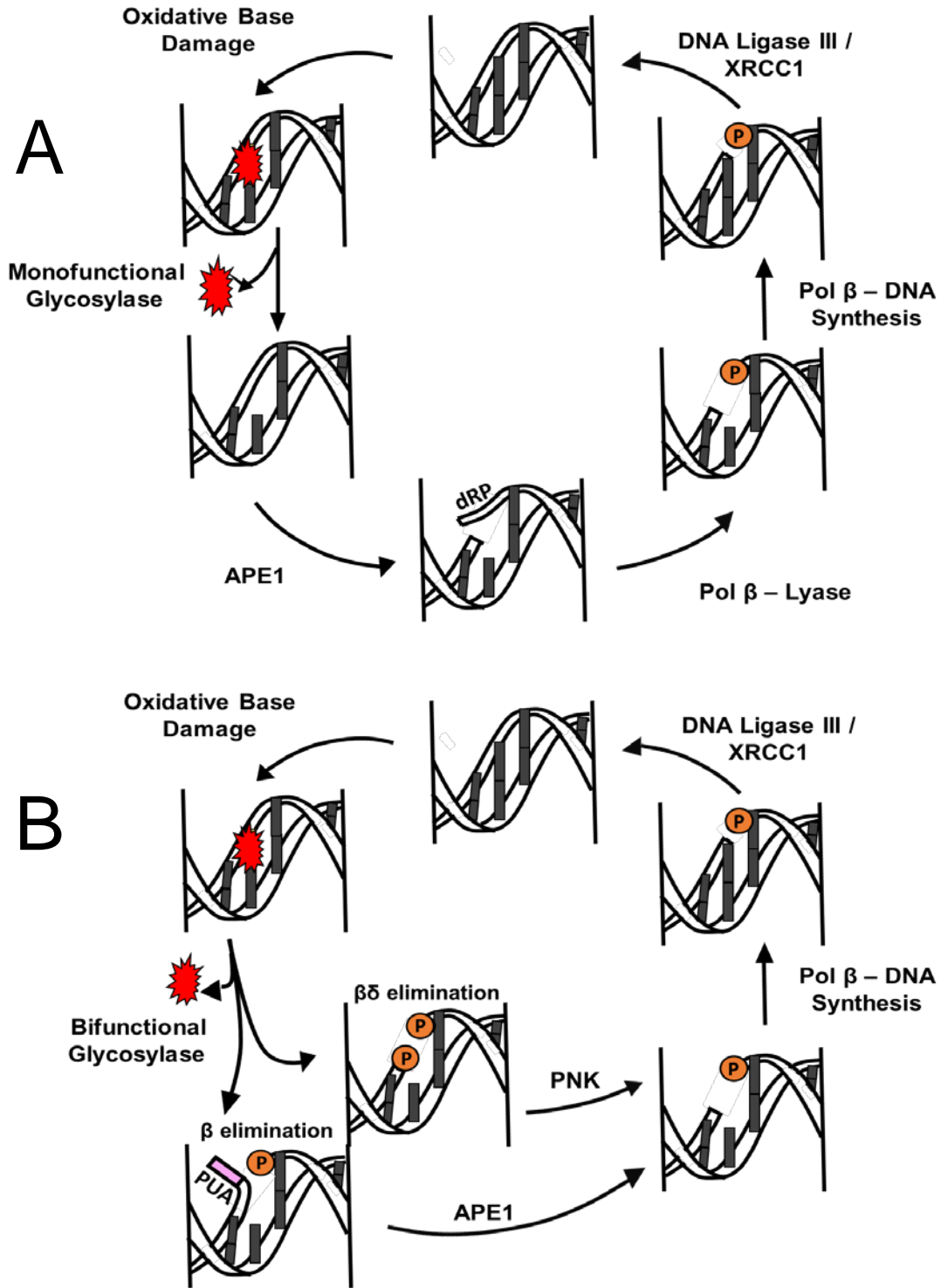


Figure 1.2 Scheme of the proteins and intermediates in the base excision repair pathway.

A) The pathway scheme by which a monofunctional glycosylase is used to remove the lesion B) The pathway scheme after lesion removal by a bifunctional glycosylase. Figure reused with permission from (4).

1.2. DNA Polymerase Beta (pol β)

1.2.1. A structural and kinetic model for replicative DNA polymerases

There are 15 mammalian DNA polymerases that are grouped into four different families, whereby A- and B- families are broadly replicative polymerases, Y-family polymerases bypass DNA damage during DNA replication (*i.e.* translesion synthesis), and X-family polymerases perform DNA synthesis during DNA repair. While all DNA polymerases utilize the nucleotidyl transferase reaction, their structures are highly specialized to their individual functions. Replicative polymerases (pols α , δ , ϵ , and γ) have many regulatory components, conformational selection, and an exonuclease domain that help ensure a high fidelity and processivity. Y-family polymerases (pols η , ι , κ , and REV1) have a lower fidelity because they are specialized to allow DNA replication to progress when encountering damaged DNA. Lastly, X-family polymerases (pols β , λ , μ , and TdT) are simpler polymerases with a medium-high fidelity that function mostly in gap-filling but some have been observed to have non-canonical functions like inserting ribonucleotides or *de novo* DNA synthesis (36). For a comprehensive structure-function review of the all mammalian DNA polymerases, refer to reference (37).

Pol β is a well-established biochemical model for characterizing the nucleotidyl transferase reaction used universally by DNA polymerases (38). As an X-family polymerase, pol β has a moderate fidelity and functions best with small gapped DNA substrates. Pol β makes an excellent biochemical model for several reasons, the first being that it features an open to closed subdomain conformational change that is akin to the conformational change found in replicative polymerases (39). Second, pol β is the smallest mammalian polymerase and structurally simple in comparison to other

polymerases, containing only two domains and no exonuclease domain (lack of exonuclease domain simplifies biochemical assays). Third, no coenzymes or cofactors are required for pol β to perform catalysis, except for two divalent metals (physiologically, Mg^{2+}). Lastly, pol β is amenable to crystallographic studies at high resolution with more than 400 published structures in the Protein Data Bank as of January 2020. Furthermore, the nucleotidyl transferase reaction can occur *in crystallo* which allows pol β to be amenable for time-lapse crystallography. To perform time-lapse crystallography, a crystallized pol β :DNA complex is first placed in a solution containing an incoming nucleotide and a metal that does not support catalysis (*i.e.* Ca^{2+}), creating a ground state complex of a bound substrate prior to catalysis. This complex can then be subjected to subsequent soaks with a metal that supports catalysis (usually Mg^{2+} or Mn^{2+}) at varying timepoints to capture catalytic intermediates and eventually product structures. Crystallographic time-lapse approaches provide a robust characterization of substrate discrimination during DNA synthesis by DNA polymerases. Time-lapse crystallography of pol β can reveal mechanisms by which damaged dNTPs (or rNTPs) enter the genome, and unambiguously show how DNA polymerases defend against noncanonical nucleotides.

1.2.2. Substrate discrimination and the nucleotidyl transferase reaction

Transferring a nucleotide to an acceptor hydroxyl group is a chemical reaction that is essential to many biological processes and is termed the nucleotidyl transferase reaction (40). The nucleotidyl transferase reaction occurs broadly across 10 distinct superfamilies, including all DNA polymerases, and is essential for propagating genetic information in all forms of life (40). The most fundamental property of propagating of genetic information is

accurate base selection based on the templating strand sequence. DNA polymerases have evolved to closely associate the substrate discrimination step, *i.e.* selecting the correct base, with the nucleotidyl transferase reaction, *i.e.* catalysis. In doing so, the polymerase can tailor the insertion efficiency for each nucleotide depending on the identity of the templating base, ensuring the correct nucleotide is inserted and incorrect nucleotides are excluded. In a similar fashion to replicative polymerases, pol β is proposed to synthesize DNA using an induced fit mechanism, outlined below (41-43).

First, pol β binds its DNA substrate (a gapped double-stranded DNA duplex) to make a binary complex and then binds the triphosphate moiety of the incoming nucleotide triphosphate to become a ternary complex. The negatively charged triphosphate group is coordinated by a divalent nucleotide metal (Me_n) to neutralize the triphosphate group for efficient binding. After triphosphate binding, the Watson-Crick base pairing compatibility is assessed between the templating base and the newly bound nucleotide triphosphate. If the bound nucleotide properly base pairs, pol β undergoes a conformational change, moving its N-subdomain (also referenced as N-helix) from an open to a closed position around the bound nucleotide, [Figure 1.3](#). In concurrence with adopting a closed conformation, the active site rearranges to become catalytically competent. The conformational change effectively gates for correct nucleotides and subsequently primes pol β for the nucleotidyl transferase reaction. The reaction then proceeds as follows: the 3' hydroxyl group (3'-OH) at the end of the primer (primer terminus) serves as the nucleophile in an S_N2 reaction, attacking the phosphorous of the incoming dNTP α -phosphate (αP) group to form a phosphodiester linkage. Proton abstraction from the 3'-OH is facilitated by a divalent catalytic metal (Me_c) and Asp256, which is one of three

required aspartic acid residues that are referred to as the catalytic triad. The two divalent cation metals required for the nucleotidyl transferase reaction are widely accepted to be Mg^{2+} in a physiological context (44,45). Following the nucleotidyl transferase reaction, the nucleotide monophosphate is now added to the DNA strand and the inorganic pyrophosphate (PP_i) byproduct dissociates (46,47).

In summary, the induced fit mechanism must be able to discriminate between correct and incorrect nucleotides that may only differ by as little as one atom, such as ribonucleotides, oxidized deoxyribonucleotides, and mismatched deoxyribonucleotides. Therefore, the induced fit mechanism evaluates whether each incoming dNTP satisfies Watson-Crick hydrogen bonding, base-stacking, and steric constraints that are instructed by the templating base identity and the nucleotide binding pocket in the active site (48,49). When the constraints are satisfied (*i.e.* correct dNTP binding) conformational changes of the N-subdomain and templating DNA strand induce the proper alignment of catalytic residues to promote catalysis (48,50). The ability for pol β to modulate the steps of the induced mechanism to discriminate against oxidized base damage is investigated in the following chapters

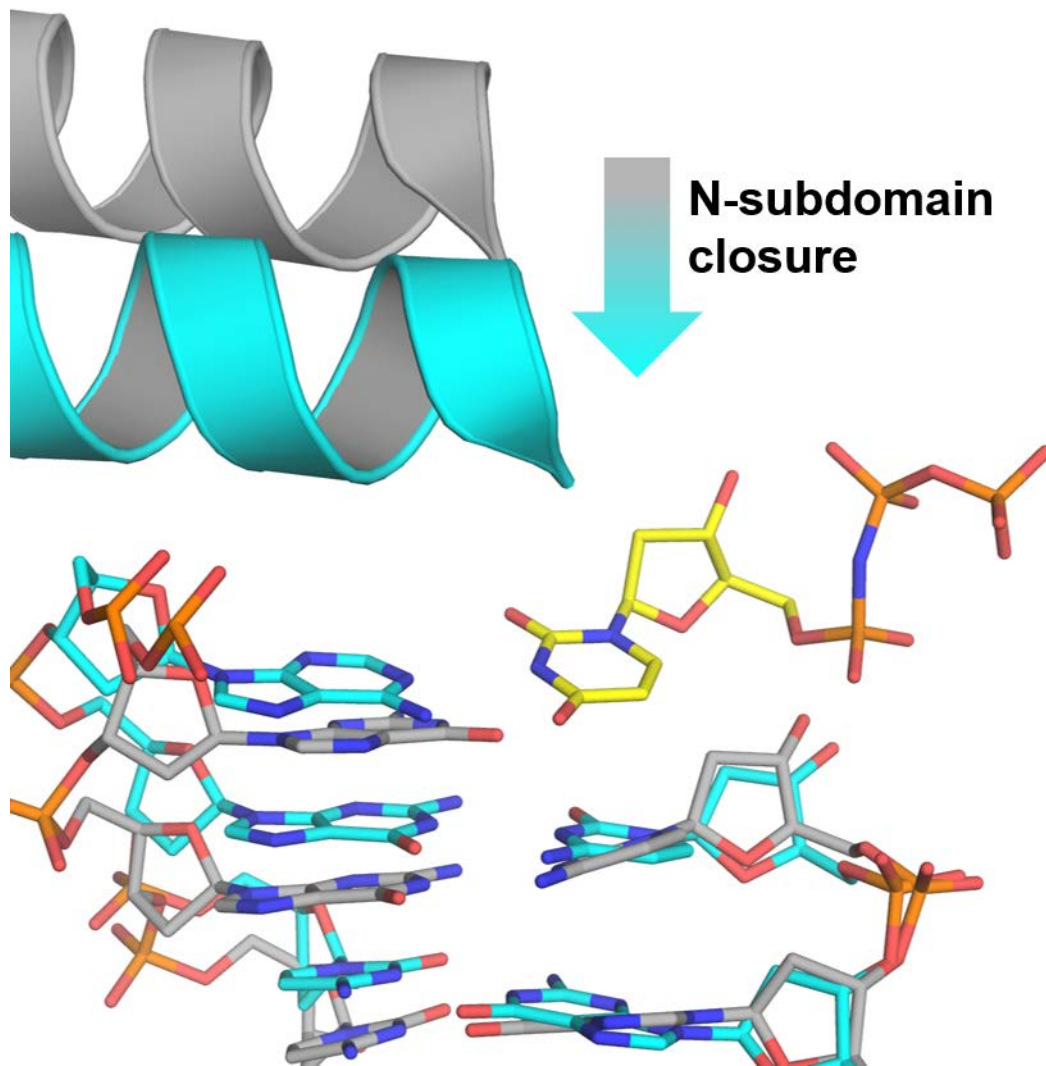


Figure 1.3 N-subdomain closure of DNA polymerase β upon binding a correct incoming nucleotide.

A binary pol β complex (gray, PDB ID: 3ISB) that is poised for binding is overlaid with a competent ternary pol β complex (cyan, PDB ID: 2FMS) that has bound a correct incoming nucleotide triphosphate (yellow sticks) and is poised for catalysis.

1.2.3. DNA synthesis mechanisms that involve DNA Damage

Replicative DNA polymerases are estimated to make more than a million errors during one round of DNA replication (28). Understanding how these errors occur provides insight into how mutagenic events are initiated and potentially persist to progress to cancer and aging phenotypes. DNA polymerases may be faced with replicating past DNA damage in a variety of different positions or registries. Some possibilities include: a damaged templating position (bypass), a damaged incoming nucleotide (insertion), and the next replication event following damaged nucleotide insertion (extension). As discussed above in **Section 1.2.2.**, pol β is an excellent model for replicative polymerases and its entire catalytic cycle has been elucidated at atomic resolution using time-lapse X-ray crystallography (47,51,52). Importantly, this system has already been utilized to understand how DNA polymerases process non-canonical DNA substrates such as mismatches, damaged nucleotides, anti-viral drugs, and therapeutic nucleotides (51-56). Therefore, pol β is an ideal model to resolve these mechanistic questions and begin to identify patterns and common polymerase strategies to process DNA damage for novel lesions and at novel positions.

1.3. Guanine Adducts

Of the four DNA bases, guanine is particularly susceptible to oxidative damage due to its low reduction potential (10,57). When guanine is oxidized, the most common oxidation intermediate is a C8-OH adduct. Subsequently, the C8-OH adduct is either further oxidized to the well-studied 8-oxo-G lesion or the C8-OH is reduced, breaking the imidazole ring to produce 2,6-diamino-4-hydroxy-5-formamidopyrimidine (Fapy•G),

Figure 1.4. Previous characterizations of these lesions and the ribo- counterpart of 8-oxo-Gua (r8-oxo-Gua) are reviewed here (58), summarized in the sections below, and further investigated in the following chapters.

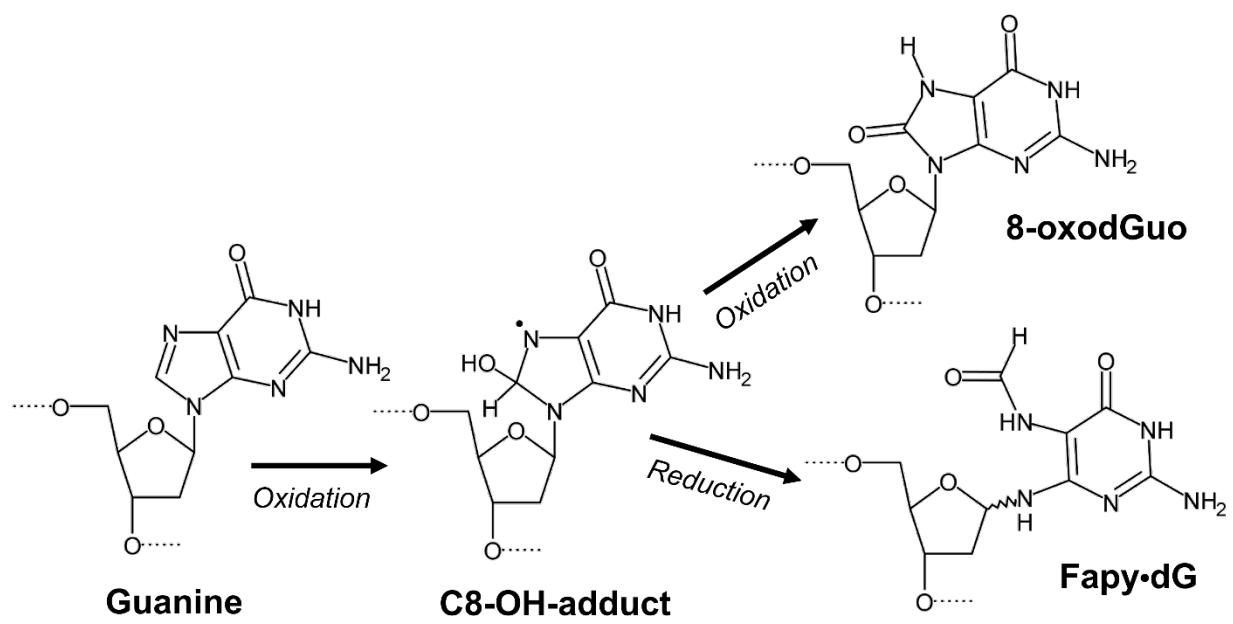


Figure 1.4 Formation of 8-oxo- and formamidopyrimidine guanine lesions.

Adapted from (39) and reused with permission from (54).

1.3.1. 8-Oxo-7,8-dihydro-2'-deoxyguanosine (8-oxo-dG)

8-Oxo-dG is the “prototypical” oxidative lesion and has been thoroughly investigated with respect to formation, prevalence, structural properties, mutagenic mechanisms, and human disease. This lesion even serves as a biomarker of oxidative stress in cellular studies (59). Historically, levels of guanine oxidation were difficult to interpret due to artificial oxidation during DNA extraction (60). With better extraction methodologies, it is now estimated that 8-oxo-dG is present at a steady-state level of 0.03-4.2 per 10⁶ guanines, which corresponds to approximately 10,000 8-oxo-dG residues per single human nucleus (61,62). Estimates suggest that up to 100,000 8-oxo-dG lesions could be formed in DNA per cell daily and are estimated to be much higher during oxidative stress (63-65). 8-oxo-dG is a stable lesion that inflicts minimal helix distorting properties, as is detailed in the review by Delaney et. al (58). Furthermore, it was also shown that 8-oxo-dG causes neighboring DNA bases to be more sensitive to oxidation, thus forming oxidative DNA damage ‘hot spots’ (66).

The 8-oxo-dG lesion contains an adducted oxygen off of the C8 carbon (O8) which results in protonation of N7. Through the adducted O8 and protonated N7, 8-oxo-dG is able to adopt either an *anti*- or *syn*- conformation during base pairing (67). 8-Oxo-dG was observed to base pair with cytosine using an *anti*- conformation and conventional Watson–Crick hydrogen bonding like that of undamaged guanine. Alternatively, 8-oxo-dG can rotate about the glycosidic bond into the *syn*-conformation and use the protonated N7 to form a mutagenic base pair with adenine (68,69). This base pair interaction is termed ‘Hoogsteen base pairing’, and accordingly the edge of 8-oxo-dG used in this base pairing is termed the ‘Hoogsteen edge’ (69,70). Because 8-oxo-dG can modulate

between these conformations in the absence of a base pair (71), DNA polymerases are tasked with trying to interpret the mutagenic versus non-mutagenic interactions of 8-oxo-dG lesion. The rate of incorporating of dATP (mutagenic) versus dCTP (non-mutagenic) when faced with a templating 8-oxo-dG lesion is largely dependent on the polymerase identity, but is widely considered mutagenic due to a general loss of fidelity (72). Replicative human DNA polymerase α may be the highest mutagenic human polymerase, preferring dATP over dCTP at a 200:1 ratio (73). However, 8-oxo-dG is only mildly mutagenic *in vivo*, likely due to the extensive repair systems evolved to protect against 8-oxo-dG accumulation (74).

1.3.2. 4,6-Diamino-5-formamidopyrimidine (Fapy•dG)

The quantity of Fapy•dG rivals that of its sister lesion, 8-oxo-dG, under mildly oxidative cellular conditions (12,75-78). Furthermore, the mutation frequency of Fapy•dG in mammalian cell lines has been reported to be up to ~400% and ~75% more mutagenic than 8-oxoG (79,80). However, the field is still unsure if Fapy•dG contributes significantly to the mutagenic load of the cell due to conflicting mutagenicity reports in bacterial and yeast systems (81-83). Despite the prevalence and potential mutagenicity of the Fapy•dG lesion, it is not as well characterized as 8-oxo-dG (84,85). This is largely due to the difficulty in synthesizing the Fapy•dG lesion to sufficient and pure quantities. Synthesis of Fapy•dG is difficult and laborious because Fapy•dG can readily anomerize between α - and β - glycosidic bonds, [Figure 1.5](#). Anomerization occurs due to its reactive lone pair on the nitrogen of the formamide group resulting from the broken imidazole ring which is free to attack the ribose sugar. Fapy•dG predominantly adopted the β - anomer when templated with a cytosine in duplex DNA (86). Later, thermodynamic and kinetic

investigations supported the physiological preference for the β -anomer by concluding that the α -anomer was unable to form a stable base pair (87). With a consensus on the β -anomer being preferred within the confines of DNA, β -analogs of Fapy•dG have been developed that eliminate anomerization and simplify the synthesis (81,88). This was done by replacing one of the reactive atoms (either the cyclic ribose oxygen or the glycosidic nitrogen) with carbon.

Fapy•dG and its analogs have been investigated sparsely with sometimes conflicting results. In cultured human cells, Fapy•dG mutation frequency appears to be highly dependent on sequence context, but predominantly promotes G to T transversion mutations, akin to 8-oxo-dG (79,80,89-91). Fapy•dG was therefore speculated to mimic 8-oxo-dG and rotate into a *syn*- conformation to base pair favorably with adenine, [Figure 1.5](#) (92). However, thermodynamic and structural studies using a carbocyclic analog of Fapy•dG later contradicted the presence of *syn*-Fapy•dG (82,83). Instead, Fapy•dG underwent base shifting and tautomerization during non-mutagenic and mutagenic bypass by DNA Polymerase I (82). In *Escherichia coli*, Fapy•dG was shown to be less efficiently bypassed than 8-oxo-dG, suggesting that Fapy•dG is not as mutagenic as 8-oxo-dG (91). A solution study of the β -carba-Fapy-dG analog within a DNA duplex showed no significant perturbations to the DNA helix and was observed to be quite stably base paired with cytosine (93). This suggested that Fapy•dG may not be easily detected by DNA repair enzymes. When the Fapy•dG:dC base pair was studied as a substrate for formamidopyrimidine (Fapy) DNA glycosylase (Fpg), a base excision repair glycosylase, the lack of helix distortion resulted in a poorly repaired Fapy•dG in contrast to the mutagenic base pair (Fapy•dG:dA) (94). This suggests that Fapy•dG may persist in the

genome in non-mutagenic base pairs, eliciting other biological ramifications, such as replication stalling. The inconsistent mutagenic profiles and unclear biological outcomes of Fapy•dG warrants further investigation of this elusive lesion.

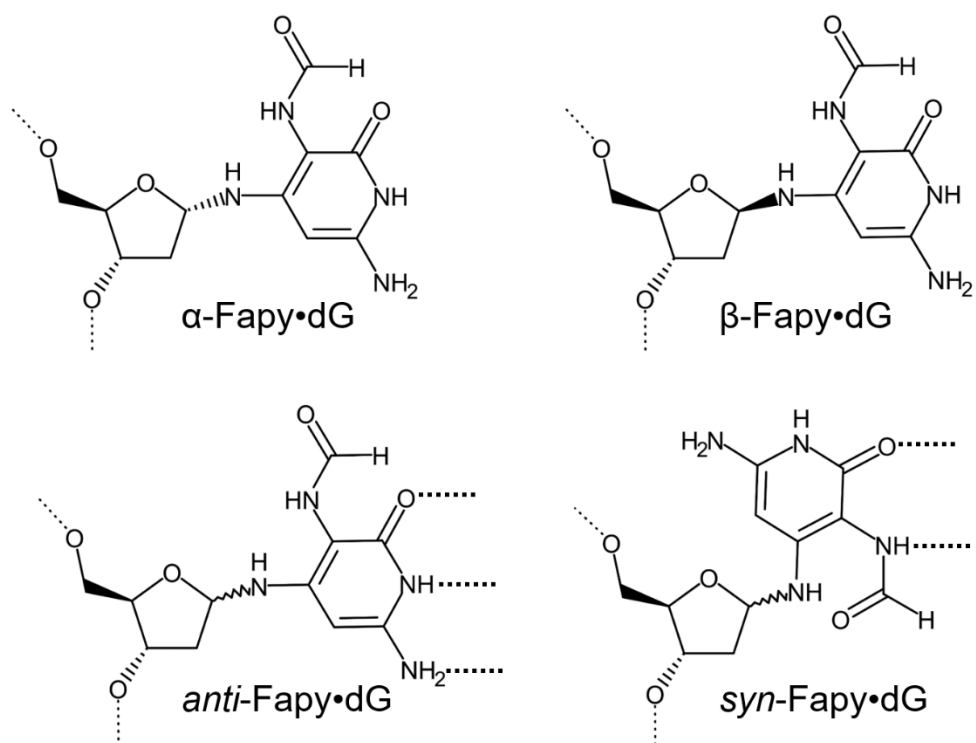


Figure 1.5 The different possible conformations of Fapy•dG.

1.3.3. 7,8-Dihydro-8-oxo-ribo-guanosine triphosphate (r8-oxo-GTP)

The production of guanine adducts can occur regardless of the identity of the sugar moiety (deoxyribose or ribose sugar). Therefore, nucleic acid lesions occur in DNA, RNA, and potentially all nucleic acid structures, warranting a thorough investigation of all sugar identities. Guanines with ribose sugars are oxidized approximately 10 times more frequently than those with deoxyribose sugars, which poses a unique threat to the cell that extends past the scope of this dissertation (65,95,96). Oxidation to the ribonucleotide pool (rNTPs) is particularly significant because more than a million ribonucleotides are estimated to be inserted into DNA every cell division. During mildly oxidative conditions, 0.2 - 5% of free guanine ribonucleotides (rGTP) are oxidized to form r8-oxo-GTP, which creates many opportunities for DNA polymerases to insert oxidized rNTPs into the genome (12,97,98).

Recently, r8-oxo-GTP was shown to be incorporated into DNA in studies using yeast, bacteria, and human polymerases (29-31). In those studies, r8-oxo-GTP exhibited different catalytic efficiencies depending on the specific DNA polymerase and the templating base identity. A unique polymerase in *Schizosaccharomyces pombe*, Pol4, inserted r8-oxo-GTP opposite a cytosine template at a similar rate to 8-oxo-dGTP, but r8-oxo-GTP insertion opposite adenine was 8-fold slower than r8-oxo-GTP opposite cytosine (30). With the bacterial polymerase, DinB2, from *Mycobacterium smegmatis*, r8-oxo-GTP was shown to have a slight preference for mutagenic insertion opposite adenine over cytosine (29). With the human polymerase, pol β , r8-oxo-GTP had a strong preference for inserting opposite adenine that was only 36-fold less efficient than 8-oxo-dGTP when examined with a repeat expansion substrate (31). Of note, the substrate used in this study

differs from the canonical substrate of pol β , which is conventionally a one nucleotide gap. Altogether, the high abundance oxidized rGTPs (r8-oxo-GTP) may be potential substrates for DNA polymerases, but the issue is likely dependent on specific mechanisms of differing DNA polymerases as well as the biological context.

Chapter 2: Extension from the 8-oxo-dG adduct is favored opposite a mutagenic base

Previously published as an open access article and is reprinted here with adaptations and with permission from Oxford University Press. Amy M. Whitaker*, Mallory R. Smith*, Matthew A. Schaich, Bret D. Freudenthal, *Capturing a mammalian DNA polymerase extending from an oxidized nucleotide*, *Nucleic Acids Research*, Volume 45, Issue 11, 20 June 2017, Pages 6934–6944, <https://doi.org/10.1093/nar/gkx293>

This chapter includes the work of Dr. Amy Whitaker and Matthew Schaich as contributing authors. Dr. Whitaker and I share co-first authorship of the following publication whereby the structures and figures were provided by myself apart from four structures collected and refined by Matthew Schaich. The kinetic data were provided by Dr. Amy Whitaker. Preparation of the manuscript was provided by Dr. Amy Whitaker and me with editing from Dr. Bret Freudenthal.

2.1 Significance and Hypothesis

As described in Section 1.3.1, 8-oxo-dGTP was demonstrated to insert mutagenically opposite adenine more efficiently than non-mutagenically opposite cytosine (16). In order for replication to continue, the polymerase must extend from the inserted lesion to avoid stalling the replication fork. Stalled replication events must be avoided to prevent dangerous replication fork collapse and potential double strand breaks. Our central question was whether a primer terminal 8-oxo-dGMP is efficiently extended when at the primer terminal position to prevent stalling, and whether it would retain the same mutagenic pattern as 8-oxo-dGTP. We hypothesized that 8-oxo-dGMP would be capable of extending beyond either templating base as to prevent replication stalling, but it would prefer to extend from a mutagenic 8-oxo-GMP base pair based on previous observations from 8-oxo-dGTP insertion. Previously, non-mutagenic 8-oxo-dGTP insertion opposite cytosine (dC) caused steric clashes between the adducted O8 and the phosphate backbone of 8-oxo-dGTP in the *anti*- conformation. In contrast, mutagenic 8-oxo-dGTP insertion opposite adenine (dA) stably accommodated the O8 during in the minor groove using the *syn*- conformation. Because the adducted O8 would likely still clash with the phosphate backbone in the primer terminal position investigated in this chapter, we hypothesized that replication past 8-oxo-G would proceed more efficiently opposite dA. We show that primer terminal 8-oxo-dGMP can be efficiently extended when in a

mutagenic base pair and a non-mutagenic base pair is extended although to a lesser degree. This result builds on the previous observation that 8-oxo-dGTP inserts mutagenically and non-mutagenically at a similar proportion to 8-oxo-GMP extension. This means that 8-oxo-dGTP is preferentially inserted mutagenically opposite dA and then is efficiently extended as the next step. By allowing efficient replication beyond the mutagenic base pair, the polymerase would prevent replication stalling which minimizes the chances of incurring single-stranded DNA breaks that can lead to more dangerous double-stranded DNA breaks. Although this scenario would introduce a mutagenic base pair into the genome, DNA repair enzymes would have the opportunity to rescue the mutagenic event. In particular, the mutY DNA glycosylase (MUTYH) protein recognizes mutagenic 8-oxo-dG:dA base pair and excises the incorrect dA, giving base excision repair pathway the opportunity to correct the error.

2.2 Abstract

The oxidized nucleotide, 8-oxo-7,8-dihydro-2'-deoxyguanosine (8-oxo-dG), is one of the most abundant DNA lesions. 8-oxo-dG plays a major role in tumorigenesis and human disease. Biological consequences of 8-oxo-dG are mediated in part by its insertion into the genome, making it essential to understand how DNA polymerases handle 8-oxo-dG. Insertion of 8-oxo-dGTP is mutagenic when opposite adenine but not when opposite cytosine. However, either result leads to DNA damage at the primer terminus (3'-end) during the succeeding insertion event. Extension from DNA damage at primer termini remains poorly understood. Using kinetics and time-lapse crystallography, we evaluated how a model DNA polymerase, human polymerase β , accommodates 8-oxo-dG at the primer terminus opposite cytosine and adenine. Notably, extension from the mutagenic

base pair is favored over the non-mutagenic base pair. When 8-oxo-dG is at the primer terminus opposite cytosine, DNA centric changes lead to a clash between O8 of 8-oxo-dG and the phosphate backbone. Changes in the extension reaction resulting from the altered active site provide evidence for a stabilizing interaction between Arg254 and Asp256 that serves an important role during DNA synthesis reactions. These results provide novel insights into the impact of damage at the primer terminus on genomic stability and DNA synthesis.

2.3 Introduction

Oxidative stress, a cellular condition in which there is an imbalance between concentrations of reactive oxygen species (ROS) and antioxidant defenses, is associated with genomic instability and multiple human diseases (99). ROS can react with nucleotides to generate multiple types of oxidative DNA lesions, both in duplex DNA and the free nucleotide pool. Free deoxynucleotides are even more susceptible to oxidation than duplex DNA (100,101), and incorporation of oxidized nucleotide triphosphates into the genome during replication and repair leads to decreased genomic stability (16,101-104). Consequently, cells encode an enzyme, human MutT homologue (MTH1), to convert free oxidized nucleotides to their monophosphate form, prohibiting their insertion into the genome (105). Underscoring the significance of the incorporation of oxidized nucleotides into the genome, the inhibition of MTH1 in cancer cell lines promotes cellular death and MTH1 inhibitors are currently in clinical trials (19,106).

Given that biological impacts of damaged nucleotides are mediated in part by their insertion and subsequent extension by a DNA polymerase, it is essential to understand how these damaged nucleotides are handled by DNA polymerases at the molecular level

(16). One major oxidized nucleobase resulting from ROS is 8-oxo-7,8-dihydro-2'-deoxyguanosine, which is found in both duplex DNA (8-oxo-dG) and in the nucleotide pool (8-oxo-dGTP) (107,108). 8-oxo-dG arises by the incorporation of an adducted oxygen at C8 and protonation of N7 (109). These modifications to guanine (dG) lead to potential mutagenic hydrogen bonding interactions at the Hoogsteen edge (110). The mutagenicity of 8-oxo-dG is dictated by the *anti*- or *syn*- conformation of the damaged base. Similar to undamaged guanine, 8-oxo-dG (*anti*-) base pairs with cytosine (dC) through classical Watson–Crick hydrogen bonding interactions, forming a non-mutagenic DNA lesion. Alternatively, 8-oxo-dG (*syn*-) can exploit its Hoogsteen edge to form a mutagenic base pair with adenine (dA). The 8-oxo-dG:dA base pair promotes a dG:dC to dT:dA transversion following DNA replication (111). Because of the key role DNA polymerases play in DNA replication and repair, they are important mediators between oxidative stress and the biological outcome of 8-oxo-dG.

Mammalian DNA polymerase beta (pol β) has been characterized structurally, kinetically, and biologically (38,112). Consequently, pol β has served as a model enzyme for characterizing the nucleotidyl transferase reaction, which is utilized universally by DNA polymerases during DNA synthesis. Pol β is employed during DNA repair as part of the base excision repair pathway (BER), where it primarily preforms gap filling DNA synthesis during single nucleotide replacements. The polymerase domain of pol β , analogous to other DNA polymerases, is composed of three functionally distinct subdomains. Pol β binds to gapped DNA substrates in the open conformation using its DNA binding- or D-subdomain. This binary complex (pol β /DNA) positions the templating base and primer terminus within the active site. A conformational change from an open to closed state

occurs at the nascent base pair binding domain (N-subdomain) upon binding of the incoming nucleotide. In the closed conformation, pol β repositions the 3'-OH of the deoxyribose at the primer terminus for inline attack on the α -phosphate (α P) of the incoming dNTP. In this state, the catalytic subdomain (C-domain) of pol β coordinates two divalent metal cations that facilitate DNA synthesis. Upon catalysis, pyrophosphate (PPi) is formed and released when pol β re-opens.

Employing pol β as a model DNA polymerase, structural changes within the active site, emanating from substrates containing 8-oxo-dG in the templating strand (51,71) or the insertion of 8-oxo-dGTP, have led to mechanistic insights (16). These crystallographic studies have demonstrated that a clash, between the adducted oxygen (O8) and the phosphate backbone of 8-oxo-dG, can promote antagonistic changes to the nucleoside sugar pucker and backbone position. Additionally, insertion of 8-oxodGTP leads to overall instability at the newly generated primer terminus. During the subsequent round of DNA synthesis, the polymerase is tasked with extending from the 8-oxo-dG terminated primer strand. Unfortunately, very little is known about how polymerases extend from a damaged primer terminus. In this study, we utilized kinetics and time-lapse X-ray crystallography to decipher the impact of 8-oxo-dG at primer termini during DNA synthesis. These studies revealed mutagenic extension from 8-oxo-dG:dA is substantially favored in comparison to the non-mutagenic pairing of 8-oxo-dG:dC. Reduced extension proficiency with non-mutagenic 8-oxo-dG:dC primer termini arises from active site rearrangements accommodating O8 of 8-oxo-dG in a base pair dependent fashion.

2.4 Materials and Methods

2.4.1 Expression and purification of DNA Polymerase β

Human wild-type DNA pol β was overexpressed from a pET-30 vector in the BL21-CodonPlus(DE3)-RP *Escherichia coli* strain. Purification of pol β was carried out as previously described and briefly summarized here (113). Cell lysate containing pol β was run over GE HiTrap Heparin HP, GE Resource S, and HiPrep 16/60 Sephacryl S-200HR columns and fractions containing pure pol β were concentrated and stored at -80°C in 20 mM BisTris propane, pH 7.0 for crystallization and 50 mM HEPES, pH 7.4 for kinetics. Pol β was determined to be pure by SDS page and the final concentration was determined by A280 using a NanoDrop One UV-Vis Spectrophotometer ($\epsilon = 23\,380\text{ M}^{-1}\text{ cm}^{-1}$).

2.4.2. DNA sequences and oligonucleotide annealing

The following DNA sequences were used to generate the 16-mer DNA duplexes used in crystallization studies (the nucleotide opposite 8-oxo-dG is underlined): template, 5'-CCGACG(C/A)CGCATCAGC-3'; primer, 5'-GCTGATGCG-3'; downstream, 5'-GTCGC-3'. The downstream sequence was 5'-phosphorylated. The kinetic studies required extending the downstream and upstream sequences to employ a 34-base DNA substrate. The sequence of the template strand was 5'-GTACCCGGGGATCCGTACG(C/A)CGCATCAGCTGCAG-3'. DNA substrates for single-nucleotide gap filling DNA synthesis reactions were prepared by annealing three purified oligonucleotides. Each oligonucleotide was suspended in 10 mM Tris-HCl, pH 7.4 and 1 mM EDTA and the concentration was determined from their ultraviolet absorbance at 260 nm. The annealing reactions were performed by incubating a solution of primer with

downstream and template oligonucleotides (1:1.2:1.2 molar ratio, respectively) at 95°C for 5 min, followed by 65°C for 30 min, and finally cooling 1°C min⁻¹ to 10°C in a thermocycler.

2.4.3. Pol β /DNA complex crystallization and time-lapse crystallography

Pol β was initially complexed with 2-nt gapped DNA and incubated with 8-oxo-dGTP. This incubation resulted in a 1-nt gap DNA substrate with 8-oxo-dG at the primer terminus inserted across from either dA or dC. Binary complex crystals with 8-oxo-dG:dA or 8-oxo-dG:dC at the primer terminus were grown as previously described in a solution containing 50 mM imidazole, pH 7.5, 13–19% PEG3350 and 350 mM sodium acetate (114). In order to visualize multiple enzymatic states, time-lapse crystallography was utilized as previously described and summarized here (51). First, binary pol β /DNA crystals were soaked in a cryosolution containing 25% ethylene glycol, 50 mM imidazole, pH 7.5, 19% PEG3350 and 70 mM sodium acetate, 2 mM dCTP and 50 mM CaCl₂ for 20 min. These ground state ternary pol β /DNA/dNTP crystals were subsequently transferred to a cryosolution containing 25% ethylene glycol, 50 mM imidazole, pH 7.5, 19% PEG3350, 70 mM sodium acetate, and 200 mM MgCl₂ or MnCl₂ for the varying, indicated times.

2.4.4. Crystallographic data collection and refinement

Data were collected at 100 K on a Rigaku MicroMax-007 HF rotating anode diffractometer equipped with a Dectris Pilatus3R 200K-A detector system at a wavelength of 1.54 Å . Data were processed and scaled using the HKL3000R software package (115). Initial models were determined using molecular replacement with the previously determined open (PDB: 3ISB), closed (PDB: 2FMS), or mismatch (PDB: 3C2M) structures of pol β as

a reference. All R_{free} flags were taken from the starting model. Refinement was performed using PHENIX and model building using Coot (116,117). The metal ligand coordination restraints were generated by ReadySet (PHENIX). Partial catalysis models were generated with both the reactant and product species, and occupancy refinement was performed. The figures were prepared in PyMOL (Schrödinger LLC). Ramachandran analysis determined 100% of non-glycine residues lie in the allowed regions and at least 98% in favored regions.

2.4.5. Kinetic characterization using steady-state kinetics

The steady-state kinetic parameters for the extension from 8-oxo-dG by pol β were determined by performing initial velocity measurements of a single-nucleotide gap filling reaction as previously described (118). DNA substrates contained a 5',6-carboxyfluorescein (6-FAM) and were designed with an 8-oxo-dG or non-damaged dG at the 3'-terminus base paired with dC or dA. The reaction mixture used to obtain activity measurements contained 50 mM Tris-HCl, pH 7.4 (37°C), 100 mM KCl, 10 mM MgCl₂, 1 mM dithiothreitol, 100 μ g/ml bovine serum albumin, 10% glycerol and 200 nM single-nucleotide gapped DNA. 50 μ l reactions were stopped by addition of an equal volume of a quenching solution containing 100 mM EDTA, 80% deionized formamide, 0.25 mg/ml bromophenol blue and 0.25 mg/ml xylene cyanol. Enzyme concentrations and reaction times were selected to maintain initial velocity conditions. Product and substrate DNA were separated on a 16% denaturing (8M urea) polyacrylamide gel. The resulting bands were quantified using a GE Typhoon 8600 imager in fluorescence mode using a 532 nm excitation laser and 526 nm short-pass emission filter. Steady-state kinetic parameters (K_M , k_{cat}) were determined by fitting the data to the Michaelis-Menten equation. The

relative extension efficiency, f_{ex} , was calculated from the ratio of catalytic efficiencies for correct dCTP insertion on a matched, non-damaged (dG–dC) and modified primer terminus. The mean and standard error of at least three independent experiments are shown on the graphs in [Figure 2.1](#)

2.5 Results

2.5.1. Kinetic characterization of extension from 8-oxo-dG

The ability of a DNA polymerase to extend from 8-oxo-dG at primer termini was evaluated using pol β and steady-state kinetic analysis. This approach utilized a 1-nt gapped DNA substrate with a templating dG and either 8-oxo-dG:dC, 8-oxo-dG:dA, dG:dC or dG:dA at the primer terminus. This array of substrates allowed for a thorough comparison of extension from non-damaged and damaged primer termini. Results are summarized in [Figure 2.1](#) and kinetic parameters are listed in [Table 1](#). The apparent affinity of an incoming dCTP to pol β with a 1-nt gapped DNA substrate (K_M) with each 3'-terminus combination was determined. The presence of 8-oxo-dG at the primer terminus, in the form of either an 8-oxo-dG:dA or 8-oxo-dG:dC base pair, resulted in similar K_M values for the incoming dCTP of 0.3 and 0.2 μM , respectively ([Figure 2.1A](#), [Table 1](#)). These apparent binding affinities are comparable to the pol β /DNA complex with a matched, non-damaged dG:dC base pair at the primer terminus ($K_M = 0.09 \mu\text{M}$), but in contrast to a dG:dA ($K_M = 24 \mu\text{M}$). On the other hand, enzymatic turnover rates (k_{cat}) are considerably different depending on which base is across from 3'-8-oxo-dG, with dC and dA producing rates of 0.017 and 0.30 s^{-1} , respectively ([Figure 2.1](#), [Table 1](#)). In comparison, the rate of enzymatic turnover for the nondamaged, mismatched dG:dA is 0.092 s^{-1} , while matched

dG:dC is 0.26 s^{-1} . The dG:dC k_{cat} is nearly identical to 8-oxo-dG:dA, in contrast to 8-oxo-dG:dC which is ~ 15 -fold slower. The resulting catalytic efficiencies, k_{cat}/K_M , are $0.09 \mu\text{M}^{-1} \text{ s}^{-1}$ (8-oxo-dG:dC) and $1.2 \mu\text{M}^{-1} \text{ s}^{-1}$ (8-oxo-dG:dA), compared to 2.9 and $0.0040 \mu\text{M}^{-1} \text{ s}^{-1}$ for non-damaged dG:dC and dG:dA,

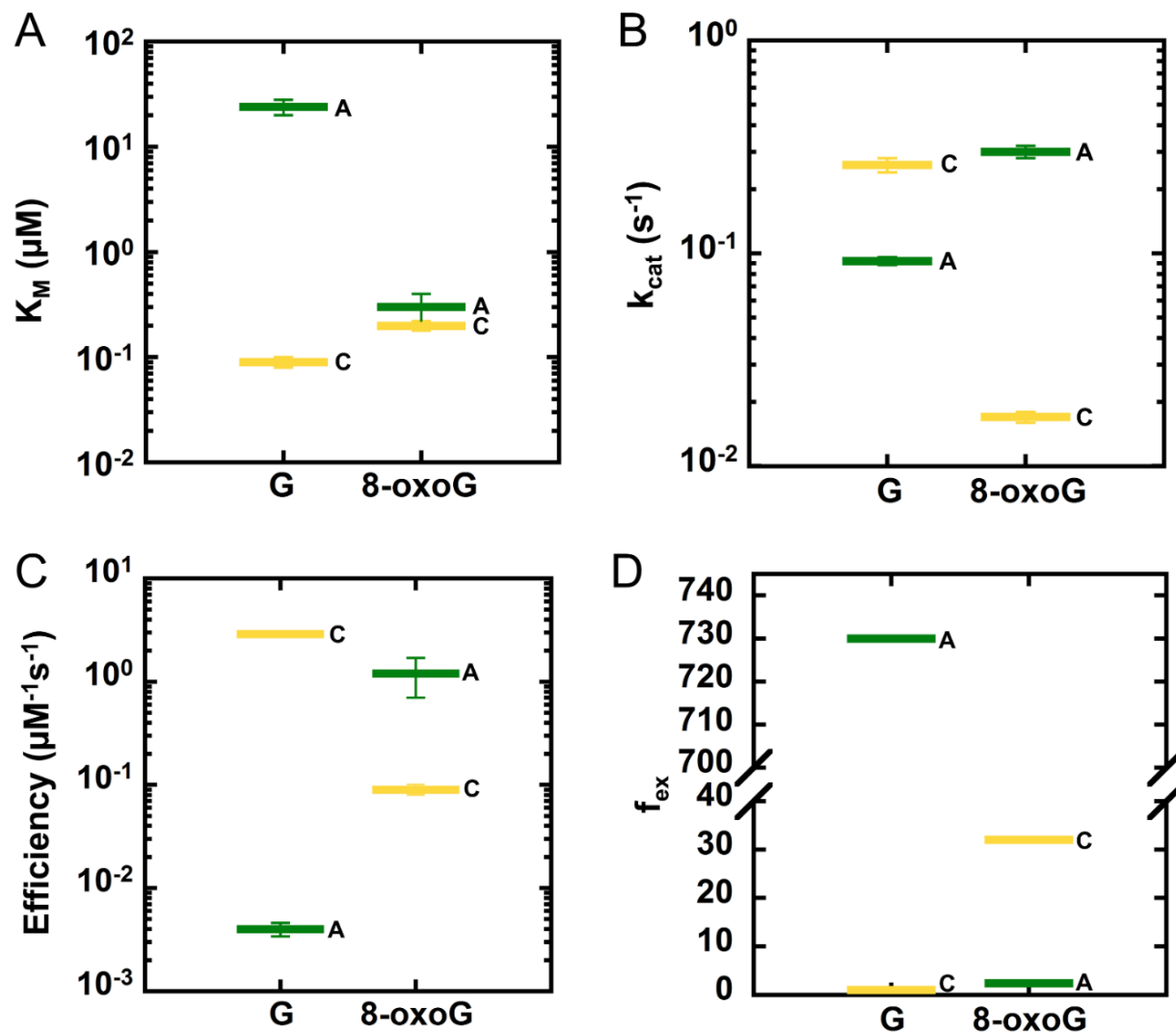


Figure 2.1 Kinetic characterization of extension from 8-oxo-dG by pol β .

(A) K_M , (B) k_{cat} and (C) catalytic efficiencies pol β dCTP insertion opposite dG with substrates containing either dGTP or 8-oxo-dGTP at the primer terminus opposite dC and dA. (D) f_{ex} values corresponding to (C). Green bars represent dA, and yellow represents dC. The results represent the mean of at least three independent determinations with the standard error (SE) graphed in each despite the width being smaller than some of the bars. The identity of the primer terminus is given as primer nucleotide/template nucleotide.

Table 1. Steady-state kinetic parameters for correct dCTP insertion on 8-oxo-dG primer termini.

3'-terminus	K_M (μM)	k_{cat} (s^{-1})	Efficiency ($\mu\text{M}^{-1} \text{s}^{-1}$)	f_{ex}
G/C	0.09 (0.01)	0.26 (0.02)	2.9 (0.2)	1
8oxoG/C	0.20 (0.02)	0.017 (0.001)	0.09 (0.01)	33
G/A	24 (4)	0.092 (0.004)	0.0040 (0.0006)	720
8oxoG/A	0.3 (0.1)	0.30 (0.02)	1.2 (0.5)	2.3

The results represent the mean (standard error) of at least three independent determinations. The identity of the primer terminus is given as primer nucleotide/template nucleotide.

To provide a rational method for comparing the differences in catalytic efficiency between the matched, nondamaged dG:dC primer terminus and either mismatched (dG:dA) or 8-oxo-dG containing termini, we have also reported relative extension efficiency (f_{ex}) values (Figure 2.1D, Table 1) (19). For each 3'-terminus, the f_{ex} value represents the fold change in catalytic efficiency between the substrate with the terminus of interest and the substrate with a dG:dC terminus. Hence, f_{ex} describes the efficiency of extension relative to that from the matched, non-damaged primer terminus, where values >1 correspond to termini with reduced extension efficiencies and larger magnitudes represent reduced efficiency. Experimental f_{ex} values for 8-oxo-dG:dA and 8-oxo-dG:dC are 2.3 and 32, respectively.

The large reduction in relative extension efficiency observed with 8-oxo-dG at the primer terminus opposite dC, but not dA, implies 8-oxo-dG alters the active site differently depending on its base-pairing partner. Furthermore, the measured differences in catalytic efficiency between the two damaged termini stem from variation in the enzymatic turnover rates (k_{cat}) as opposed to their comparative apparent nucleotide binding affinities (K_M). Additionally, extension efficiencies vary greatly between the damaged mismatch 8-oxo-dG:dA ($f_{ex} = 2.3$) and the nondamaged mismatch dG:dA ($f_{ex} = 730$). This is presumably from the reduced K_M for substrate, demonstrated by the 80-fold larger K_M with dG:dA at the primer terminus, indicating O8 of 8-oxo-dG promotes a primer terminus conformation suitable for nucleotide binding. Because pol β binds DNA in an open conformation, we do not expect 8-oxo-dG at the primer terminus to alter the affinity of pol β for single-nucleotide gapped DNA. Additionally, it has previously been shown that mismatched primer termini do not affect single-nucleotide gapped DNA binding affinity for pol β (118,119).

2.5.2. 8-oxodG forms stable base pairs opposite dC (*anti*-) and dA (*syn*-) in binary complexes at the primer terminus position

To gain molecular insight into the impact an 8-oxo-dG terminated primer has on the polymerase active site, we employed X-ray crystallography of pol β . To generate 1-nt gapped DNA substrates with 8-oxo-dG at the primer terminus, we utilized pol β polymerase activity prior to crystallization ([Figure 2.2A](#)). Pol β was incubated with 8-oxodGTP and a 2-nt gapped DNA substrate containing dC or dA followed by dG in the gap, resulting in 8-oxo-dG incorporation opposite either dC or dA at the primer terminus with a dG in the 1-nt gap. This protein/DNA mixture was subsequently used during crystallization to form binary pol β /DNA complexes with either an 8-oxo-dG:dC or 8-oxo-dG:dA base pair at the primer terminus. Our binary pol β structures, described below, confirmed that 8-oxo-dG was inserted at the primer terminus adjacent to a 1-nt gap containing a dG ([Figure 2.2 B and C](#)).

Binary X-ray crystal structures show pol β in its open conformation while bound to 1-nt gapped DNA with 8-oxo-dG at the primer terminus opposite either dC or dA at 1.80 and 1.95 Å resolution, respectively ([Figure 2.2B](#), [Figure 2.2C](#), [Table 2](#) and [Table 3](#)). These structures provide insight into how 8-oxo-dG is situated at primer termini in the binary state prior to nucleotide binding. When 8-oxo-dG is opposite either dA or dC, it forms an ordered and stable primer terminus as indicated by clear density and a low B-factor ([Table 2](#), [Table 3](#), and [Figure 2.3 A and B](#)). This stability is achieved by hydrogen bonding interactions between 8-oxo-dG and the opposing base. 8-oxo-dG (*anti*) hydrogen bonds with dC using its canonical Watson-Crick face ([Figure 2.3A](#)) and to dA in the *syn*-conformation using its Hoogsteen face ([Figure 2.3B](#)).

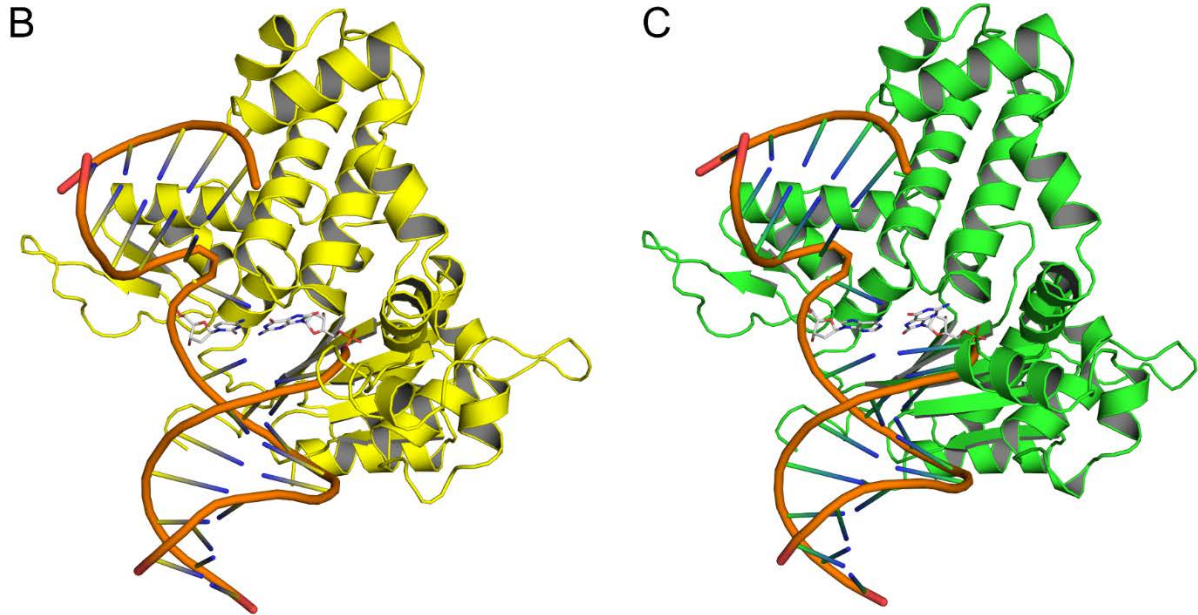
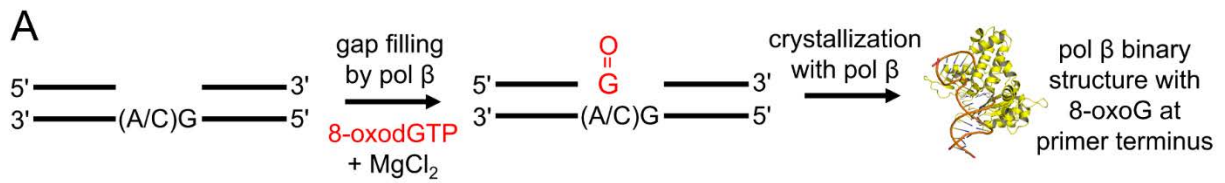


Figure 2.2 Construction of 8-oxo-dG terminated pol β DNA substrates.

(A) Schematic demonstrating pol β insertion of 8-oxo-dGTP (red) to generate substrates for subsequent crystallization with 8-oxo-dG opposite dA and dC at the primer terminus. (B) Binary structure showing 8-oxo-dG at the primer terminus opposite dC (yellow). (C) Binary structure showing 8-oxo-dG opposite dA at the primer terminus (green). The primer terminal base pairs are shown as sticks in gray.

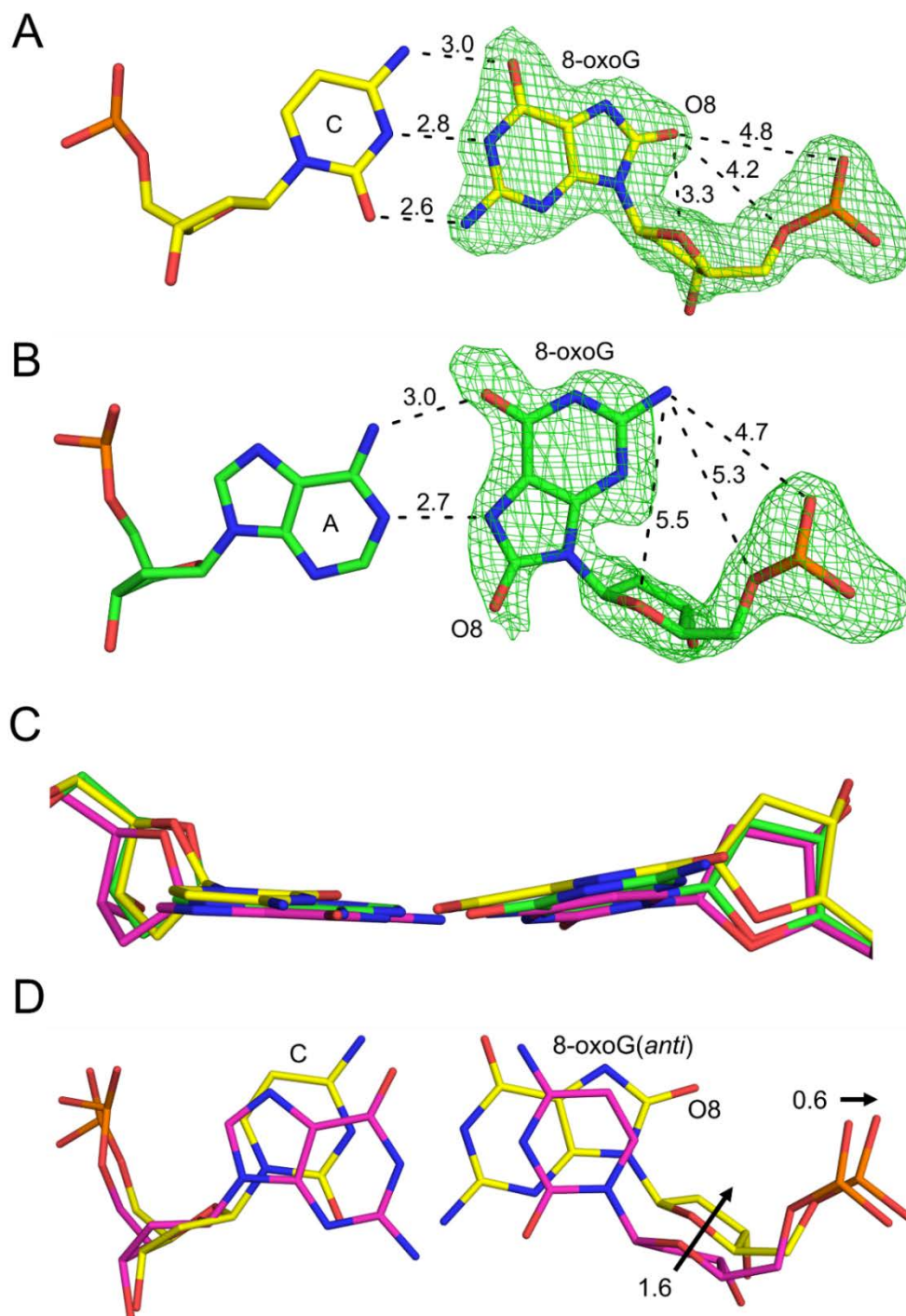


Figure 2.3 Binary complex structures with 8-oxo-dG at the primer terminus.

(A) Primer terminus 8-oxo-dG:dC Watson–Crick base pair (yellow). (B) Primer terminus 8-oxo-dG:dA Hoogsteen base pair (green). (C) A 90° rotation demonstrates planarity of 8-oxo-dG containing base pairs overlaid with non-damaged, matched binary reference structure (magenta, PDB 3ISB). (D) In reference to 3ISB (magenta), a primer terminus 8-oxo-dG:dC (yellow) results in shifts (arrows) in the sugar and α P of 8-oxo-dG (*anti*). The omit maps (green) are contoured at 3σ . Distances are labeled and indicated as dashed lines.

Both 8-oxo-dG containing base pairs sit planar at the primer terminus and there is no significant repositioning compared to non-damaged, correctly paired DNA (*i.e.* dG:dC) ([Figure 2.3C](#)). The sugar pucker of 8-oxo-dG at the primer terminus is O4'-endo while paired with either dA or dC, which contrasts to binary non-damaged, matched primer termini that adopt C4'-exo at the primer terminus (PDB 3ISB). In addition to the sugar pucker change, when 8-oxo-dG (*anti*) is opposite dC the nucleoside shifts by 1.6 Å toward the major groove ([Figure 2.3D](#)). This movement may arise from the phosphate backbone shifting 0.6 Å away from O8 when 8-oxo-dG is in the anti-conformation. When 8-oxo-dG is in the syn-conformation, O8 of 8-oxo-dG is in the minor groove of the DNA, which prevents clashing with active site residues.

2.4.3. 8-oxodG opposite dC breaks the Arg254 and Asp256 salt bridge

To obtain ternary pol β complexes, we started with binary pol β/DNA complexes with 8-oxo-dG:dC at the primer terminus generated as described above. These crystals were transferred to a cryoprotectant solution containing Ca²⁺, which does not support catalysis, and dCTP to promote the formation of the closed pre-catalytic ternary pol β complex. The crystal diffracted to 2.2 Å, [Table 2](#).

Table 2. Data collection and refinement statistics of binary and ternary polymerase β /DNA co-complexes with dCTP extending from 8-oxodGTP across from cytosine.

	Binary	Ground State dCTP	Ground State dCMPCPP	Reactant	Product Closed	Product Open
Data collection						
Space group	P2 ₁	P2 ₁	P2 ₁	P2 ₁	P2 ₁	P2 ₁
Cell dimensions <i>a, b, c</i> (Å)	54.3,79.1,54.9	50.2,79.0,55.6	50.7,80,55.7	50.6,79.7,55.6	50.6,79.8,55.5	55.3,79.8,55.9
α, β, γ (°)	90,104.9,90	90,107.0,90	90,107.5,90	90,107.5,90	90,107.6,90	90,110.3,90
Resolution (Å)	25-1.80	50-2.2	25-2.0	25-2.08	25-2.05	50-2.62
R_{sym} or R_{merge}^a (%)	0.068 (0.294)	0.102 (0.659)	0.068 (0.501)	0.069 (0.39)	0.078 (0.452)	0.118 (0.859)
$I/\sigma I$	20.6 (3.5)	16.5 (2.1)	17.4 (2.3)	17.3 (2.1)	14.4 (2.7)	14.3 (2.0)
Completeness (%)	98.3 (92.6)	99.4 (98.1)	98.1 (89.5)	99.4 (98.3)	98.3 (91.3)	99.6 (99.9)
Redundancy	3.9 (2.1)	4.4 (2.6)	3.8 (2.1)	4.1 (2.21)	3.7 (1.9)	3.8 (3.6)
Refinement						
Resolution (Å)	1.80	2.18	1.99	2.08	2.05	2.62
No. reflections	69873	36996	51341	44071	47251	25305
$R_{\text{work}}/R_{\text{free}}$	17.61/22.15	22.5/29.76	17.6/23.1	18.0/23.8	18.5/23.8	21.1/29.7
No. atoms						
Protein	2580	2614	2574	2540	2590	2588
DNA	611	611	632	652	652	630
Water	442	45	44	227	235	42
B-factors (Å ²)						
Protein	23.48	47.4	24.8	33.56	25.50	62.99
DNA/8OG/dCTP	24.9/24.9/NA	56.5/48.1/38.0	35.5/20.2/15.3	46.5/34.0/32.0	37.8/23.5/NA	56.4/60.5/NA
Water	30.88	47.4	31.54	39.45	30.90	51.84
R.m.s deviations						
Bond length (Å)	0.011	0.009	0.007	0.007	0.018	0.010
Bond angles (°)	1.216	1.057	0.948	0.941	1.411	1.132
Ratio of RS/PS	NA	1/0	1/0	0.8/0.2	0/1	0/1
PDB ID	5V1G	5V1F	5V1P	5V1R	5V1I	5V1J

^a Highest resolution shell is shown in parentheses.

RS and PS correspond to the amount of reactant and product states, respectively.

Figure 2.4A shows a close-up of the active site with the dCTP bound, Ca^{2+} in the nucleotide (Me_n) and catalytic (Me_c) metal binding sites, and 8-oxo-dG:C at the primer terminus. The metal ions and incoming dCTP adopt a nearly identical conformation as observed with a non-damaged, matched primer terminus (Figure 2.5A). The only major structural changes are localized around the 8-oxo-dG:dC primer terminus base pair. Upon binding dCTP, the sugar pucker of 8-oxo-dG shifts from O4'-endo to C3'-endo, likely as a result of the 8-oxo-dG 3'-OH coordinating Ca^{2+} in the Me_c site. 8-oxo-dG maintains the *anti*-conformation and planar Watson-Crick hydrogen bonding interactions with dC. In this conformation, the clash between O8 and the phosphate backbone forces a 1.7 Å shift of the backbone away from O8. This shift leads to a 110° rotation and 5.5–6 Å displacement of Arg254 in the pol β active site (Figure 2.4B), causing a disruption of the salt bridge between Arg254 and Asp256 (Figure 2.4C) that is postulated to stabilize Asp256 in pol β structures with non-damaged primer termini (see discussion) (120). To ensure the rotation of Arg254 was not Ca^{2+} dependent, a higher resolution structure was obtained after a soak in the biological polymerase co-factor Mg^{2+} and a nonhydrolyzable nucleotide analog, 2'-deoxycytidine-5'-[(α,β)-methylene]triphosphate (dCpCpp), to prevent the catalysis. The 2.0 Å resolution structure showed a rotated Arg254 and therefore, confirmed metal independence (Figure 2.5B).

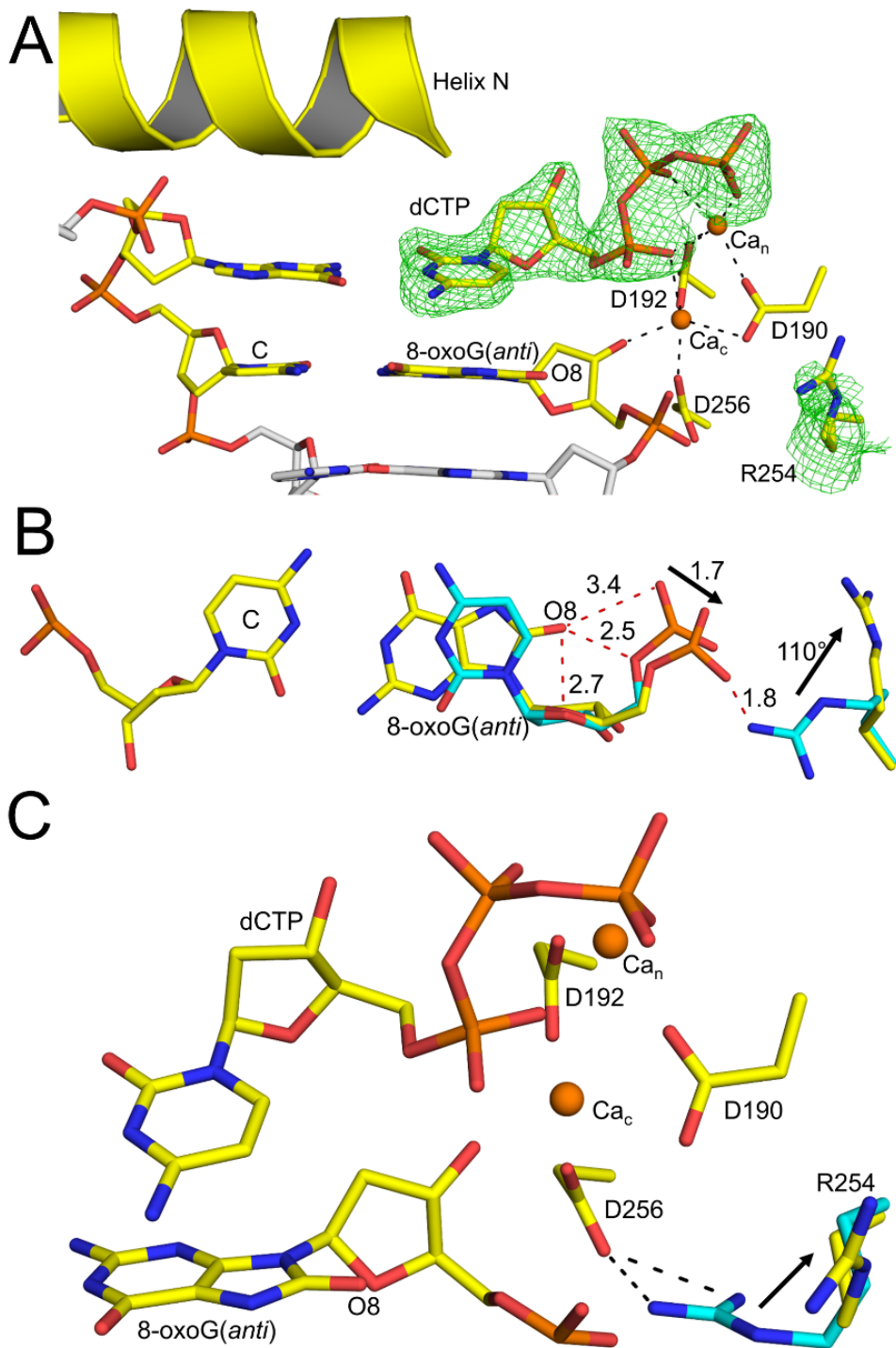


Figure 2.4 Ternary ground state structures with 8-oxo-dG:dC at the primer terminus.

A) Pre-catalytic complex with dCTP and inert Ca²⁺. B) A 90° rotation relative to (A). Clashing at O8 and αP is shown as red dashes and shifts are indicated with arrows in reference to a non-damaged primer terminus (cyan, PDB 2FMS). C) Close- demonstrating the loss of the interaction between Asp256 and Arg254 (2FMS, cyan) when 8-oxo-dG:dC is at the primer terminus (yellow). The omit map (green) is contoured at 3σ. H-bonds are shown as black dashed lines.

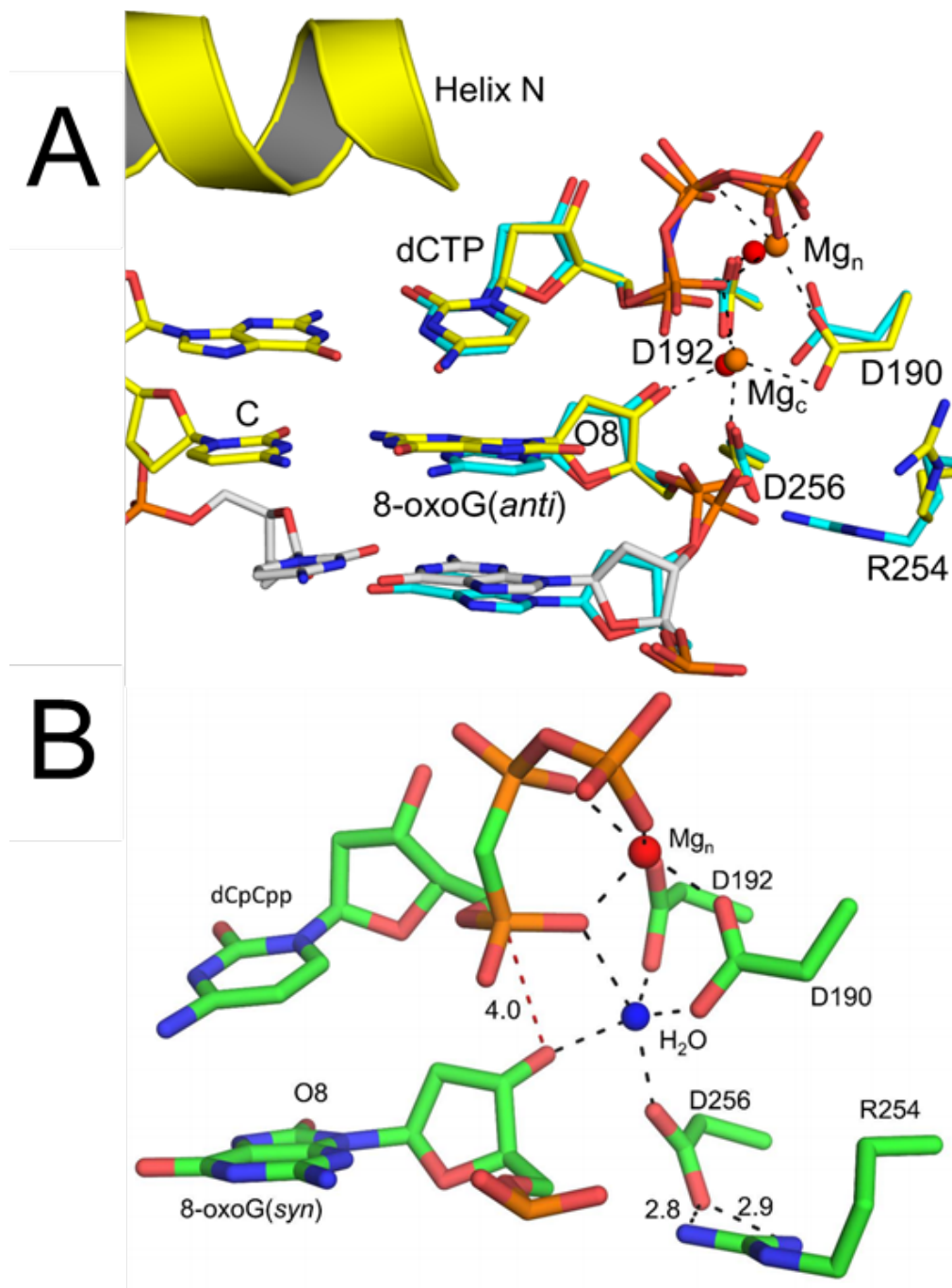


Figure 2.5 Overlays of 8-oxo-dG:dC primer terminus with reference structure containing a dG:dC base pair.

A) Overlay of closed ternary ground state pol β structures with 8-oxoG:dC (yellow) and dG:dC (cyan, 2FMS) at the primer terminus. B) Overlay of open product structure after extension from 8-oxoG:C (yellow) and reference closed ground state structure (cyan, 2FMS).

2.5.4. Arg254 realigns into a catalytically competent position following catalytic initiation

Both the kinetic binding constant (K_M) and ternary ground state structure ([Table 1](#) and [Figure 2.4C](#)) indicate that pol β can accommodate dCTP binding easily with an 8-oxo-dG at the primer terminus opposite dC. The active site residue Arg254 shifts out of the catalytically optimal orientation, however the mechanism of extension is indecipherable from the pre-catalytic structure alone. In order to understand how 8-oxo-dG:dC alters catalytic efficiency, we utilized time-lapse X-ray crystallography to look at structural changes at the molecular level over the course of catalysis. This approach captures reactant state structures undergoing nucleotidyl transfer by first generating crystals of ternary complexes (pol β /DNA/dCTP) in the presence of the inert metal Ca^{2+} before initiating the reaction by soaking the crystal in a solution of $MgCl_2$ (51). The reaction is subsequently stopped in a time dependent fashion by flash freezing, followed by structure determination of the crystal. A structure with 8-oxo-dG:C at the primer terminus was collected after a 60 s soak in $MgCl_2$ that diffracted to 2.08 Å. Density corresponding to both the reactant and product states was observed ([Figure 2.6A](#)), indicating the reaction was 20% complete. [Figure 2.6B](#) shows a comparison of this reactant structure with the ground state. Upon initiation of catalysis, Arg254 realigns into a catalytically competent position where it coordinates Asp256 ([Figure 2.6B](#)), as observed for the non-damaged primer terminus (PDB: 2FMS). Thus, indicating Arg254 must first swing back to coordinate Asp256 for catalysis, providing a structural basis for the reduced k_{cat} observed in the steady-state kinetic analysis ([Figure 2.1](#) and [Table 1](#)).

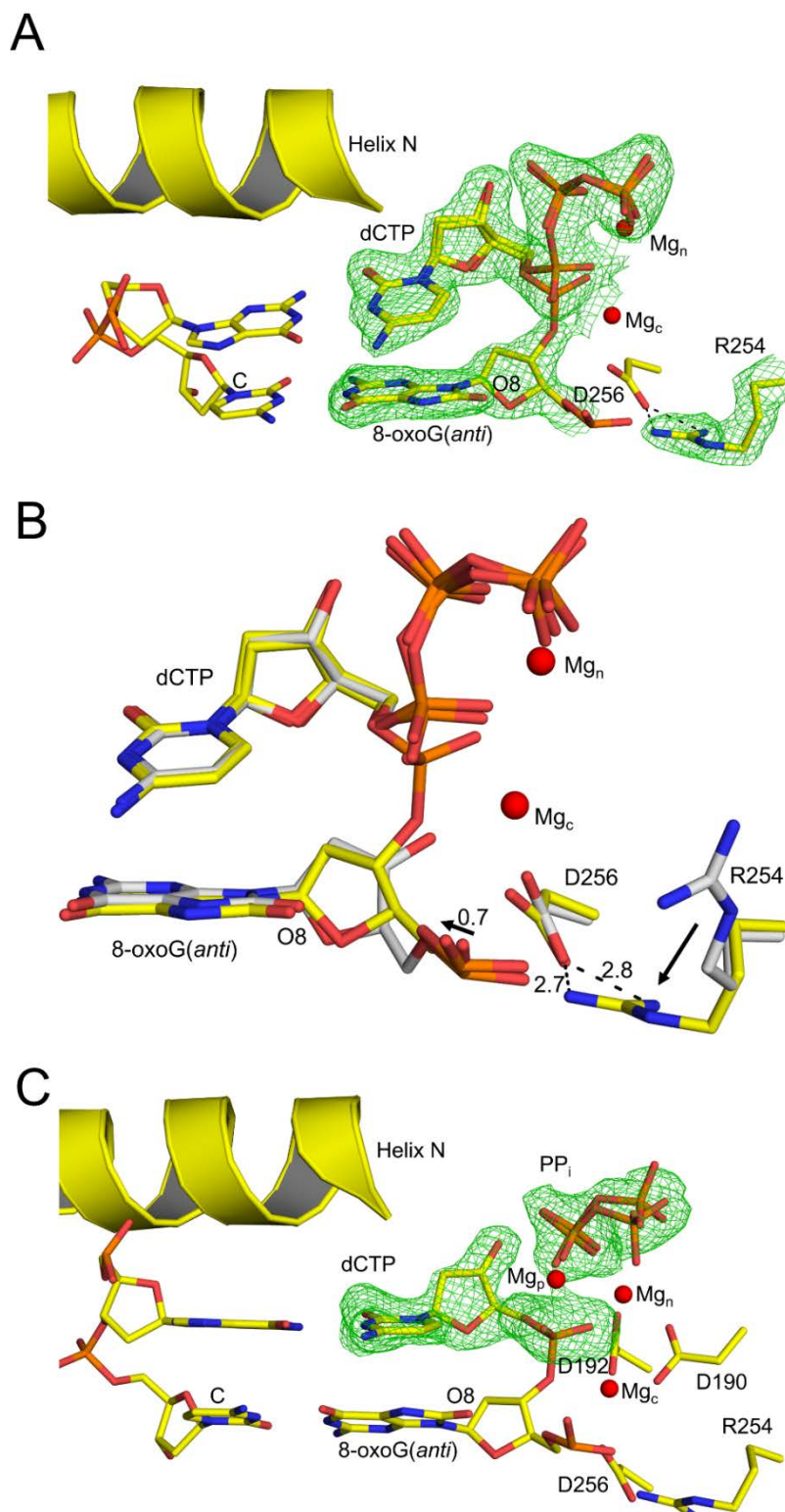


Figure 2.6 Pol β extension from 8-oxo-dG:dC by time-lapse X-ray crystallography.

A) The active site after a 60 s soak in $MgCl_2$. B) An overlay of the reactant state (yellow) and the ground state (gray) active sites demonstrating the swing of Arg254 back into the catalytically competent position. C) The closed, completed product active site after a 120 s soak in $MgCl_2$. The omit maps (green) are contoured at 3σ . Red spheres are Mg^{2+} . H-bonds are shown as black dashed lines.

To observe the product complex with 8-oxo-dG:dC at the primer terminus, we utilized the same approach, but extended our MgCl₂ soak time to 120 s prior to collecting the 2.05 Å resolution product structure ([Table 2](#)). At this point, the synthesis reaction was complete, shown by insertion of dCMP and formation of pyrophosphate ([Figure 2.6C](#)). The sugar pucker of 8-oxo-dG maintains C3'-endo. In this product complex, Arg254 remains in a stable salt bridge with Asp256. As shown in previous pol β product structures, a third product associated metal ion is present (16,51,121). In this product complex, the polymerase remains in the closed conformation. It has previously been shown that the closed to open conformational change of pol β following insertion is altered depending on the identity of the nucleotide (*i.e.* matched, mismatched, damaged) (16,51). To establish whether 8-oxo-dG promotes re-opening of the polymerase *in crystallo*, we extended the time of our soak in MgCl₂. This resulted in pol β undergoing the closed to open transition accompanied by a loss of hydrogen bonding interactions between the inserted dCMP and templating dG while 8-oxo-dG remained base paired to dC.

To determine the molecular structure of 8-oxo-dG:dA at the primer terminus, we soaked a binary 8-oxo-dG:dA pol β crystal in a cryoprotectant solution with CaCl₂ and dCTP. The resultant closed ternary ground state crystal diffracted to 2.1 Å. This structure has an incoming dCTP base pairing with a templating dG and the primer terminal 8-oxo-dG in the *syn*-conformation hydrogen bonding to dA through its Hoogsteen face ([Figure 2.7A](#)). The sugar pucker changes to C2'-endo in the ground state, a conformation that has been demonstrated to inhibit insertion (122). This is as opposed to the 8-oxo-dG:dC pre-catalytic structures which shifted into the catalytically optimized C3'-endo upon nucleotide binding. In this conformation, the N2 of 8-oxo-dG(*syn*) hydrogen bonds to the

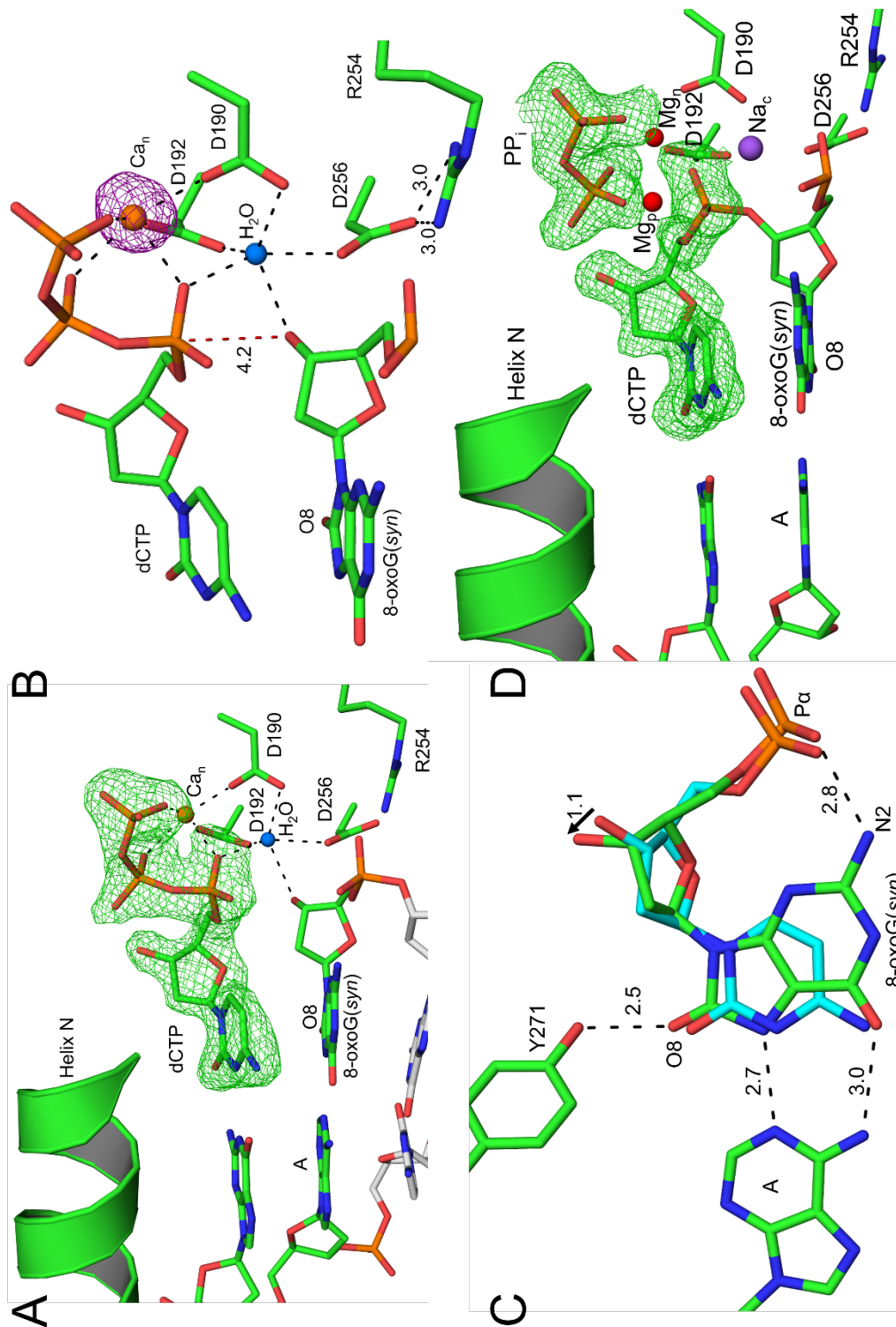


Figure 2.7 Ternary ground state structures with 8-oxo-dG:dA at the primer terminus.

A) Pre-catalytic complex with dCTP, Ca^{2+} in Me_n , and water in Me_c bound. B) A close up of the active site. Interaction between Asp256 and Arg254 is maintained. Distance between 3'-OH and α P of dCTP is shown as a red dashed line. C) Stabilizing interactions are shown at the terminal base pair. Shift in 3'-OH is indicated by an arrow. D) The closed, completed product active site after a 20 s soak in MgCl_2 . Ca^{2+} , Mg^{2+} , Na^+ , and H_2O are orange, red, purple, and blue spheres, respectively. Magenta is an anomalous map contoured at 4σ . H-bonds are shown as black dashed lines. (copyrights received)

non-bridging oxygen of the phosphate backbone and Arg254 maintain the salt bridge with Asp256 ([Figure 2.7B](#) and [Figure 2.7C](#)). In addition, Tyr271 is within hydrogen bonding distance of O8 ([Figure 2.7C](#)). These favorable interactions contrast the unfavorable interactions between the phosphate backbone and O8 with 8-oxo-dG in the *anti*-conformation ([Figure 2.4B](#)). A close-up of the active site in [Figure 2.7B](#) shows 8-oxoG:dA at the primer terminus with Ca²⁺ bound in the Me_n site and a water molecule in the Me_c site. The lack of a metal in the Me_c site results in the 3'-OH shifting to a non-catalytic conformation that does not support in-line nucleophilic attack. The distance between the 3'-OH and the P α is 4.2 Å, as opposed to 3.4 Å, which is optimized for catalysis in the reference structure (PDB 2FMS). Similarly, when the ternary complex was crystallized with the non-hydrolysable analog, dCpCpp, in the presence of MgCl₂ a water molecule is in the Me_c site and the 3'-OH is shifted (data not shown). This suggests that even though Me²⁺ does bind at the catalytic metal site per its ability to form product and bind Na²⁺ ([Figure 2.7D](#)), the Me²⁺ binding is less efficient than when dC is at the template-primer terminus across 8-oxo-dG. This is indicated by the corresponding ternary structure with dC, which has Ca²⁺ ions bound in both metal sites, [Figure 2.4A](#). When interpreted in the context of the catalytic efficiencies, it appears additional stabilizing features at the primer terminus between Tyr271 and O8, and N2 with the phosphate backbone compensate for the weakened Me²⁺ binding at the catalytic metal site.

Attempts to observe catalysis by soaking ground state crystals in a solution containing MgCl₂ failed to produce reactant state structures that contain a mixture of both substrate and product. We either obtained structures that were in the ground state (dCTP bound) or had been converted to all product (dCMP inserted). One possibility for the

difficulty in capturing a reactant state is that the Mg^{2+} ion can quickly bind to the Me_c site to initiate catalysis, which contrasts with other time-lapse structures with a Ca^{2+} in the Me_c that must exchange prior to catalysis occurring. Therefore, the reaction likely undergoes catalysis faster than we can capture using a manual approach. The resulting product structure was obtained at a resolution of 1.8 Å with Mg^{2+} bound at the Me_n site, and Na^+ bound at the Me_c site. This structure indicates as soon as Mg^{2+} binds to the Me_c site, catalysis occurs with minimal changes between the ground and product state structures (Figure 2.7D and Table 3). After catalysis has occurred, the Mg^{2+} exchanges for Na^+ in the Me_c site (51). The only major change is the appearance of a third metal ion upon complete product formation that is consistent with previous early product structures observing catalysis *in crystallo* (51). Of note, 8-oxo-dG remains in the syn-conformation with potential hydrogen bonding interactions between Tyr271 and O8, and N2 and the phosphate backbone oxygen. The only structural change observed upon catalysis, which occurs upon nucleotide binding with 8-oxo-dG:dC, is a shift in the sugar pucker to C3'-endo. As was previously observed for correct insertion of dCTP across from dG with a non-damaged substrate, pol β with the 8-oxo-dG:dA base pair remained in a closed conformation after an extended soak, in contrast to the 8-oxo-dG:dC structure. Overall, the ground state and product structures obtained with dA across from the primer terminus indicate minimal structural rearrangements are required for catalysis.

Table 3. Data collection and refinement statistics of binary and ternary polymerase β /DNA co-complexes with dCTP extending from 8-oxodGTP across from adenine.

	Binary	Ground State dCTP	Ground State dCpCpp	Product
Data collection				
Space group	P2 ₁	P2 ₁	P2 ₁	P2 ₁
Cell dimensions				
<i>a, b, c</i> (Å)	54.3,79.1,54.9	50.5,79.2,55.5	50.5,79.7,55.5	50.6,79.7,55.4
α, β, γ (°)	90,105.5,90	90,107.3,90	90,107.5,90	90,107.8,90
Resolution (Å)	50-1.95	50-2.01	50-2.04	50-1.8
<i>R</i> _{sym} or <i>R</i> _{merge} ^a (%)	0.119 (0.692)	0.124 (0.513)	0.06 (0.458)	0.057 (0.501)
<i>I</i> / σ <i>I</i>	14.6 (3.0)	13.9 (2.2)	18.5 (1.9)	22.8 (2.3)
Completeness (%)	100 (100)	99.4 (97.8)	99.0 (96.6)	99.6 (98.3)
Redundancy	6.1 (5.9)	3.7 (1.9)	3.8 (2.1)	4.1 (2.2)
Refinement				
Resolution (Å)	1.95	2.01	2.04	1.8
No. reflections	61220	51707	46175	71975
<i>R</i> _{work} / <i>R</i> _{free}	22.1/27.3	18.1/23.6	19.3/22.6	17.3/21.1
No. atoms				
Protein	2579	2663	2642	2655
DNA	613	613	663	633
Water	424	306	253	333
B-factors (Å ²)				
Protein	19.8	27.5	34.6	22.8
DNA/8OG/dCTP	22.2/25.6/NA	35.2/19.9/15.9	41.4/32.7/23.5	29.9/16.2/NA
Water	25.6	35.1	36.5	32.0
R.m.s deviations				
Bond length (Å)	0.007	0.008	0.009	0.011
Bond angles (°)	0.9	1.01	1.051	1.094
Ratio of RS/PS	NA	1/0	1/0	0/1
PDB ID	5V1H	5V1N	5VEZ	5V1O

^a Highest resolution shell is shown in parentheses.

RS and PS correspond to the amount of reactant and product states, respectively.

2.6. Discussion

Insertion of a modified nucleotide by a DNA polymerase results in DNA damage positioned at the primer terminus, which will be the substrate during subsequent rounds of DNA synthesis. The oxidized purine 8-oxo-dG, generated by oxidative stress, is the most abundant of the various modified DNA bases and plays a major role in mutagenesis and tumorigenesis. Using kinetics and time-lapse X-ray crystallography, we have evaluated how pol β accommodates 8-oxo-dG at the primer terminus and revealed the molecular contacts involved during extension from both mutagenic and non-mutagenic 8-oxo-dG base pairs ([Figure 2.8](#)).

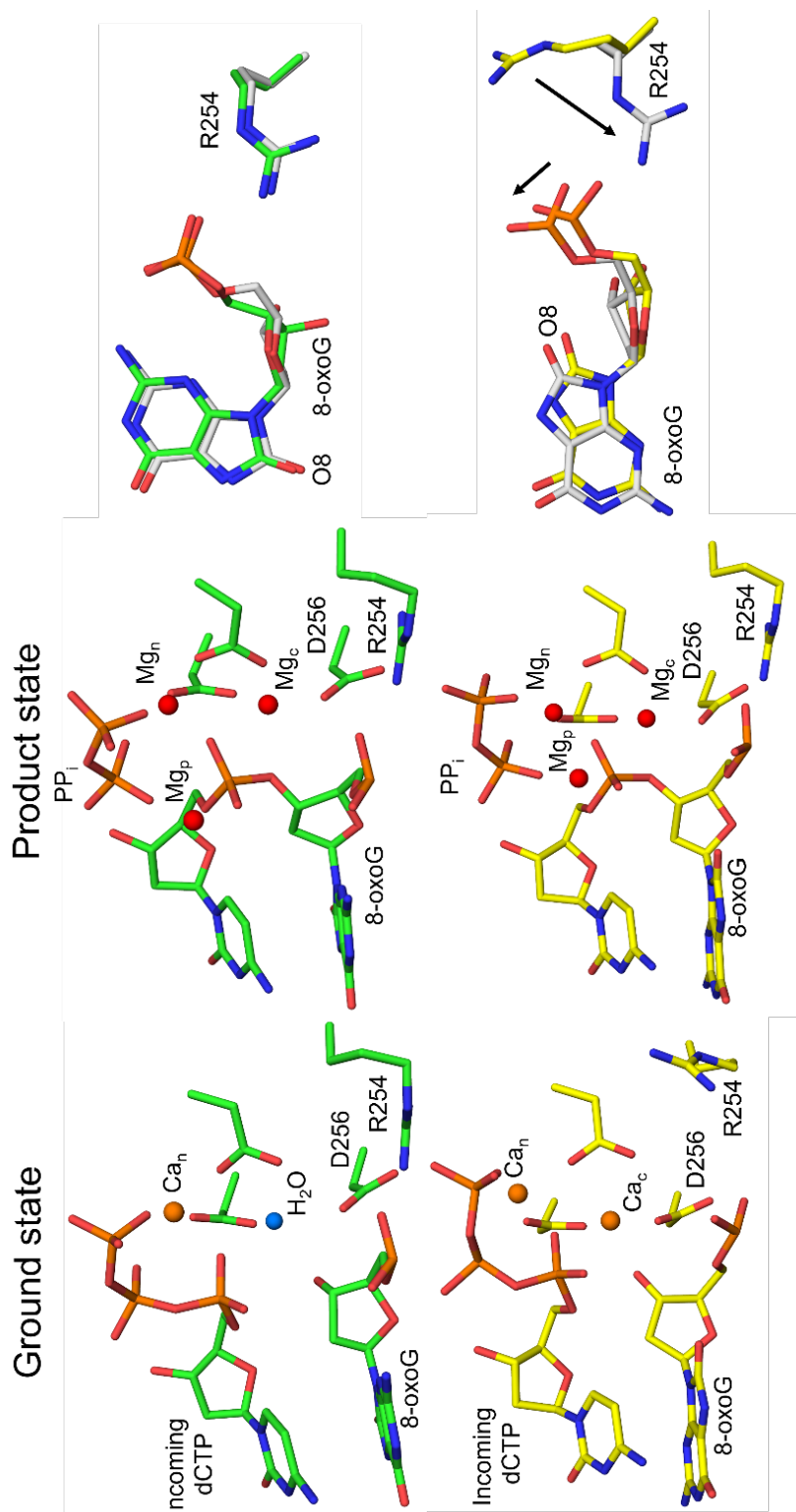


Figure 2.8 Overall scheme demonstrating the structural insights from mutagenic and non-mutagenic extension of 8-oxo-dG that inform on their differing extension efficiencies.

Extension from 8-oxo-dG:dA (green) and 8-oxo-dG:dC (yellow), are shown in both ground and product state complexes. In the last column, the gray sticks are the product state that have been overlaid with the ground state complexes shown as color sticks (yellow:dC, green:dA).

2.6.1. 8-oxo-dG:C results in a clash at the phosphate backbone

Our binary structure shows stable (B-factor = 24.9 Å²) Watson–Crick hydrogen bonds between 8-oxo-dG (*anti*) and dC at the primer terminus. As also recognized in the mutagenic case with dA, previously reported product structures characterizing the insertion of 8-oxodGTP across from dC displayed a high B-factor (65.4 Å²) for the inserted 8-oxo-dG (*anti*) and a loss of Watson–Crick base pairing interaction at the newly generated primer terminus post-catalysis. This is also in contrast to recent structures of pol β with terminal mispairs, which indicate that the mismatched termini adopt various distorted conformations (119). Ternary ground state structures, with 8-oxo-dG:dC at the primer terminus and an incoming dCTP, show a clash between O8 and a non-bridging oxygen of the phosphate backbone that promotes a shift of the DNA backbone towards the protein active site. This shift is accommodated by a rotation of Arg254, which prevents the formation of a salt bridge between Arg254 and Asp256 ([Figure 2.4C](#)). Time lapse X-ray crystallography established that in order for catalysis to occur, Arg254 shifts back into position to coordinate Asp256. The observed requirement for this structural rearrangement is in agreement with the kinetics that show a substantially decreased catalytic efficiency with 8-oxo-dG:dC at the primer terminus ([Figure 2.1](#)).

The clash between O8 and the phosphate backbone is also observed when 8-oxo-dG is in alternative registries. When 8-oxo-dG (*anti*) is in the template position with an incoming dCTP, the phosphodiester backbone shifts 3 Å away from O8. This shift is accommodated by the flexibility of the DNA at the bend in the templating strand and does not alter any active site residues or alter the catalytic efficiency. The 8-oxo-dG:dC base pair at the template n-1 position also maintains its catalytic efficiency; however, it does

not require adjustment of the phosphodiester backbone (71). In the case of 8-oxo-dGTP insertion across from dC, the clash between O8 and the oxygens of α P are accommodated by an additional divalent metal cation during non-mutagenic insertion. Overall, it appears the templating strand can more effectively accommodate 8-oxo-dG (*anti*) than either the primer terminus or when the damage is the incoming nucleotide. This is reflective of the templating strand being more solvent exposed and therefore superiorly positioned to accommodate the clash between O8 and the non-bridging oxygens of the phosphate.

2.6.2. *Pol β accommodates the mutagenic 8-oxo-dG:A base pair at the primer terminus*

Our open binary complex structures demonstrate that 8-oxo-dG (*syn*) across from dA at the primer terminus forms a stable (25.6 Å²) Hoogsteen base pair in the absence of an incoming dNTP. This contrasts what was seen in previous reported structures characterizing the insertion of 8-oxo-dG (*syn*) across from dA, where a high B-factor (57 Å²) and a loss of hydrogen bonding between the bases was observed at the new primer terminus in the post-catalysis open product complex (112). Of note, in this product structure, the primer terminus is not in the correct registry for insertion of the next nucleotide, as it is in the structures reported here, suggesting that active site contacts stabilize 8-oxo-dG (*syn*) at the primer terminus when in the proper registry. Once the nucleotide is bound and the enzyme shifts into the closed conformation, the only repositioning required for catalysis to occur is a change in the sugar pucker, and the binding of the catalytic metal. The lack of substantial structural rearrangements required for extension from a mutagenic 8-oxo-dG:dA base pair is supported by the high catalytic efficiency. Additionally, our structures showed the damage, O8, is accommodated at the

primer terminus by being positioned in the minor groove of the DNA. Similarly, accurate replication beyond a bulky major benzo[a]pyrene adduct by human DNA polymerase kappa was shown to be accomplished by positioning the damage in the nascent DNA minor groove (123).

Because the biological outcomes of 8-oxo-dG are mediated in part by the perturbations to the DNA synthesis reaction provoked by the modified structure of the lesion, it is important to have a thorough understanding of how DNA polymerases respond to the damage. Accordingly, previous studies have determined the effects of 8-oxo-dG on the mechanism of model mammalian DNA polymerase, pol β , both structurally and kinetically, with the damage in the templating position, the template strand primer terminus ($n-1$), and as the incoming nucleotide (16,56,71,124). While the catalytic efficiencies are similar to that with a non-damaged substrate, the strategies employed by pol β to accommodate 8-oxo-dG (*syn*) adapt, depending upon which registry contains the damage. Insertion of 8-oxo-dGTP (*syn*) across from dA relies on interactions between α P and N2 of 8-oxo-dG (*syn*) and active site residue Asn279 with O8 (16). In the case of a templating 8-oxo-dG, the transition to the *syn*-conformation with an incoming dATP requires contacts between 8-oxo-dG (*syn*) and residue Arg283, which is a key minor groove contact in the pol β active site (124). The template strand has a 90° bend at the position of the templating base, resulting in an absence of protein interactions and intrinsic flexibility of the phosphodiester backbone. This flexibility allows for a 3.4 Å shift in the phosphate backbone of 8-oxo-dG in the template position. No shift of the phosphodiester backbone is observed when the 8-oxo-dG (*syn*):dA base pair is at the template primer terminus ($n - 1$) (71). Overall, the different strategies indicate a registry dependent

processing of 8-oxo-dG within the pol β active site, emphasizing the importance of characterizing each of these positions.

2.6.3. The Asp256 and Arg254 salt bridge serves an important role during catalysis

The nucleotidyl-transfer reaction is initiated by deprotonation of the primer DNA strand 3'-OH. The catalytic Mg^{2+} facilitates deprotonation by lowering the pKa of the hydroxyl group and stabilizing the negative charge of the nucleophilic oxygen that attacks the phosphate of the incoming nucleotide. The nature of the 3'-OH proton acceptor is an ongoing debate with two main theories for pol β (120,125-127). One theory is that the proton acceptor is a hydroxide anion in bulk water via a specific base mechanism. The second theory is that the proton acceptor is an active site group via a general base mechanism. In the former case, the proton transfer can be described by a pH dependent equilibrium between the protonated and deprotonated O3', where the activated species forms a covalent bond with αP of the dNTP and thus extends the primer DNA stand by one nucleotide. In the latter case, the pKa values of both the donor (primer O3') and the acceptor group (Asp256) are modulated by the catalytic Mg^{2+} . This results in the proton being transferred to the active site aspartic acid residue (Asp256) prior to it being transferred to bulk solvent.

The experimental data presented here supports a role for the carboxylate group of Asp256 in the deprotonation of the 3'-OH during catalysis and suggests a key stabilizing role for Arg254. This is in agreement with quantum mechanical/molecular mechanical calculations indicating that the O3' proton transfers to the OD2 oxygen of Asp256, which serves as a general base upon activation (127). Additionally, these computational studies suggested the critical role of Asp256 (OD2) is facilitated by a stabilizing salt bridge interaction between Asp256 (OD1) and the nearby Arg254. This is consistent with an

experimental study that showed mutation of the homologous Arg254 residue in rat pol β to Ala decreases the k_{cat} from 51 to 1 min^{-1} (128). In a mutant of human pol β (D256E), a water molecule replaces OD2 of Asp256 and coordinates the catalytic metal (120). In contrast to the wild-type scenario, quantum calculations show this water is not involved in charge transfer to the catalytic metal. Additionally, the D256E pol β variant exhibited a three order of magnitude decrease in activity, and the structure demonstrates Arg254 repositions into a conformation where it does not interact with D256E (120). Thus, Arg254 appears to play a critical role in positioning and stabilizing the carboxylate of Asp256. Our experiments also perturbed the nucleotidyl transfer reaction, but by altering the DNA substrate as opposed to using a variant enzyme. Experimental data presented here, and previously reported by others, suggests Asp256 is likely the proton acceptor in the nucleotidyl transferase reaction by pol β with Arg254 playing a key role in stabilizing Asp256 through a salt bridge interaction.

2.6.4. Broader implications for 8-oxo-dG at primer termini

It was unexpected for the extension from the mutagenic base to be favored, as it potentially augments the ability of the lesion to become hidden within the genome in its mutagenic form. Alternatively, in the case of 8-oxo-dG:dC, rearrangements of key residues slow down catalysis and the polymerase 'pauses' on the DNA. This could potentially serve as a signal to other repair enzymes. The insertion of 8-oxo-dG opposite dC, which would occur directly prior to the extension, is also catalytically disfavored relative to dA. This would further delay the polymerase on the DNA in response to the lesion. Similarly, this contrast between mutagenic and non-mutagenic extension was observed during extended soaks in which 8-oxo-dG:dC, but not 8-oxo-dG:dA, at the

primer terminus results in the reopening of the enzyme post-catalysis. This is in contrast to the correct insertion of a dNTP with a non-damaged primer terminus where pol β remains in the closed conformation upon extended soaks (51). 8-oxo-dG:dC at the primer terminus promotes instability by exposing the cytotoxic nicked DNA repair intermediate, similarly to the insertion of 8-oxo-dGTP or incorrect insertion (16,51). Together, these results indicate the mutagenic 8-oxo-dG:dA base pair is catalytically favored during DNA replication and repair, underscoring the danger this common oxidative lesion poses to genome stability.

While the results presented here utilized pol β and a 1-nt gapped DNA substrate, the contacts and active site changes are likely applicable to other DNA polymerases. This is because the changes observed during extension from 8-oxo-dG are DNA centric, arising from the clash between O8 and the phosphate backbone, which would need accommodation by any polymerase's active site. The backbone α P and 3'-OH move together and mediate the catalytic efficiency through altering the turnover rate. A phylogenetic analysis of DNA polymerase X-family members, of which pol β is a member, shows active site residues are conserved among many members. Specifically, Asp256 is highly conserved among X-family members (129). In pol λ , salt bridges between Arg488 (Arg254 in pol β) and Asp490 (Asp256 in pol β) are observed in the X-ray structures with an average distance of 2.8 Å. Therefore, it is likely that Arg488 plays an analogous stabilizing role in the nucleotidyl transfer reactions of pol β , as proposed based on ab initio quantum mechanical/molecular mechanical methods (127,130). By performing MSA for the three X-family closed ternary complexes pol β (PDB 2FMS), pol λ (PDB 2PFO), and pol μ (PDB 2IHM) it was shown that two arginine residues likely contribute to

substantial stabilization of the active site: Arg254 and Arg183 (pol β), Arg488 and Arg420 (pol λ) and Arg418 and Arg323 (pol μ). Therefore, the shift in the phosphate backbone arising from O8 will likely alter these X-family polymerases during DNA replication and repair.

It remains to be elucidated how 8-oxo-dG at the primer termini is handled by other polymerase families (A, B and Y). Outside of this study, the ability of polymerases to extend from DNA damage and the consequences of this extension have not been assiduously investigated. However, 8-oxo-dG regulation of telomerase activity was recently examined. In this study, it was uncovered that 8-oxo-dGTP insertion by telomerase terminates the chain, thereby preventing telomere restoration and promoting cell death (131). As the effects of 8-oxo-dG on the primer terminus presented here are DNA centric, it is likely that the clash observed between O8 and α P in the 8-oxo-dG:dC structures also occurs in the telomerase active site. The chain termination by 8-oxo-dG in telomerase could potentially be the result of an analogous clash, which alters key active site residues, thus providing a possible explanation for the fascinating result.

Chapter 3: β -C-Fapy•dGTP insertion hinders the open-closed DNA polymerase transition

Previously published as an open access article and is reprinted here with adaptations and with permission from Oxford University Press. Mallory R. Smith, David D. Shock, William A. Beard, Marc M. Greenberg, Bret D. Freudenthal, Samuel H. Wilson, A guardian residue hinders insertion of a Fapy•dGTP analog by modulating the open-closed DNA polymerase transition, *Nucleic Acids Research*, Volume 47, Issue 6, 08 April 2019, Pages 3197–3207, <https://doi.org/10.1093/nar/qkz002>.

This chapter includes contributions by Drs. David Shock, William Beard, Marc Greenberg, and Bret Freudenthal. Dr. Shock performed the kinetic experiments, Dr. Greenberg synthesized the nucleotide analog, and Dr. Freudenthal collected preliminary structural datasets (some of which I re-collected). All other contributions, such as data analysis, structure collection, structure refinement and deposition, and manuscript preparation were my own.

Fapy•dG (**Section 1.3.2**) is a frequent DNA lesion. However, the field is still unsure if Fapy•dG contributes significantly to the mutagenic load of the cell. The few studies performed with Fapy•dG and its analogs report conflicting rates of mutagenicity. Therefore, we utilized our model polymerase (**Section 1.2.1**), pol β , and a stable nucleotide analog of Fapy•dGTP, β -C-Fapy•dGTP, opposite either a dC (non-mutagenic) or dA (mutagenic base) to evaluate whether Fapy•dGTP was mutagenic as an incoming nucleotide lesion. We hypothesized that β -C-Fapy•dGTP would be slightly mutagenic and use similar base pairing properties as 8-oxo-dG based on the similar properties of the adducted O8 and ability to adopt a *syn*- conformation. However, we found that β -C-Fapy•dGTP preferred non-mutagenic insertion, retained a *syn*- conformation opposite both templating bases, and polymerase closure was greatly impaired by the flexibility of this lesion. These results suggest that Fapy•dGTP may not be as strongly mutagenic as an incoming base in comparison to 8-oxo-dGTP and implies that the Fapy•dGTP nucleotide does not contribute strongly to the mutagenic load of a cell. Future studies using natural Fapy•dGTP are needed to confirm our findings.

3.1 Abstract

4, 6-Diamino-5-formamidopyrimidine (Fapy•dG) is an abundant form of oxidative DNA damage that is mutagenic and contributes to the pathogenesis of human disease. When Fapy•dG is in its nucleotide triphosphate form, Fapy•dGTP, it is inefficiently cleansed from

the nucleotide pool by the responsible enzyme in *E. coli* MutT and its mammalian homolog MTH1. Therefore, under oxidative stress conditions, Fapy•dGTP could become a pro-mutagenic substrate for insertion into the genome by DNA polymerases. Here, we evaluated insertion kinetics and high-resolution ternary complex crystal structures of a configurationally stable Fapy•dGTP analog, β -C-Fapy•dGTP, with DNA polymerase β . The crystallographic snapshots and kinetic data indicate that binding of β -C-Fapy•dGTP impedes enzyme closure, thus hindering insertion. The structures reveal that an active site residue, Asp276, positions β -C-Fapy•dGTP so that it distorts the geometry of critical catalytic atoms. Removal of this guardian side chain permits enzyme closure and increases the efficiency of β -C-Fapy•dG insertion opposite dC. These results highlight the stringent requirements necessary to achieve a closed DNA polymerase active site poised for efficient nucleotide incorporation and illustrate how DNA polymerase β has evolved to hinder Fapy•dGTP insertion.

3.2 Introduction

During oxidative stress, oxygen and nitrogen radicals accumulate and damage DNA bases in duplex DNA and the nucleotide pool. These damaged DNA lesions promote cytotoxicity and/or mutagenesis, leading to adverse human health outcomes (4,132,133). Understanding how damaged nucleotides are inserted into the genome is imperative for improving cancer therapies that utilize DNA damaging mechanisms, such as radiation therapy, nucleotide analog inhibitors, and MTH1 inhibitors (19,134-138). Under endogenous and exogenous oxidative stress, guanine (dG) in both duplex DNA and the nucleotide pool (dGTP) undergoes increased damage in comparison to other DNA bases

because of its oxidation potential (10). Of the possible damaged guanine intermediates, the C8-OH-adduct radical generates two of the most prominent DNA lesions, 8-oxo-7,8-dihydro-2'-deoxyguanosine (8-oxo-dG) and 4,6-diamino-5-formamidopyrimidine (Fapy•dG) (139,140). 8-oxo-dG results from oxidation of the C8-OH intermediate, while Fapy•dG is formed via opening of the imidazole ring and subsequent reduction (Figure 1.4) (84). The formation of these two species are therefore in competition with each other, with both being prevalent DNA lesions found in cellular DNA (75-77,139). The biological importance of the lesions is highlighted by the elaborate cellular defense mechanisms that have evolved to remove these lesions from DNA and the nucleotide pool (141).

Fapy•dG poses a threat to genomic integrity through mismatched base pairing, which can cause transversions and transitions in the genome if not removed. The mutagenic profile of Fapy•dG during replication bypass is that Fapy•dG predominantly promotes G to T transversion mutations, akin to 8-oxo-dG, but also promotes G to A transitions (79,80,89). Despite the lesion's mutagenicity and the levels at which it is formed, our mechanistic understanding of Fapy•dG mediated mutagenesis lags behind that of 8-oxo-dG due to challenges generating suitable substrates containing the Fapy•dG lesion (142). Although Fapy•dG is believed to exist predominantly as the β -anomer in duplex DNA, monomeric formamidopyrimidines undergo facile epimerization (86,88,142). Therefore, obtaining a pure sample containing a single Fapy•dG anomer for biochemical assays has been challenging. To bypass these prohibitive synthetic challenges, configurationally stable analogs of Fapy•dG have been used to elucidate biochemical mechanisms that confer the biological consequences of this prevalent DNA lesion (81,82,94,143). Accordingly, we utilized a similar approach to generate a nucleotide

Fapy•dGTP analog, β -C-Fapy•dGTP, in which the glycosidic nitrogen is replaced with a methylene group to preserve the biologically relevant β -anomer (Figure 3.1). For simplicity, the analog will be referred to as Fapy•dGTP.

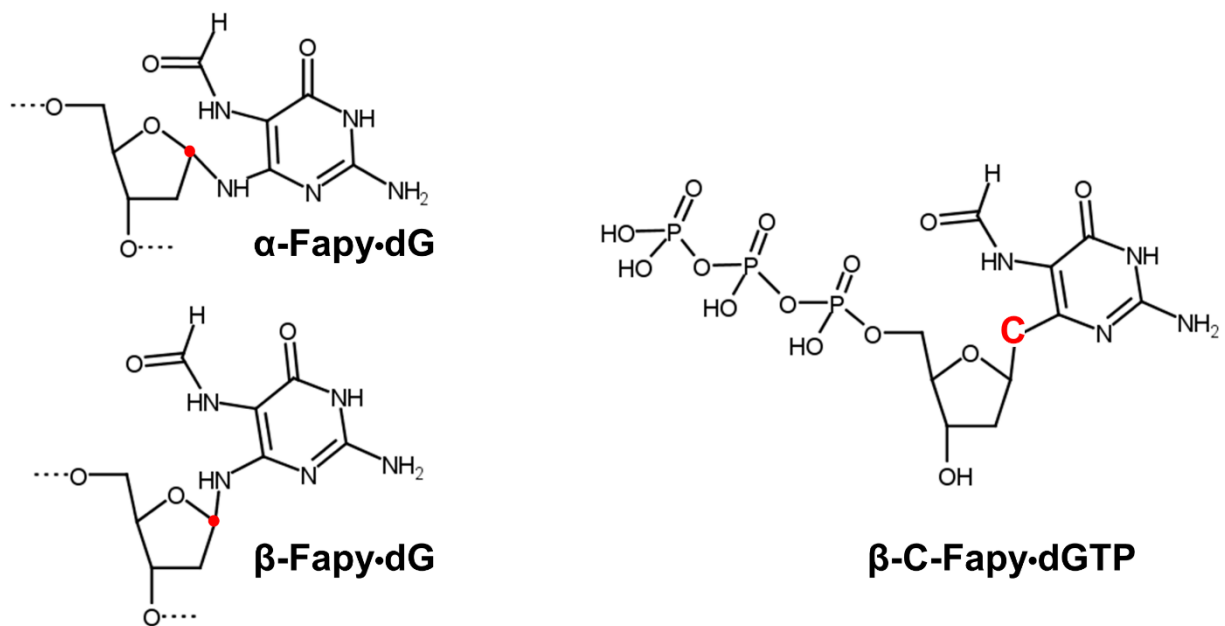


Figure 3.1 Chemical structures of Fapy•dG α - and β -anomers and Fapy•dG Analog, β -C-Fapy•dGTP.
 Figure adapted from (81).

Previous studies have elicited that Fapy•dG bypass in prokaryotes is weakly mutagenic (81,89,91,143). In contrast, it is highly mutagenic in eukaryotes, even more so than 8-oxo-dG in some sequence contexts (79,80). 8-oxo-dG is frequently thought of as a significant, highly mutagenic DNA lesion. The contrasting results in different species, and especially the mutagenicity compared to 8-oxo-dG in eukaryotes emphasizes the significance of understanding Fapy•dG-induced effects at the molecular level. Previous structural studies of templating Fapy•dG bypass revealed that Watson-Crick base pairing and base tautomerization confer mutagenicity (82). Here, we expand on the molecular understanding of Fapy•dG mutagenesis by examining the nucleotide form of Fapy•dG. Importantly, Fapy•dGTP is poorly cleansed from the nucleotide pool by the sanitizing enzyme MutT in *E. coli* and its mammalian counterpart MTH1 (81,144). These enzymes are responsible for removing oxidized nucleotides in the nucleotide pool by hydrolyzing the triphosphate form and generating the monophosphate form (145); this effectively prevents oxidized nucleotides from being inserted in the genome thereby deterring mutagenesis. However, since Fapy•dGTP is not efficiently hydrolyzed by MutT/MTH1, it could accumulate and be utilized by DNA polymerases during DNA replication and repair. To gain mechanistic insight into Fapy•dGTP insertion, we report high resolution pre-catalytic ternary substrate crystallographic structures of Fapy•dGTP opposite templating adenine (dA) or cytosine (dC), as well as kinetic characterization for the insertion reaction of Fapy•dGTP using the model mammalian DNA polymerase (pol) β . These results provide mechanistic molecular insight into how Fapy•dGMP incorporation into DNA is deterred by DNA polymerases.

3.3 Methods

3.3.1. Expression and purification and crystallization of DNA Polymerase β D276G

Human pol β was overexpressed in *E. coli* and purified as previously described (146). Pol β was incubated with prepared single-nucleotide gapped DNA (1:1.2) containing either a templating dA or dC. To form binary complex crystals, they were grown in a solution containing 50 mM imidazole, pH 8.0, 13–19% PEG3350 and 350 mM sodium acetate as previously described (147). Binary pol β :DNA complex crystals were then soaked in a cryosolution containing 25% ethylene glycol, 50 mM imidazole, pH 7.5, 19% PEG3350 and 70 mM sodium acetate, 3 mM β -C-Fapy•dGTP (prepared as previously described (81)) and 50 mM CaCl₂ for 1 h. This resulted in “ground state” ternary pol β :DNA: β -C-Fapy•dGTP crystals for X-ray crystallography.

3.3.2. DNA sequences and oligonucleotide annealing

The following DNA sequences were used to generate the 16-mer DNA duplexes used in crystallization studies (the templating base is underlined): template, 5'-CCG ACX GCG CAT CAG C-3', where X represents the coding templating base (dA or dC); primer, 5'-GCT GAT GCG C-3'; downstream, 5'-pGTC GG-3'. Each oligonucleotide was suspended in 10 mM Tris–HCl, pH 7.4 and 1 mM EDTA, and the concentration was determined from their ultraviolet absorbance at 260 nm. DNA substrates were prepared by annealing the three purified oligonucleotides. The annealing reactions were performed by incubating a solution of primer with downstream and template oligonucleotides (1:1.2:1.2 molar ratio, respectively) at 95°C for 5 min, followed by 65°C for 30 min, and finally cooling 1°C min⁻¹ to 10°C in a PCR thermocycler.

For use in our kinetic experiments, a 34-mer oligonucleotide DNA substrate containing a single nucleotide gap was prepared by annealing 3 gel-purified oligonucleotides to create a single-nucleotide gap at position 16. Each oligonucleotide was resuspended in 10 mM Tris-HCl, pH 7.4, and 1 mM EDTA, and the concentration determined from their UV absorbance at 260 nm. The annealing reactions were carried out by incubating a solution of 10 μ M primer with 12 μ M each of downstream and template oligonucleotides at 90–100 °C for 3 min followed by 30 min at 65 °C, and then slow cooling to room temperature. The sequences of the gapped DNA substrate were primer, 5'-CTG CAG CTG ATG CGC-3', downstream, 5'-GTA CGG ATC CCC GGG TAC-3', and template, 3'-GAC GTC GAC TAC GCG XCA TGC CTA GGG GCC CAT G-5' where the X represents the coding templating base (dA or dC).

3.3.4. Crystallographic data collection and refinement

Fapy•dGTP insertion opposite dC with either wild-type (WT) or D276G pol β (PDB accession numbers: 6DIA.pdb and 6DIC.pdb, respectively) were collected at 100 °K on an SATURN92 CCD (charge-coupled device) detector system mounted on a MiraMax-007HF rotating anode generator at a wavelength of 1.54 Å. Fapy•dGTP insertion opposite dA with either WT or D276G pol β (6MR7.pdb and 6MR8.pdb, respectively) were collected on a Rigaku MicroMax-007 HF rotating anode diffractometer equipped with a Dectris Pilatus3R 200K-A detector system at a wavelength of 1.54 Å. Data were processed and scaled using the HKL3000R software package (148). Initial models were determined using the PHENIX single one-component interface molecular replacement program by searching as a whole with the previously determined open binary (3ISB.pdb) or closed

ternary (2FMS.pdb) structures of pol β bound to DNA with all ligands removed. The R_{free} flags were taken from the starting model 2FMS.pdb for 6DIC.pdb. R_{free} flags were generated randomly for the three open-ternary complexes, 6DIA.pdb, 6MR7.pdb, 6MR8.pdb, due to a lack of isomorphism with the open binary model used for molecular replacement (3ISB.pdb). Simulated annealing was performed to ensure no model bias. Refinement was performed using PHENIX and model building using Coot (116,117). The metal ligand coordination restraints were generated by ReadySet (PHENIX). The figures were prepared in PyMOL (Schrödinger LLC) and density maps were generated as polder maps within the phenix suite (149,150). Ramachandran analysis determined 100% of non-glycine residues lie in the allowed regions and at least 97% in favored regions (Table 4).

Table 4. Data collection and refinement statistics of ternary polymerase β :DNA co-complexes with incoming β -C-Fapy•dGTP.

	Wild-type Templating Cy	Wild-type Templating Ad	D276G Templating Cy	D276G Templating Ad
Data collection				
Space group	P2 ₁	P2 ₁	P2 ₁	P2 ₁
Cell dimensions				
<i>a, b, c</i> (Å)	54.9,80.6,55.3	55.0,79.8,55.5	50.6,79.6,55.6	55.0, 80.3, 55.6
α, β, γ (°)	90,109.9,90	90,110.6,90	90,107.5,90	90, 110.5, 90
Resolution (Å)	22.57-1.97	25.00-2.15	20.74-1.99	25.00-1.90
<i>R</i> _{sym} or <i>R</i> _{merge} ^a (%)	4.9 (55.7)	7.5 (41.5)	4.7 (36.8)	7.6 (83.1)
<i>R</i> _{pim} ^a	0.013 (0.451)	0.033 (0.287)	0.023 (0.330)	0.033 (0.605)
<i>CC</i> _{1/2} ^a	0.999 (0.621)	0.995 (0.808)	0.997 (0.670)	0.998 (0.893)
<i>I</i> / σ <i>I</i> ^a	21.2 (2)	13.1 (2.5)	17.5 (2.4)	16.6 (1.2)
Completeness ^a (%)	99.9 (100)	99.1 (97.9)	96.4 (89.8)	98.8 (94.6)
Redundancy ^a	5.9 (3.4)	3.0 (2.8)	3.4 (2.3)	4.3 (2.5)
Refinement				
Resolution (Å)	1.97	2.15	1.99	1.90
No. reflections	61239	43797	27588	65469
<i>R</i> _{work} / <i>R</i> _{free}	0.20/0.25	0.19/0.25	0.18/0.23	0.20/0.24
No. atoms	3616	3532	3718	3605
Protein	2574	2529	2643	2548
DNA	629	631	629	631
Water	375	286	390	372
B-factors (Å ²)				
Protein	32.8	35.8	27.4	29.9
DNA/Fapy	29.5/37.4	33.3/41.7	33.8/18.3	28.1/45.2
Water	36.0	40.0	33.5	34.2
R.m.s deviations				
Bond length (Å)	0.008	0.011	0.008	0.010
Bond angles (°)	0.988	1.140	0.979	1.088
Ramachandran plot:				
Outliers (%)	0.00	0.00	0.00	0.00
Allowed (%)	1.56	2.83	2.47	2.55
Favored (%)	98.44	97.17	97.53	97.45
PDB ID	6DIA	6MR7	6DIC	6MR8

3.3.5. Kinetic characterization using single-turnover kinetics

Catalytic efficiencies (k_{pol}/K_d) for single-nucleotide gap filling reactions were determined by single-turnover analysis (*i.e.*, enzyme \gg DNA). At least 7 time points were gathered for each single-exponential time course determined with at least three sub-saturating concentrations of β -C-Fapy•dGTP. The standard reaction mixture contained 50 mM Tris-HCl, pH 7.4 (37 °C), 40 mM KCl, 10 mM MgCl₂, 1 mM dithiothreitol, 100 μ g/ml bovine serum albumin, 10% glycerol, 100 nM single-nucleotide gapped DNA, and 500 nM enzyme. Reactions were stopped with 150 mM EDTA and mixed with formamide dye. The substrates and products were separated on 16% denaturing (8 M urea) polyacrylamide gels. Since a 6-carboxyfluorescein 5'-labeled primer was used in these assays, the products were quantified using the GE Typhoon phosphorimager in fluorescence mode. Because sub-saturating concentrations of β -C-Fapy•dGTP were used (5–200 μ M, dependent on the templating base), the data were fitted to an alternate form of the Michaelis equation to extract apparent catalytic efficiencies (k_{pol}/K_d): $k_{\text{obs}} = ((k_{\text{pol}}/K_d) * S) / (1 + (S/K_d))$, where S refers to the concentration of β -C-Fapy•dGTP ([Figure 3.2](#)).

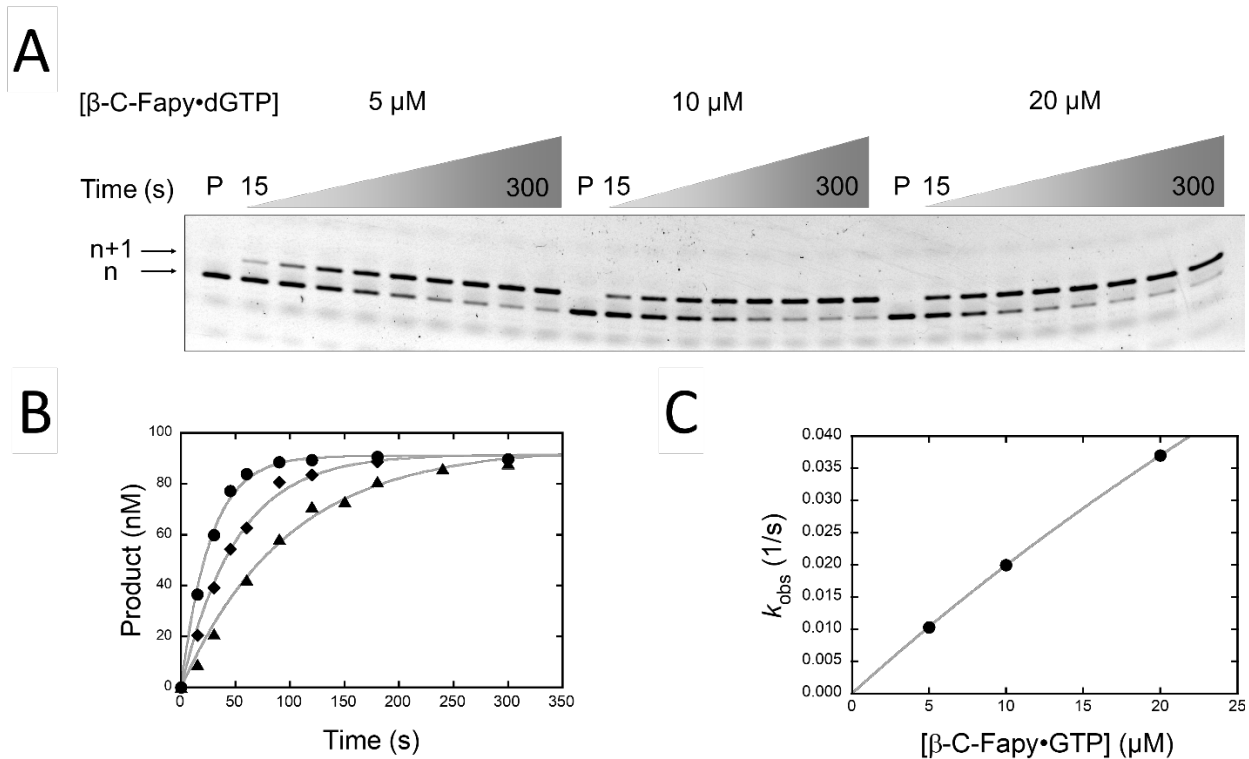


Figure 3.2 Single-turnover analysis for gap filling insertion with β -C-Fapy•dGTP opposite cytosine.

A) Image of a representative sequencing gel showing the time dependence (15–300 s) of single nucleotide gap filling by the D276G mutant of pol β in the presence of 5, 10 and 20 μ M β -C-Fapy•dGTP opposite cytosine. In this assay, the 5'-labeled primer (15-mer, n) can be extended one nucleotide (16-mer, n+1). The lanes including primer only (P) are indicated. B) D276G pol β dependent single-nucleotide gap filling DNA synthesis with 5 μ M (\blacktriangle), 10 μ M (\blacklozenge), and 20 μ M (\bullet) β -C-Fapy•dGTP. Time courses were fit to a single exponential (gray lines). C) A secondary plot of the β -C-Fapy•dGTP concentration dependence of the observed first-order rate constants (k_{obs}). These data were fit to a modified hyperbola (gray line) to extract k_{pol}/K_d .

3.4 Results

3.4.1. β -C-Fapy•dGTP is inefficiently inserted by DNA polymerase β

The catalytic efficiencies for insertion of Fapy•dGTP opposite dC and dA were determined by single-turnover kinetic analysis ([Figure 3.3](#)). These results help contextualize the structural information described below. In comparison to undamaged dGTP opposite dC, the insertion efficiency of Fapy•dGTP is dramatically lower (nearly 4-orders of magnitude), and Fapy•dGTP insertion opposite dA is even less efficient. Consequently, insertion across from dA is only 82- fold less efficient than dC, resulting in a ~750-fold reduction in discrimination compared to dGTP. Nevertheless, pol β is effective in excluding a Fapy•dGTP analog under circumstances where the oxidatively-generated nucleotide has accumulated in the nucleotide pool. The reduction in catalytic efficiency for this substrate is likely a result of unique and unfavorable binding within the polymerase active site as highlighted by the inability to saturate the polymerase with reasonable (<20 μ M) concentrations of oxidized nucleotide ([Figure 3.2](#)). To provide molecular insight into the origin of these observations, we turned to X-ray crystallography.

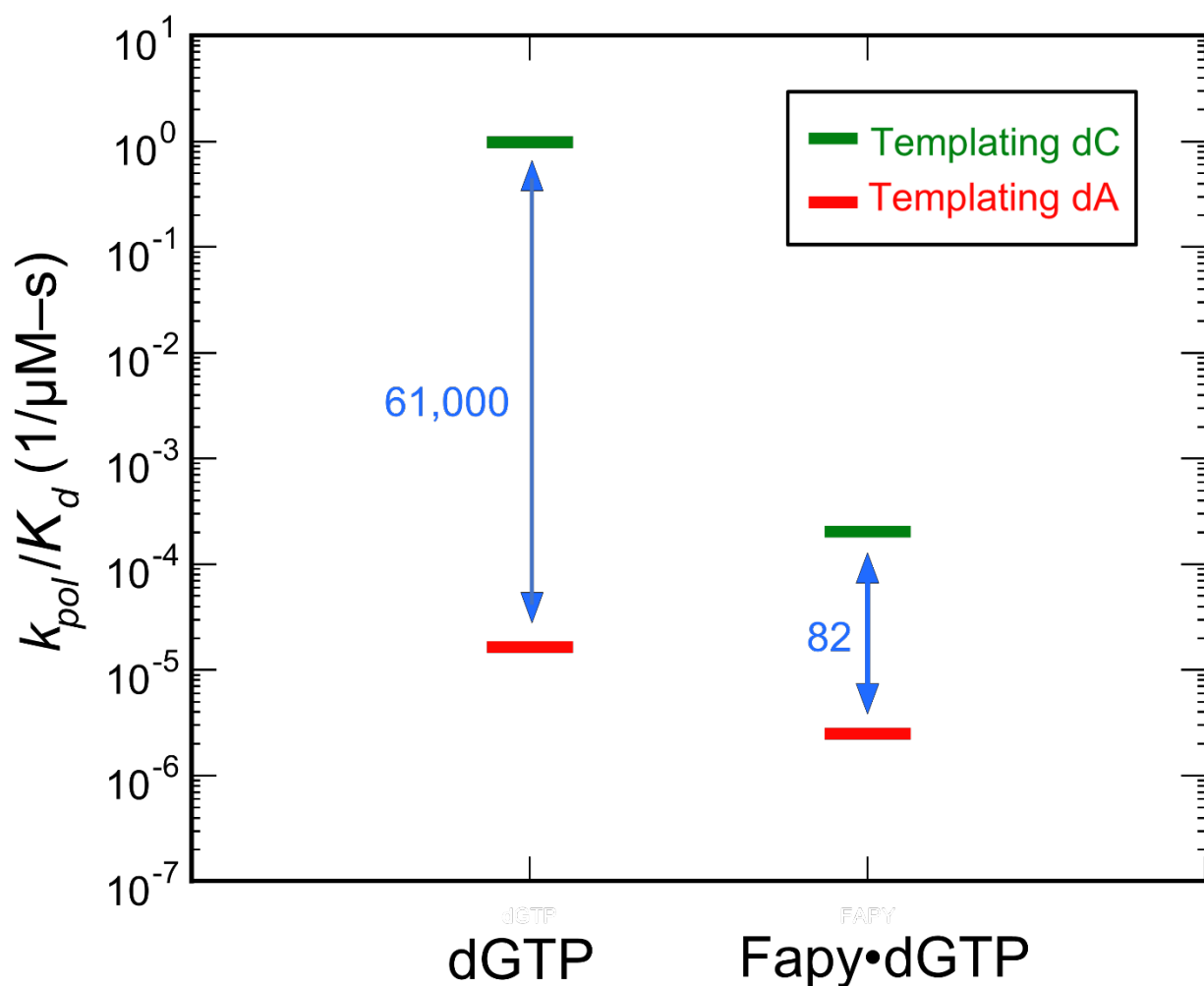


Figure 3.3 Discrimination plot for insertion of β -C-Fapy•dGTP.

The catalytic efficiencies (k_{pol}/K_d) for insertion of β -C-Fapy•dGTP opposite dC (green) or dA (red) for wild-type (WT) pol β are shown. The distance between the respective catalytic efficiencies is a measure of discrimination/fidelity. Each horizontal short bar represents the mean of duplicate independent determinations. The insertion efficiencies for dGTP opposite dC and dA were taken from (16).

3.4.2. *Fapy•dGTP* adopts an altered nucleotide binding position during insertion opposite dC and dA

The general enzymatic steps of DNA polymerization by pol β are structurally and biochemically characterized and provide a comparison for evaluating *Fapy•dGTP* insertion. Upon binding duplex DNA, pol β assumes an “open” conformation. Selection of the correct nucleotide occurs via an induced fit mechanism, requiring closure of the N-subdomain (fingers of replicative polymerases) resulting in proper alignment of active site residues with duplex DNA and incoming nucleotide, as well as proper coordination of active site metals that hasten catalysis. This subdomain repositioning also occurs with replicative polymerases, making pol β an applicable crystallographic model for evaluating nucleotide insertion. The resultant conformational rearrangement is termed the ternary-closed conformation. Catalysis occurs via a two metal mechanism, where nucleophilic attack by the oxyanion of O3' of the primer terminus on α -phosphate (α P) of the incoming nucleotide results in incorporation of a deoxynucleoside monophosphate and release of pyrophosphate (38). Here, we evaluated the alignment of the catalytic atoms within pre-catalytic *Fapy•dGTP* insertion complexes containing either a templating dC or dA to provide molecular insight into the insertion of *Fapy•dGTP*.

To observe the pre-catalytic complex of non-mutagenic insertion of *Fapy•dGTP* by pol β , we crystallized a binary 1-nucleotide gapped DNA:pol β complex with templating dC. Crystals were placed in a cryoprotectant solution containing CaCl_2 and *Fapy•dGTP*, whereby Ca^{2+} prevents catalysis, but allows for nucleotide binding (16,151). The resulting complex diffracted to 1.97 Å, [Table 4](#). Pol β retains an open conformation, and *Fapy•dGTP* is located in a stable but distorted position within the nucleotide binding

pocket ([Figure 3.4](#)). The open ternary conformation is here-on referred to as ternary-open, as opposed to the canonical ternary-closed conformation. Within the nucleotide binding site, calcium binding is observed in the nucleotide metal site and absent in the catalytic metal site. Despite the absence of a catalytic metal, the O3' (primer terminus) and α P (Fapy•dGTP) are 3.8 Å apart ([Figure 3.4A](#)), which is similar to the 3.7 Å distance observed in the undamaged pre-catalytic pol β :DNA:dGTP:Ca²⁺ complex (16). The Watson-Crick edge of Fapy•dGTP faces upstream with its pyrimidine ring in the DNA minor groove perpendicular to the primer terminus base ([Figure 3.4B](#)). The formamide carbonyl oxygen (O8) resulting from the broken imidazole ring interacts weakly with the templating dC (3.3 Å, [Figure 3.4C](#)). The Fapy•dG base is stabilized by several protein contacts and rotated about its glycosidic bond into a *syn*-conformation. The N-helix residue Asp276 is within hydrogen bonding distance of the O3' of Fapy•dGTP (2.6 Å), while Arg258 forms stabilizing contacts with the analog through hydrogen bonds with N1 and O6 of the Watson-Crick edge (3.0 and 3.2 Å, respectively; [Figure 3.4C](#)). We also observed a Ca²⁺ ion coordinating the O2 of the templating dC. The presence of this metal is likely dependent on the identity of the templating base and the open polymerase conformation that accommodates the metal ion within the minor groove of pol β . The altered position of Fapy•dGTP observed in this open complex provides structural justification for previous assertions that damaged or incorrect nucleotides deter incorporation by stabilizing an unfavorable open conformation (152,153).

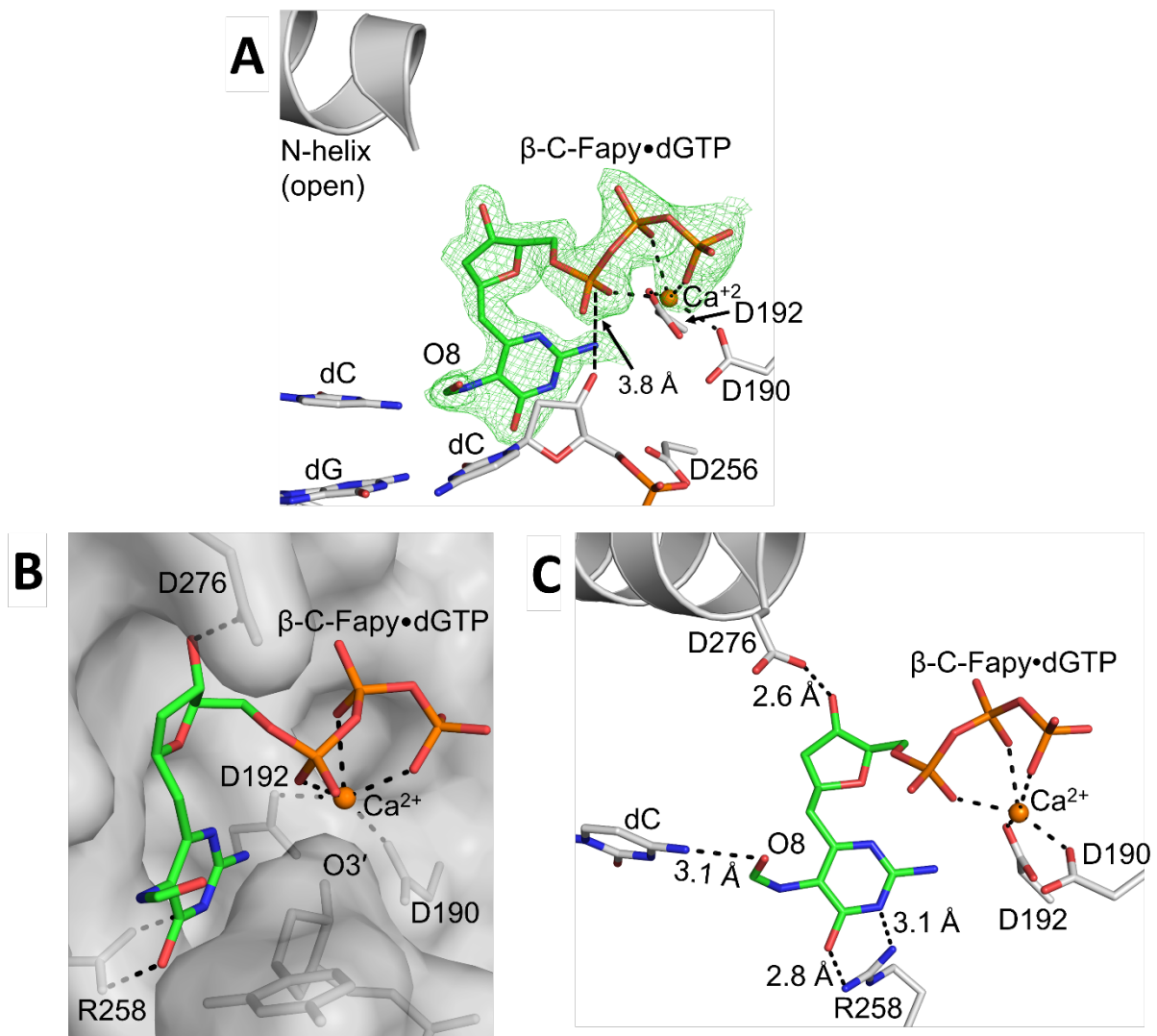


Figure 3.4 Pre-catalytic non-mutagenic pol β :DNA: β -C-Fapy•dGTP complex.

A) Pre-catalytic ternary-open complex of wild-type pol β (gray) with β -C-Fapy•dGTP (green sticks) bound across from dC; Ca^{2+} ions are shown in orange. A polder map (green mesh) contoured at 3.0σ is shown for the incoming β -C-Fapy•dGTP. B) β -C-Fapy•dGTP is shown as green sticks with the nucleotide binding pocket in surface representation looking into the minor groove behind the primer terminus (O3'). The Watson-Crick edge (W-C edge) is indicated. C) Active site residues (gray sticks) that contact β -C-Fapy•dGTP (green) or Ca^{2+} (orange) are shown. Potential hydrogen bonds are shown as black dashed lines.

Because Fapy•dG has been reported to generate G to T transversion mutations, it is assumed that Fapy•dGTP insertion occurs opposite templating dA. To evaluate the mechanism of this type of insertion of Fapy•dGTP, we crystallized a binary DNA/pol β complex with templating dA in a 1-nucleotide gapped DNA substrate and soaked in CaCl₂ and Fapy•dGTP to generate a pre-catalytic ternary complex. The crystal complex diffracted to 2.05 Å, [Table 4](#). Similar to what was observed with insertion opposite dC, pol β adopts a ternary-open conformation and Fapy•dGTP is positioned with the Watson-Crick edge in the minor groove facing upstream ([Figure 3.5A](#)). The distance between the O3' of the primer terminus and α P of Fapy•dGTP increased subtly from 3.8 Å (opposite dC) to 4.1 Å (opposite dA). Additionally, the formamide group of Fapy•dG adopted multiple conformations opposite dA. Among the two conformations, one conformation is positioned within hydrogen bonding distance to N1 of dA via the formamide carbon (3.1 Å) and the formamide oxygen (3.2 Å), [Figure 3.5B](#). In contrast, the formamide O8 interacts weakly with N4 of the templating dC (3.3 Å) ([Figure 3.5C](#)). When both the template dA and dC structures are overlaid the result is nearly identical ternary-open complexes ([Figure 3.5C](#)). However, slight changes were observed in the contacts between Fapy•dGTP and residues Arg258, Lys234, and the templating base ([Figure 3.5D](#)). In the templating dA complex, Arg258 adopts a different rotamer such that only NH2 comes within hydrogen bonding distance of O6 of the Fapy•dG Watson-Crick edge (2.6 Å). In the template dC complex, these two nitrogens of Arg258, NH1 and NH2, contact N1 (3.0 Å) and O6 (3.2 Å), respectively ([Figure 3.5D](#)). Lastly, a contact between Lys234 and O6 of the Fapy•dG base (3.2 Å) in the templating dC structure is not observed with templating dA.

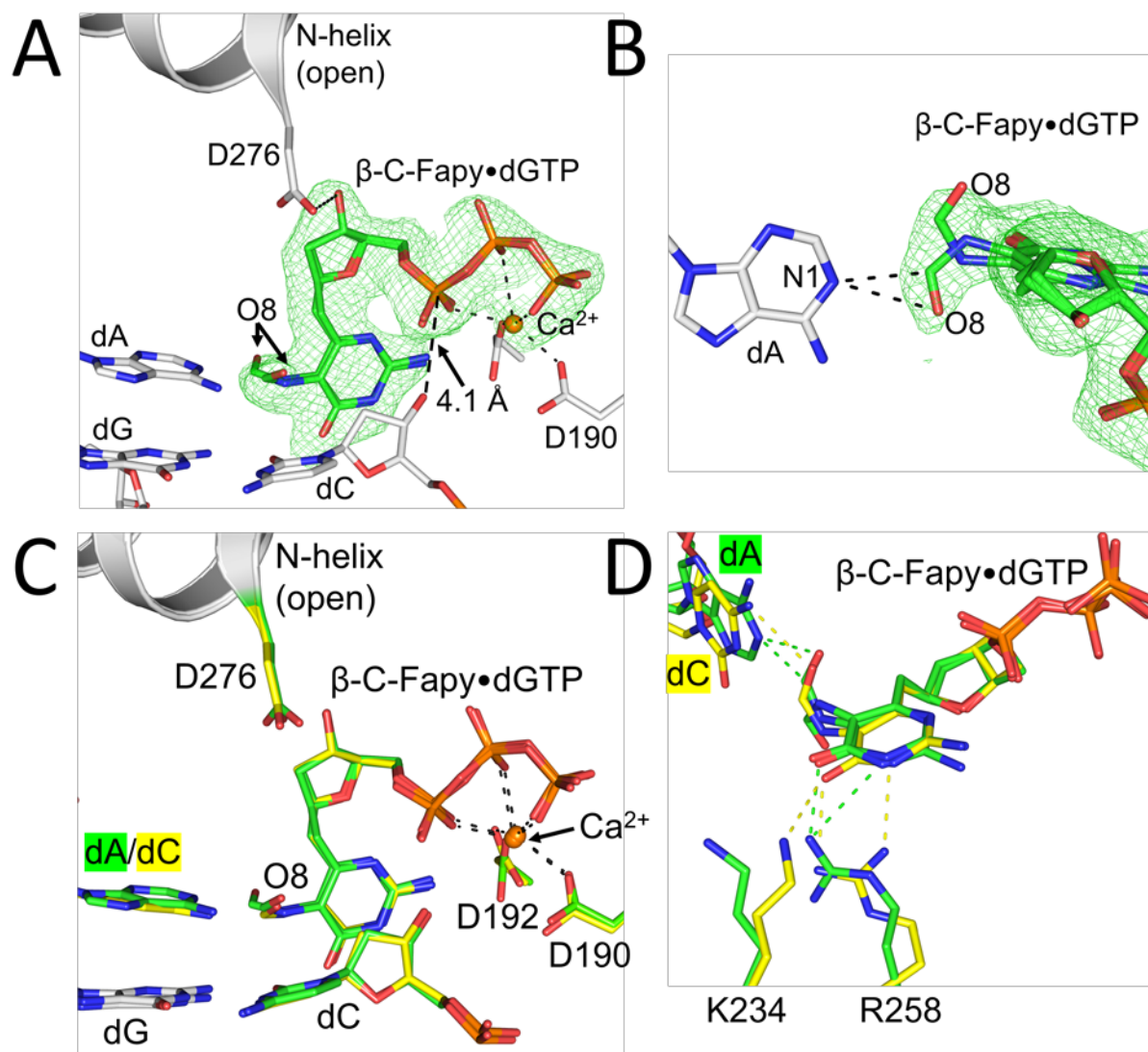


Figure 3.5 Pre-catalytic mutagenic pol β :DNA: β -C-Fapy•dGTP complex.

A) Pre-catalytic ternary-open complex of wild-type pol β (gray) with β -C-Fapy•dGTP (green sticks) bound across from dA; Ca^{2+} ions are shown in orange. A polder map (green mesh) contoured at 3.0σ is shown for the incoming β -C-Fapy•dGTP. B) An alternate viewpoint demonstrating the two formamide conformations of β -C-Fapy•dGTP (green sticks) opposite adenine (gray sticks) with the polder map contoured to 3.0σ (green mesh). C) An overlay between the pre-catalytic ternary-open structures of β -C-Fapy•dGTP across from dA (green) or dC (yellow). Key residues are shown as gray sticks and the N-helix in gray cartoon. D) An overlay between the pre-catalytic ternary-open structures of β -C-Fapy•dGTP across from dA (green) or dC (yellow) highlighting altered amino acids in stick format and potential hydrogen bonds as dashed lines.

3.4.3. *Pol β active site residue (Asp276) impedes insertion by hindering polymerase closure*

As revealed in the structures shown in [Figure 3.4](#) and [Figure 3.5](#), the Fapy•dG base and sugar are stabilized by contacts with Asp276 in a fashion that hinders formation of the closed conformation and this, in turn, deters catalytic metal binding and chemistry. We chose to evaluate the significance of these distorting contacts by changing this residue to glycine, *i.e.*, yielding the D276G variant. Consistent with the structural observation, the mutant enzyme partially restored efficiency for Fapy•dGTP insertion opposite dC ([Figure 3.6](#)). In contrast, there was little effect on insertion efficiency opposite template dA ([Figure 3.6](#)). Therefore, Asp276 functionally guards against Fapy•dG insertion opposite template dC.

Both template dA and dC insertions of the Fapy•dGTP analog result in a similarly distorted position of the incoming nucleotide in the active site of wild-type (WT) pol β, and the distortion is stabilized by active site residue Asp276. To further elucidate the role of Asp276 as a “guardian” against the insertion of Fapy•dGTP opposite template dC and dA, we solved structures with the D276G pol β variant, [Figure 3.7](#). We chose to replace Asp276 with glycine in order to remove the interaction between residue Asp276 in α-helix N of pol β and the sugar moiety of Fapy•dGTP. The loss of the Asp276 side chain was confirmed via an isomorphous difference map between our D276G pol β complex (PDB accession number: 6DIC) and a WT pre-catalytic complex (PDB accession number: 2FMS) (data not shown). Notably, changes in nucleotide and templating base identity between the two structures are also easily observed.

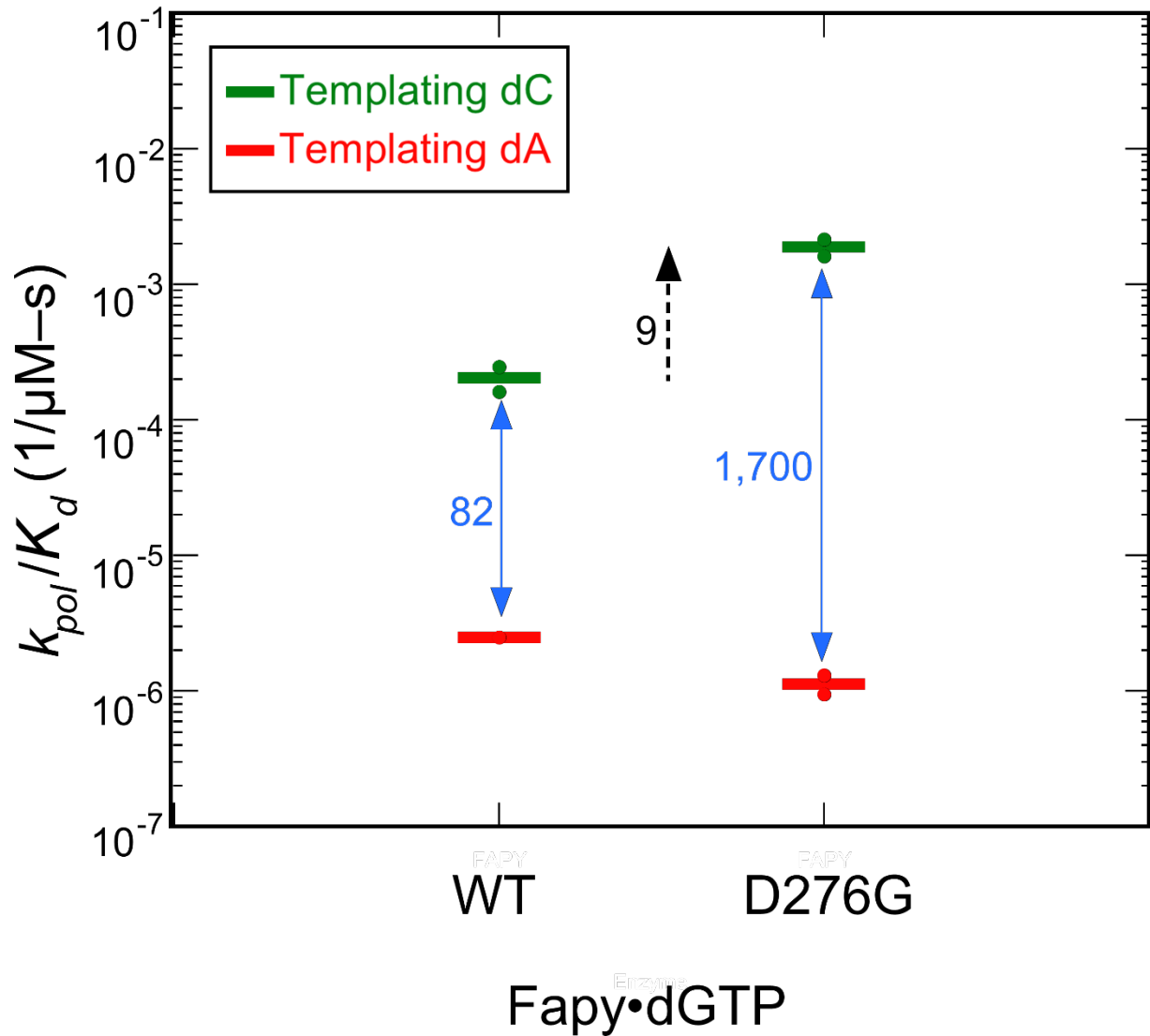


Figure 3.6 Discrimination plot for insertion of β -C-Fapy•dGTP.

The catalytic efficiency of β -C-Fapy•dGTP insertion opposite dC or dA for wild-type pol β and the mutant where Asp276 was substituted with glycine (D276G) are shown. Each horizontal short bar represents the mean of duplicate independent determinations. Additionally, the value for each determination is plotted (small solid circle) to illustrate the reproducibility of these assays.

A pre-catalytic complex of Fapy•dGTP insertion by D276G across from dC revealed that removing the aspartate side chain enables stabilization of the ternary-closed conformation ([Figure 3.7A](#)). In this structure, (*anti*) Fapy•dGTP forms a planar Watson-Crick base pair with the templating dC. Both metal binding sites are occupied and the O3' (primer terminus) and α P of the incoming damaged nucleotide are in proximity (3.7 Å, [Figure 3.7A](#)) for chemistry. The formamide group of Fapy•dG is located out of plane with the remaining pyrimidine ring, likely interacting via a weak hydrogen bond with Arg40 in one of two conformers (3.2 Å or 3.3 Å; [Figure 3.7A](#)). An overlay of an undamaged ternary-closed complex with a correct nucleotide (PDB accession number: 4UB4) ([Figure 3.7B](#)) reveals that the formamide group (O8, C8, N7) would clash with one of the γ -oxygens, C γ , and C β of the WT location of Asp276 ([Figure 3.7C](#)), suggesting that these Asp276 contacts prevent pol β closure. Furthermore, Asp276 stabilizes the open conformation through a hydrogen bond between Asp276 and the O3' of the incoming nucleotide.

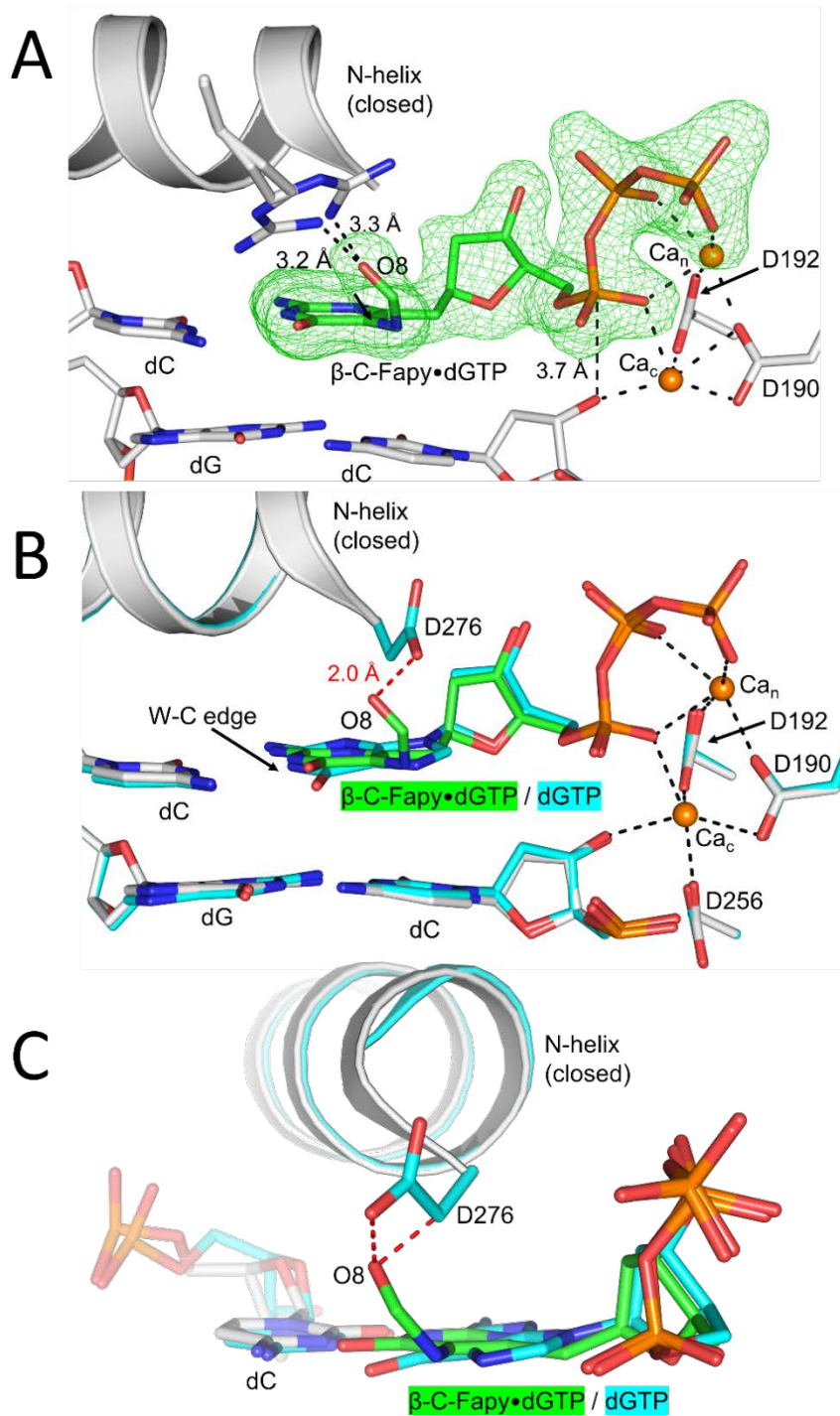


Figure 3.7 Pre-catalytic mutant (D276G) pol β non-mutagenic complex.

A) Pol β D276G mutant in a ternary-closed ground state (gray) with incoming β -C-Fapy•dGTP base (green sticks) pairing with dC in a canonical conformation. The polder map is shown as green mesh and contoured to 3.0σ . B) Overlaid is PDB ID: 4UB4 demonstrating undamaged dGTP pre-catalytic insertion (cyan). The Watson-Crick edge (W-C edge) is indicated. Potential hydrogen bonds are shown as black dashed lines. The D276 and formamide/O8 clash is demonstrated via red dashed lines. C) A rotated viewpoint of panel B highlighting the extent of the Asp276 and formamide/O8 clashes (red dashed lines).

A pre-catalytic complex of D276G pol β and Fapy•dGTP across from dA revealed that loss of the aspartate side chain alters the nucleotide conformation within the open-ternary complex ([Figure 3.8](#)). The coordination of the Fapy•dGTP O3' by residue Asp276 is lost upon glycine mutation and the incoming nucleotide refines to an occupancy of 85% for the most occupied conformation of the incoming Fapy•dGTP. Per this conformation, the Fapy•dGTP places the Watson-Crick edge of Fapy•dG towards the DNA major groove with the formamide oriented towards the minor groove ([Figure 3.8A](#)). The distance between O3' of the primer terminus and α P of Fapy•dGTP increases from 4.1 Å for the WT structure with Fapy•dGTP opposite dA to 5.8 Å ([Figure 3.8A](#)). We also observed an additional Ca^{2+} ion whose presence likely arises from the unique triphosphate orientation ([Figure 3.8B](#)). These structural changes are consistent with kinetic data ([Figure 3.6](#)).

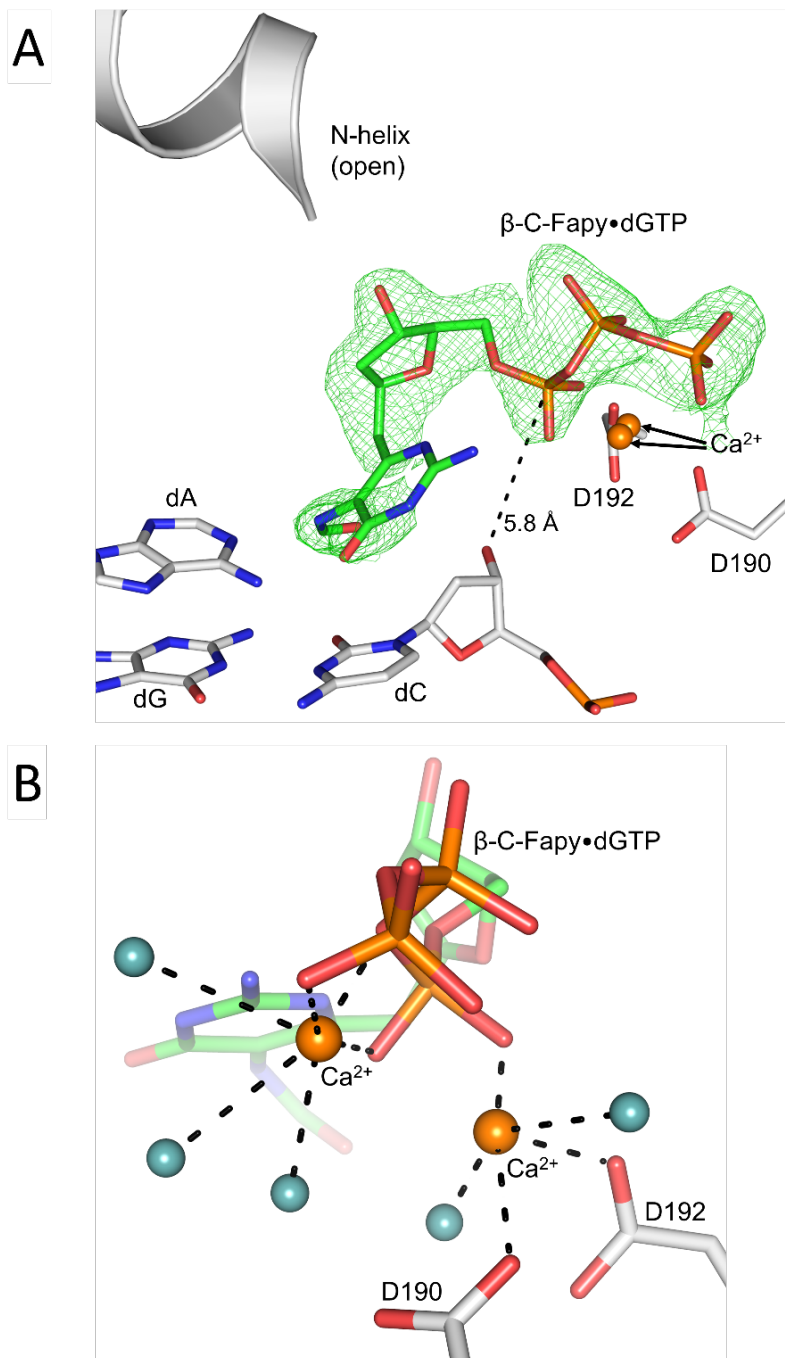


Figure 3.8 Pre-catalytic mutant (D276G) pol β mutagenic complex.

A) Pol β D276G mutant (gray) in a ternary-open ground state with incoming β -C-Fapy•dGTP nucleotide (green sticks) opposite a templating dA in a destabilized non-canonical conformation. The polder map is shown as green mesh and contoured to 3.0σ . B) A rotated viewpoint for illustrating the position of the additional Ca²⁺ ion (orange spheres) and coordinating waters (light teal spheres).

3.5 Discussion

The mutagenic Fapy•dGTP lesion was found to be poorly cleansed from nucleotide pools by *E. coli* MutT and mammalian MTH1, making it both a menacing and available substrate for DNA polymerases during oxidative stress (81,144). Here, we utilized X-ray crystallography and kinetic analyses to evaluate the insertion of Fapy•dGTP into DNA by the model mammalian DNA polymerase, pol β . The catalytic subdomain of pol β is structurally homologous to the corresponding subdomain (palm) of the bacterial replicative enzymes (154,155). In addition, pol β serves as an excellent model polymerase given that it is structurally well-characterized and exhibits open and closed structural states during transitions between different liganded states, which directly pertain to the mechanisms of eukaryotic replicative B-family polymerases (156). Through our kinetic studies, we observed that pol β inserts Fapy•dGTP with dramatically reduced catalytic efficiency opposite both dC and dA in comparison to undamaged dGTP and 8-oxodGTP (16). This is at least, in part, due to the weak binding affinity of the modified nucleotide ([Figure 3.2](#)). Additionally, insertion of Fapy•dGTP was decreased relative to the mismatch insertion efficiency of dA:dGTP by nearly an order of magnitude ([Figure 3.3](#)). Our structures revealed that Fapy•dGTP adopts an altered and distorted position in the pol β active site via flexibility of the ring-opened base ([Figure 3.4](#) and [Figure 3.5](#)). Pol β active-site residues were observed to stabilize an altered position of Fapy•dGTP and prevent closure of the N-subdomain upon nucleotide binding across from either dA or dC.

3.5.1. β -C-Fapy•dGTP insertion may be facilitated in the open conformation of DNA polymerase β

Although our kinetic data indicates catalysis occurs at a decreased efficiency, Fapy•dGTP can be inserted by pol β . Therefore, either a minor fraction of pol β is eventually able to close or catalysis occurs in the open or intermediate conformation. Let's consider that the ternary-closed structure of D276G pol β with a templating Cy shows Fapy•dGTP formamide is placed in the cavity formerly occupied by the Asp276 side chain. In WT pol β , the formamide group clashes with the γ -oxygens and C β of Asp276 should the enzyme adopt the closed conformation (Figure 3.7B). To avoid this clash, the formamide would be forced into the major groove, similar to what was previously observed with other nucleotides containing modifications at the major groove C5 position (157). This transiently closed pol β conformation could be accommodated to a limited extent; however, the stabilizing contact with Asp276 and the templating base in the observed open pol β conformation must be preferred. This suggests Fapy•dGTP might be inserted in a partially open intermediate state whereby the O3' proton is abstracted via an interaction with a transient catalytic metal. In this case, the O3' anion might attack α P from a more distant position (3.8 Å, Figure 3.4A). In comparison, the O3' to α P distance is 3.4 Å for the closed non-damaged insertion complex in the presence of MgCl₂ (147). Combined, our pre-catalytic structures and kinetic studies provide a rationale for a limited insertion mechanism occurring in a partially open conformation opposite dC. The reduction in catalytic efficiency for Fapy•dGTP insertion across from a templating dA indicates that catalysis likely requires further active site rearrangements. Notably, a

resultant Fapy•dG at the primer terminus has been shown to be extended during subsequent insertion events

3.5.2. Mechanistic insight into DNA polymerase β active-site residues

Correct and incorrect nucleotides are discriminated from each other on the basis of proper alignment of catalytic atoms within the polymerase active site (16,151). This alignment requires that the polymerase close around the nascent base pair. During Fapy•dGTP insertion, N-subdomain closure of pol β is prevented by interactions made between active site residues and the altered nucleotide position. Previous structures examining pol β active-site assembly have also observed ternary-open complexes with bound incoming non-damaged nucleotides (153,158). Overlaying the Fapy•dGTP ternary-open complex with a matched base pair ternary-open complex ([Figure 3.9A](#)) and a mismatched base pair ternary-open complex ([Figure 3.9B](#)) provides insight into how pol β accommodates an incoming nucleotide in the open conformation (153). Importantly, this conformation is mediated through binding of the triphosphate moiety. In contrast, the nucleoside base and deoxyribose sugar adopt different orientations depending on their unique interactions with the templating base. [Figure 3.9A](#) shows the nucleoside bases of a matched cytosine analog, dCMP(CF₂)PP, and Fapy•dGTP hydrogen bonding to the templating base in the *anti*- and *syn*-conformations, respectively. [Figure 3.9B](#) shows the different conformations adopted by a mismatched adenine analog (dAMP CPP) and Fapy•dGTP nucleoside bases, with the mismatched base failing to hydrogen bond with the templating base. Comparing the matched nucleotide insertion ternary-closed complex (dUMP NPP) with our matched Fapy•dGTP ternary-open complex revealed that the triphosphate moiety,

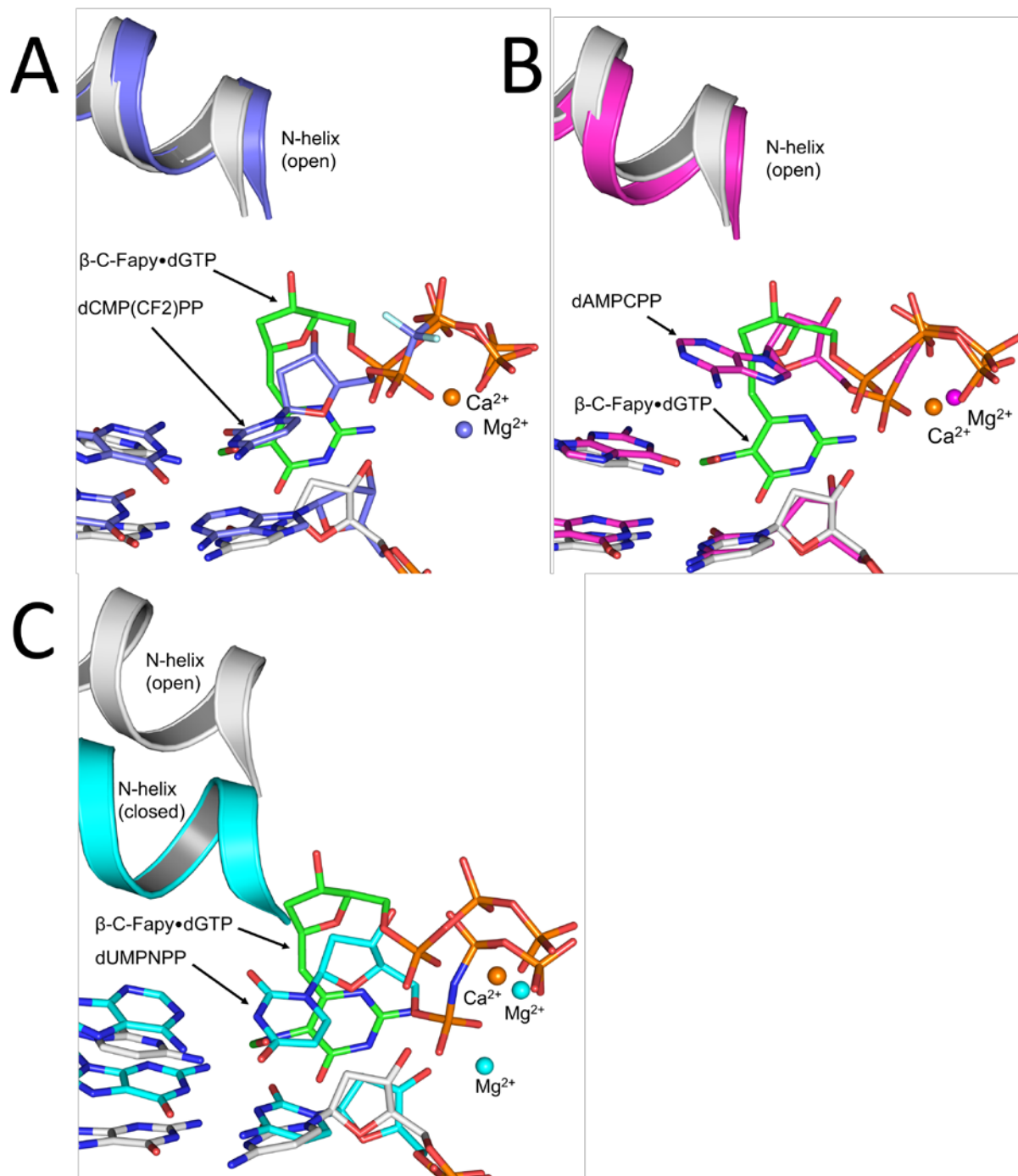


Figure 3.9 Comparison of the pol β : β -C-Fapy•dGTP complex with biologically relevant complexes.

The pre-catalytic ternary-open pol β : β -C-Fapy•dGTP:dC (gray/green) structure is overlaid with the following: A) A ternary-open complex (indigo) with an incoming nucleotide analog, dCMP(CF₂)PP, opposite a templating 8-oxo-dGuo (PDBID: 4F5O). B) A ternary-open complex (magenta) with an incoming nucleotide analog, dAMPCPP, opposite a templating dG (PDBID: 4F5P). C) A ternary-closed complex (cyan) with an incoming analog, dUMPNPP, opposite a templating dA (PDBID: 2FMS).

O3', and catalytic residues are not properly aligned in the Fapy•dGTP complex, likely preventing stable coordination of the catalytic metal ([Figure 3.9C](#)).

Both Asp276 and Arg258 stabilize the altered nucleotide position of Fapy•dGTP and have been proposed to influence nucleotide binding and subdomain closure (159,160). Arg258 forms a salt bridge with Glu295 which is key for the stabilization of the closed pol β conformation (160). Substitution of the arginine side chain with alanine decreases nucleotide binding affinity but increases the insertion rate without altering fidelity, which suggests that Arg258 aids in nucleotide binding but can generate a population of non-productive ternary complexes (128,161,162). Consistent with this, our ternary-open Fapy•dGTP complex illustrates a possible role for Arg258 in nucleotide binding prior to polymerase closure. The role for Asp276 involves stacking interactions of the side chain C β and the base of the incoming nucleotide to influence ground-state nucleotide binding during template base recognition (159). In the closed conformation, the carboxylate side chain is neutralized by Arg40. Mutation of the D276 residue to D276V, essentially removing only the charged portion of Asp276, increases the binding affinity for the incoming nucleotide, indicating Asp276 likely plays a role in the sampling and orienting of the incoming nucleotide (159).

We have shown here that during Fapy•dGTP insertion opposite dC, Asp276 stabilizes a non-productive nucleotide position, and in turn hinders subdomain closure and subsequent insertion. We further demonstrated that the D276G mutation allowed for Fapy•dGTP opposite dC to adopt a proper nucleotide orientation, closure of the N-subdomain, and catalytic metal coordination ([Figure 3.7A](#)) providing more evidence for the important role of Asp276 in nucleotide sampling and a guardian role blocking

Fapy•dGTP insertion across from dC. However, this is not the case for the insertion of Fapy•dGTP opposite dA. Our structural data show that in the case of a templating adenine, the D276G mutation does not stabilize enzyme closure nor proper nucleotide orientation ([Figure 3.8A](#)). In this conformation the insertion efficiency of Fapy•dGTP opposite dA by the D276G pol β mutant is further reduced ([Figure 3.6](#)).

3.5.3. *The mechanism of Fapy•dG mutagenesis differs from 8-oxo-dG*

8-oxo-dG, a well-studied oxidative lesion that shares a chemical intermediate with Fapy•dG, uses different glycosidic bond conformations (*syn/anti*) to promote mutagenesis (163,164). The *anti*-conformation of 8-oxo-dG base pairs with dC through the Watson-Crick edge, while the *syn*-conformation of 8-oxo-dG base pairs with dA through the Hoogsteen edge. Previous structures of a high-fidelity polymerase with a templating Fapy•dG analog demonstrated that it does not require the *syn*-conformation to base pair with dA. Instead, the flexibility of the opened ring in Fapy•dG can simply rotate the formamide group orthogonal to the aromatic heterocycle (82).

Structures of 8-oxo-dGTP insertion revealed that pol β adopts a closed conformation and planar base pairing interactions during both mutagenic and non-mutagenic insertion, whereby 8-oxo-dGTP used either an *anti*- or *syn*-conformation to base pair with dC or dA, respectively (16). As an incoming base, Fapy•dGTP does not use a similar mechanism as 8-oxodGTP. Instead, we observed pol β in the “open” conformation with Fapy•dGTP in an altered orientation and utilization of the *syn*-conformation during both template dA and dC insertions. This indicates that the ternary-open complex and the non-planar nucleotide position necessitates the rotation of the

glycosidic bond into the *syn*-conformation during insertion of Fapy•dGTP. Our results provide further evidence that opening of the imidazole ring in Fapy•dG enables a different mechanism compared with that of 8-oxo-dG mutagenesis.

3.5.4. The biological significance of characterizing Fapy•dGTP insertion with pol β

Insertion of Fapy•dGTP by pol β is biologically relevant during DNA repair, since DNA maintenance provides many opportunities for repair polymerases to utilize damaged nucleotide precursors. A robust DNA repair is especially important in non-dividing cells. Although a wide-range of persistent base excision repair intermediates have been detected (165), these steady-state values do not provide an estimate of the cellular rate of DNA repair. Lindahl has estimated that the rate of spontaneous depurination is 10,000/cell/day (63). This translates to >1 trillion abasic sites per adult per second underestimating the true burden since it does not include those generated by damage-specific DNA glycosylases. With this context of the importance of DNA repair and the processing of DNA lesions, we are poised to evaluate the contributions of the Fapy•dGTP lesion.

Previous reports indicated that DNA polymerase λ (pol λ) contributes significantly to the mutagenic signature of Fapy•dG during replication bypass (18). Pol λ is also an X-family polymerase and has been implicated in base excision repair under certain conditions (166,167). Although the Fapy•dG lesion in this previous study was limited to the DNA template strand, we chose to hypothesize on the possible effects of Fapy•dGTP in the active site of pol λ . Because the pol λ residue corresponding to Asp276 of pol β is Ala510, it can be rationalized that the smaller size and loss of hydrogen bonding capacity

with alanine would be expected to relieve some steric and electrostatic interactions that stabilize the altered conformation in the Fapy•dGTP in the ternary-open complex. However, a clash might be expected between the Ala510 C β of pol λ and the formamide of Fapy•dG based on the clashes observed in [Figure 3.7B](#) and [Figure 3.7C](#), plus the added caveat that pol λ differs from pol β in that it does not exhibit protein subdomain motions upon binding an incoming nucleotide (168). Looking further into the role of Asp 276 in pol β catalysis, previous studies replacing Asp276 with valine (159) or glycine (169) resulted in a mutant enzyme that exhibited an increased affinity for the correct incoming nucleotide. We observed that the pol β D276G mutation still discriminates against insertion opposite dA ([Figure 3.8](#)). Additionally, the similar efficiencies observed with dGTP and Fapy•dGTP insertion opposite dA for the D276G mutant suggests similar discriminating mechanisms.

Pol β has served as a model enzyme for characterizing the nucleotidyl transferase reaction, which is universally employed by DNA polymerases during DNA synthesis (38,170,171). Replicative polymerases in prokaryotic and eukaryotic organisms share structural homology to the corresponding catalytic subdomain (palm) of pol β and similarly adopt multiple subdomain conformations during the catalytic cycle as a result of different liganded states (154-156). With this in mind, the general strategies uncovered here during Fapy•dGTP insertion observed with pol β would be expected to be exploited by replicative polymerases. Specifically, we hypothesize that replicative polymerases alter their open to closed structural transition during Fapy•dGTP insertion to reduce binding and catalysis.

Chapter 4: The combined effect of oxidative damage and ribonucleotide sugar on the nucleotidyl transferase reaction.

This research was originally published in the Journal of Biological Chemistry. Smith M.R., Alnajjar K.S., Hoitsma N.M., Sweasy J.B., and Freudenthal B.D. Molecular and structural characterization of oxidized ribonucleotide insertion into DNA by human DNA polymerase beta. *Journal of Biological Chemistry*. 2020; 295:6, 3197-3207. © Smith M.R., Alnajjar K.S., Hoitsma N.M., Sweasy J.B., and Freudenthal B.D. Here, the research is presented with minor adaptations and abides by the reuse policies of the Journal of Biological Chemistry. <https://www.jbc.org/content/295/6/1613>

This chapter includes contributions by Dr. Khadijeh Alnajjar and Nicole Hoitsma. Dr. Alnajjar performed and analyzed the FRET experiments, and Nicole Hoitsma collected preliminary data for this project. My contributions included: kinetic data acquisition, X-ray crystallographic collection/refinement/deposition, data analysis, figure generation, and manuscript preparation/revision.

During DNA replication, more than a million ribonucleotides are misinserted instead of deoxyribonucleotides. During times of oxidative stress, 0.2-5% of the ribonucleotide pool has become oxidized. Moreover, nucleotide pool cleansing enzymes, such as MTH1, are 50-fold less efficient at eliminating oxidized ribonucleotides in comparison to oxidized deoxyribonucleotides. This raises the question of whether oxidized ribonucleotides are suitable substrates for DNA polymerases. We hypothesized that the prevalently formed r8-oxo-GTP lesion may be a substrate for polymerases, similar to 8-oxo-dGTP and rGTP lesions. To evaluate whether r8-oxo-GTP (**Section 1.3.3**) could be a mutagenic and/or efficient DNA polymerase substrate, we characterized r8-oxo-GTP opposite either a dC (non-mutagenic) or dA (mutagenic base) using our model polymerase (**Section 1.2.1**), pol β . We hypothesized that r8-oxo-GTP would be mutagenic and use base pairing properties as previously observed for 8-oxo-dG, but the ribose oxygen (O2') would hinder the insertion efficiency. We found that r8-oxo-GTP may be inserted into DNA using almost exclusively a mutagenic base (dA) template. Additionally, the effects of the O8 and O2' on r8-oxo-GTP were maintained in a nearly independent fashion, suggesting other ribo-DNA lesions may have similar mutagenic signatures to their deoxynucleotide counterparts.

4.1 Abstract

During oxidative stress, inflammation, or environmental exposures, ribo- and deoxyribonucleotides are oxidatively modified. 8-Oxo-7,8-dihydro-2'-guanosine (8-oxo-G) is a common oxidized nucleobase whose deoxyribonucleotide form, 8-oxo-dGTP, has been widely studied and demonstrated to be a mutagenic substrate for DNA polymerases. Guanine ribonucleotides are analogously oxidized to r8-oxo-GTP, which can constitute up to 5% of the rGTP pool. Because ribonucleotides are commonly misinserted into DNA and 8-oxo-G causes replication errors, we were motivated to investigate how the oxidized ribonucleotide is utilized by DNA polymerases. To do this, here we employed human DNA polymerase β (pol β) and characterized r8-oxo-GTP insertion with DNA substrates containing either a templating cytosine (non-mutagenic) or adenine (mutagenic). Our results show that pol β has a diminished catalytic efficiency for r8-oxo-GTP compared with canonical deoxyribonucleotides, but that r8-oxo-GTP is inserted mutagenically at a rate similar to those of other common DNA replication errors (*i.e.* ribonucleotide and mismatch insertions). Using FRET assays to monitor conformational changes of pol β with r8-oxo-GTP, we demonstrate impaired pol β closure that correlates with a reduced insertion efficiency. X-ray crystallographic analyses revealed that similar to 8-oxo-dGTP, r8-oxo-GTP adopts an anti- conformation opposite a templating cytosine and syn- conformation opposite adenine. However, unlike 8-oxo-dGTP, r8-oxo-GTP did not form a planar base pair with either templating base. These results suggest that r8-oxo-GTP is a potential mutagenic substrate for DNA polymerases and provide structural insights into how r8-oxo-GTP is processed by DNA polymerases.

4.2 Introduction

Oxygen radicals produced during oxidative stress can damage bases within both duplex DNA and the nucleotide pool causing cytotoxicity and mutagenesis (172,173). Specifically, oxidation of the nucleotide pool has been shown to be a significant contributor to DNA damage (12,100,174,175). Guanine is particularly susceptible to oxidation and readily forms 8-oxo-7,8-dihydro-2'-guanosine (8-oxo-G) (10). The deoxynucleotide form of 8-oxo-G is a highly mutagenic nucleobase substrate for DNA polymerases and consequently has been implicated in several human diseases (176-179). In contrast, the ribonucleotide form of 8-oxo-G (r8-oxo-G) remains to be fully characterized. The r8-oxo-G lesion has two deviations from the canonical nucleotide: an adducted oxygen on the nucleotide base (O8) and an additional oxygen on the ribose sugar (O2') ([Figure 4.1](#)). Importantly, the combined effect of both non-canonical oxygens during nucleotide discrimination is not well-understood.

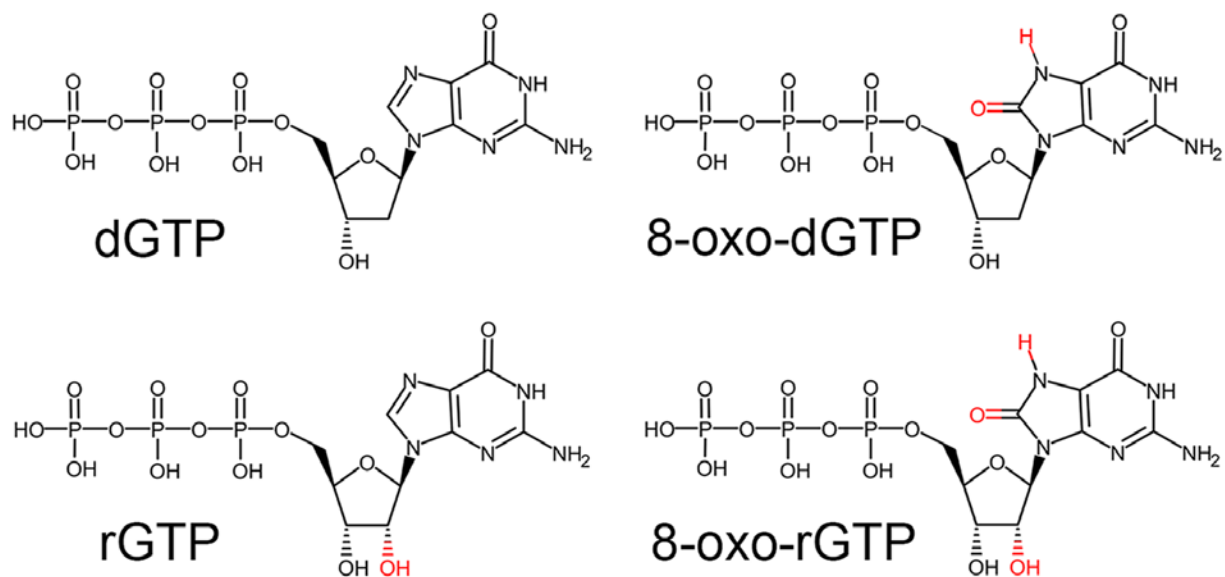


Figure 4.1 The chemical structure of various guanine nucleotides.

Deviations from the canonical DNA polymerase deoxyribonucleotide substrate are highlighted in red.

During DNA replication, polymerases must select the correct base and sugar combination to ensure high fidelity. DNA polymerase β (pol β) is an established mammalian model for studying nucleotide discrimination due to its amenability to structure-function studies and conformational nucleotide selection mechanism akin to replicative polymerases (52,180). The conformational change occurs upon correct nucleotide binding whereby the polymerase N-subdomain closes to facilitate key nucleic acid-protein interactions for efficient catalysis (52,159,180-184). Following closure, catalysis is carried out by nucleophilic attack of the primer terminus oxyanion (O3') on the α -phosphate (α P) of the incoming nucleotide, resulting in deoxynucleoside monophosphate incorporation and generation of a pyrophosphate (38).

There are several key steps involved in pol β closure and nucleotide insertion that discriminate between correct and incorrect nucleotides (119). To discriminate against ribonucleotides, Tyr 271 on α -helix M acts as a steric gate to prevent insertion of incoming ribonucleotides. Specifically, the backbone carbonyl of Tyr271 clashes with ribose O2' of the incoming nucleotide (Figure 4.2) (25,185). Although most DNA polymerases have an equivalent steric gate, misincorporation of ribonucleotides represents an extremely common replication error that is estimated to occur millions of times per cell division in normal cells (28,98,186). Moreover, mildly oxidative conditions in human cells results in oxidation of 0.2 - 5% of free guanine ribonucleotides (rGTP) into r8-oxo-GTP (12,97,98). Recent studies in yeast, bacteria, and humans have shown that r8-oxo-GTP is incorporated into DNA, thus indicating that r8-oxo-GTP is a potential polymerase substrate (29-31). Furthermore, human DNA polymerase δ is unable to proofread lesions

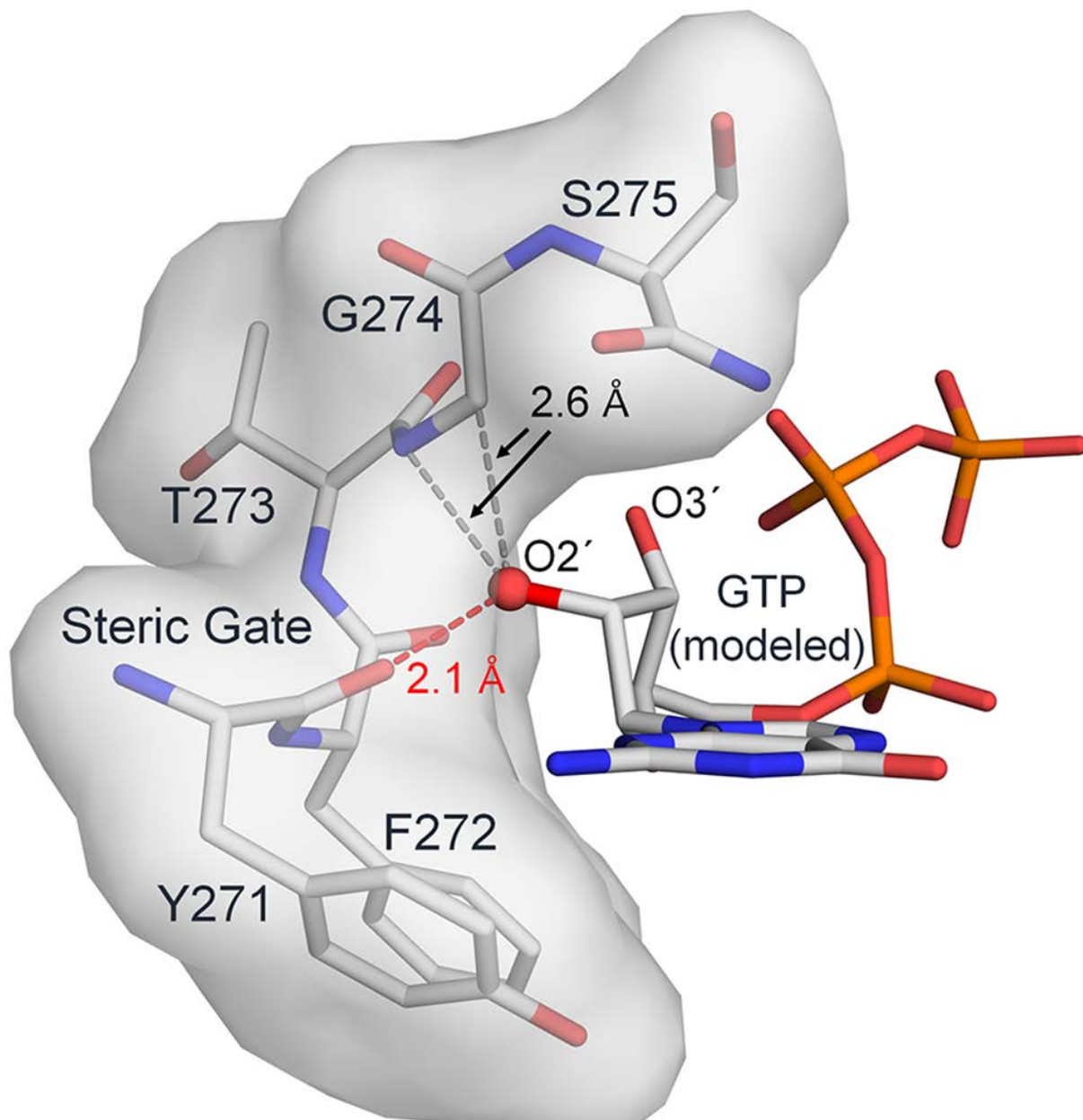


Figure 4.2 The ribonucleotide steric gate in DNA pol β .

Helix M is shown as both surface and stick representation (grey). The ribose sugar O2' (red sphere) has been added to the pol β structure with an incoming dGTP (PDBID: 4UB4). Steric clashes between the O2' and Helix M are indicated.

containing either a O2' or O8, suggesting reduced proofreading of r8-oxo-GMP during replication (98,187).

To gain mechanistic insight into r8-oxo-GTP insertion, we utilized pol β for structure-function studies of the nucleotidyl transferase reaction with an incoming r8-oxo-GTP. Here, we report pre-catalytic ternary (pol β :DNA:rNTP) substrate X-ray crystallographic structures of r8-oxo-GTP opposite templating adenine (mutagenic) or cytosine (non-mutagenic), FRET measurements of pol β closure, and kinetic characterization of r8-oxo-GTP insertion efficiencies. Our results provide molecular insight into how DNA polymerases incorporate r8-oxo-GTP into DNA.

4.3. Methods

4.3.1. Site-directed mutagenesis

Human wild-type pol β was subjected to site-directed mutagenesis to generate the Y271G mutant enzyme using the Quikchange II Site-directed mutagenesis protocol and kit. The Y271G mutation was confirmed by sequencing with the T7 forward and reverse primer. This mutant was rationally designed to provide flexibility to the steric gate backbone carboxyl of Y271 in pol β .

4.3.2. Expression and purification of DNA Polymerase β Y271G

Human DNA polymerase β Y271G was overexpressed in BL21-CodonPlus (DE3)-RP *E. coli* and purified as previously described in reference (188) and in **Section 2.3.1.** of this dissertation.

Table 5. Experimental DNA substrate sequences for characterizing r8-oxo-GTP.

Single-nucleotide gapped DNA substrates were constructed and annealed as outlined in 4.3.3. The templating position of all three duplex DNA substrates was either a dC or dA and is indicated above as (X). All downstream strands were 5'-phosphorylated (p) and the FRET/Crystallographic DNA sequences contained a dideoxy-terminated primer strand (C^{dd}). The position of the dabcyI dT FRET acceptor is indicated as D at the -8 position of the FRET primer strand. The primer strand of the kinetics DNA substrate was labeled with a 6-carboxyfluorescein (6-FAM) on the 5' end for detection and quantification of kinetic experiments.

Crystallographic DNA sequence

5' – GCTGATGCGC^{dd} pGTCGG –3'
3' – CGACTACGCG (X) CAGCC –5'

Kinetics DNA sequence

5' – ^{6-FAM}CTGCAGCTGATGCG pGTACGGATCCCCGGGTAC –3'
3' – GACGTCGACTACGC (X) CATGCCTAGGGGCCCATG –5'

FRET DNA sequence

5' – GCCTCGCAGCCGGCAGATGCGC^{dd} pGTCGGTCGATCCAATGCCGTCC –3'
3' – CGGAGCGTCGGCCGDCTACGCG (X) CAGCCAGCTAGGTTACGGCAGG –5'

4.3.3. DNA sequences and oligonucleotide annealing

The DNA sequences used in crystallization studies (16-mer), kinetic studies (34-mer), and FRET studies (45-mer) are provided in [Table 5](#). Each oligonucleotide was suspended in 10 mM Tris–HCl, pH 7.4 and 1 mM EDTA, and the concentration was determined from their ultraviolet absorbance at 260 nm. DNA substrates were prepared by annealing three purified oligonucleotides (above). The annealing reactions were performed by incubating a solution of primer with downstream and template oligonucleotides (1:1.2:1.2 molar ratio, respectively) at 95°C for 5 min, followed by 65°C for 30 min, and finally cooling 1°C min⁻¹ to 10°C in a PCR thermocycler.

4.3.4. Pol β/DNA/8-oxo-rGTP complex crystallization

Y271G pol β was incubated with 1-nt gapped/dideoxy-terminated DNA (1:1.2) containing either a templating dA or dC for 30 minutes. Binary complex crystals were grown via sitting drop vapor diffusion using 2 μL protein/DNA mix combined with 2 μL mother liquor (50 mM imidazole, pH 7.5, 16–20% PEG3350 and 350 mM sodium acetate) as previously described (114). Binary Y271G pol β:DNA complex crystals were then soaked in a cryosolution containing 20% ethylene glycol, 50 mM imidazole, pH 7.5, 16-19% PEG3350 and 70 mM sodium acetate, 5 mM r8-oxo-GTP and 50 mM MnCl₂ for 1-3 hours. This resulted in ternary pol β:DNA:r8-oxo-GTP crystals for X-ray crystallography.

4.3.5. Crystallographic data collection and refinement

Data were collected at 100 K on a MicroMax-007HF rotating anode generator at a wavelength of 1.54 Å. Diffraction images were collected using a Dectris Pilatus3R 200K-

A detector and the HKL3000 software package was used for processing and scaling the data (115). Initial models were determined using molecular replacement with the previously determined closed ternary (Protein Data Bank accession number 2FMS) structure of pol β , and R_{free} flags were taken from the starting model except for PDBID: 6UOK which had two pol β in the asymmetric unit. The metal-ligand coordination restraints were generated by ReadySet (PHENIX). Refinement was performed using PHENIX and model building using Coot (116,117). Density maps in structure figures (green mesh) were generated using Polder Maps in PHENIX. Polder OMIT maps are a reduced-bias sigma-A weighted difference density map (mF_o-DF_c) that excludes bulk solvent within a 5 Å radius when calculating OMIT maps to improve the visualization of weak densities (149). All polder maps were scaled to 3.0σ except for [Figure 4.8](#) which was scaled to 4.0σ . Ramachandran analysis determined 100% of non-glycine residues lie in the allowed regions and at least 97% in favored regions. Local base-pair parameters were calculated using 3DNA and local inter-base angles were corrected for both buckle and propeller contributions (189). The figures were prepared in PyMOL (Schrödinger LLC).

Table 6. Data collection and refinement statistics of ternary Y271G pol β :DNA co-complexes with incoming r8-oxo-GTP or rGTP.

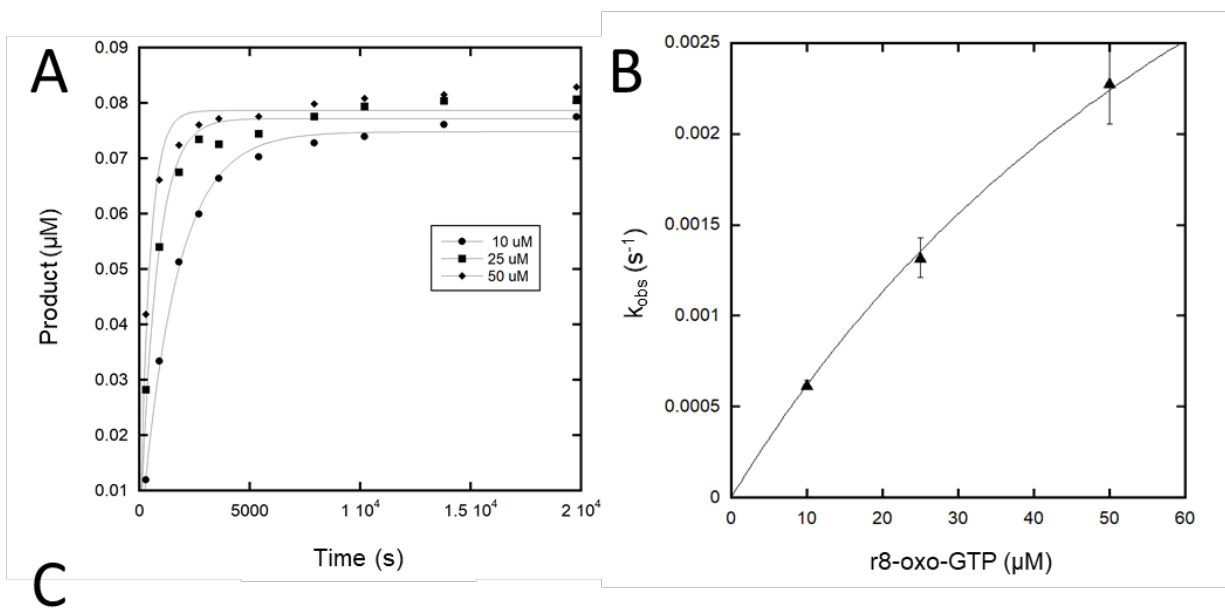
	Y271G pol β Templating Cy rGTP	Y271G pol β Templating Ad r8-oxo-GTP	Y271G pol β Templating Cy r8-oxo-GTP
Data collection			
Space group	P2 ₁	P2 ₁	P2 ₁
Cell dimensions			
<i>a</i> , <i>b</i> , <i>c</i> (Å)	51.0,80.3,55.1	51.0,80.0,54.8	54.7,80.0,100.8
α , β , γ (°)	90.0,108.6,90.0	90.0,108.4,90.0	90.0, 97.6, 90.0
Resolution (Å)	25.0-1.95	25.0-2.05	25.0-2.55
<i>R</i> _{sym} or <i>R</i> _{merge} ^a (%)	0.05 (0.87)	0.09 (.66)	0.13 (>1)
<i>R</i> _{pim} ^a	0.02 (0.68)	0.05 (0.47)	0.040 (>1)
<i>CC</i> _{1/2} ^a	0.999 (0.596)	0.994 (0.468)	0.999 (0.385)
<i> σ </i> ^a	22.6 (1.0)	12.5 (1.2)	10.5 (0.5)
Completeness ^a (%)	99.3 (98.2)	99.1 (95.8)	99.9 (99.7)
Redundancy ^a	4.0 (2.1)	3.6 (2.2)	4.8 (3.9)
Refinement			
Resolution (Å)	25.0-1.95	25.0-2.05	25.0-2.55
No. reflections	123990	93038	137585
<i>R</i> _{work} / <i>R</i> _{free}	0.186 / 0.250	0.194 / 0.244	0.224 / 0.279
No. atoms	3497	3553	6475
Protein	2615	2629	5067
DNA	628	630	1277
Water	203	223	47
B-factors (Å ²)	25.0	32.0	43.0
Protein	24.8	31.5	43.9
DNA	26.7	33.5	39.5
Water	26.6	33.5	33.8
R.m.s deviations			
Bond length (Å)	0.54	0.32	0.36
Bond angles (°)	0.66	0.54	0.55
Ramachandran plot:			
Outliers (%)	0	0	0
Allowed (%)	3	3	4
Favored (%)	97	97	96
PDB ID	6UOL	6UOM	6UOK

4.3.6. Kinetic characterization using single-turnover kinetics

Catalytic efficiencies (k_{pol}/K_d) for single-nucleotide gap filling reactions were determined by single-turnover analysis (*i.e.*, enzyme \gg DNA). At least 7 time points were gathered for each single-exponential time course determined with three sub-saturating concentrations of r8-oxo-GTP. The standard reaction mixture contained 50 mM Tris-HCl, pH 7.4, 100 mM KCl, 5 mM MgCl₂, 1 mM dithiothreitol, 100 μ g/ml bovine serum albumin, 10% glycerol, 100 nM single-nucleotide gapped DNA, and 1 μ M of pol β . Concentrations of r8-oxo-GTP were varied depending on the identity of the templating base to achieve a wide range of product concentration, while avoiding multiple insertions and/or product inhibition.

Templating dA kinetics were performed with 10 μ M, 25 μ M, and 50 μ M of r8-oxo-GTP during a four-hour time course with samples taken at 5, 15, 30, 45, 60, 90, 132, 170, 230, 330 mins. Templating dC kinetics were performed with 100 μ M, 250 μ M, and 500 μ M of r8-oxo-GTP during a time course of six and a half hours with samples taken at 15, 30, 60, 95, 132, 180, 230, 275, 400 mins. For rGTP insertion kinetics, 10 μ M, 25 μ M, and 50 μ M of rGTP were used in our reactions over a time course of 2.5 hours with samples taken at 2, 5, 15, 30, 45, 60, 90, 120, 150 mins. With the Y271G pol β mutant, kinetic experiments with a templating adenine used 50 nM, 100 nM, and 250 nM concentrations of r8-oxo-GTP over a four-hour time course with samples taken at 1, 3, 10, 30, 60, 90, 120, 180, 240 mins. Y271G pol β mutant experiments with a templating cytosine used 200 μ M, 400 μ M, and 600 μ M concentrations of r8-oxo-GTP over a six-hour time course with samples taken at 5, 15, 30, 45, 60, 90, 132, 170, 230, 330 mins.

Each reaction time course was performed at 37°C. Reactions were stopped with the addition of a quench solution containing 100 mM EDTA, 10 M urea and formamide dye. The substrates and products were separated on 22% denaturing (8 M urea) polyacrylamide gels. Since a 6-FAM 5'-labeled primer was used in these assays, the gels were quantified using the GE Typhoon phosphorimager in fluorescence mode. Substrate and product bands were quantified using ImageJ (190) and then plotted using Kaleidagraph (191), [Figure 4.3](#). For each concentration of r8-oxo-GTP, the data was fit to a single exponential curve ([Figure 4.3A](#)). Since sub-saturating concentrations of r8-oxo-GTP ($<K_d$) were used the data were fit to an alternate form of the Michaelis equation to extract apparent catalytic efficiencies (k_{pol}/K_d): $k_{obs} = ((k_{pol}/K_d) * S) / (1 + (S/K_d))$, where S refers to the concentration of r8-oxo-GTP ([Figure 4.3B](#)). Catalytic efficiencies were calculated as an average of three independent experiments \pm the error determined using standard deviation of the mean (S.D.M.), [Figure 4.3C](#).



^aRate determined in (Batra, Beard et al. 2008)

^bRate determined in (Brown, Duym et al. 2007)

Figure 4.3 Single-turnover kinetics with r8-oxo-GTP, rGTP, or dGTP.

A) A representative plot measuring pol β -dependent single-nucleotide gap filling DNA synthesis with 10 μM (●), 25 μM (■), and 50 μM (◆) r8-oxo-GTP. Data were fit to a single exponential (gray lines). B) A secondary plot of the observed first-order rate constants (k_{obs}) were fit to a modified hyperbola (gray line) to extract k_{pol}/K_d . C) Catalytic efficiencies (k_{pol}/K_d) for single-nucleotide gap filling reactions using WT and Y271G pol β . Catalytic efficiencies were calculated as an average of three independent experiments for each nucleotide concentration of rGTP and r8-oxo-GTP \pm the error determined using standard deviation of the mean (S.D.M.).

4.3.7. FRET polymerase closure assay

Human pol β containing mutations at C239S, C267S, and V303C, was used in order to fluorescently label the N-subdomain with the thiol-reactive IAEDANS, as previously described (182). Fluorescence emission of AEDANS-labeled pol β was measured in either the apoenzyme form (400 nM AEDANS-labeled pol β in 50 mM Tris pH 8.0, 20 mM NaCl, 10 mM MgCl₂), the binary complex (400 nM AEDANS-labeled pol β mixed with 400 nM of single nucleotide gapped DNA substrate with a dideoxy-terminated primer terminus containing dabcyI dT at the -8 position relative the templating base), or the ternary complex (formed by adding 1 mM of either dGTP, 8-oxo-dGTP, rGTP, or r8-oxo-GTP to the binary complex) ([Figure 4.4](#) and [Figure 4.5](#)). AEDANS was excited at 336 nm and emission was collected at 400-550 nm using QuantaMaster 800 fluorometer at room temperature ([Figure 4.5A](#) and [Figure 4.5B](#)) (182). Distances were estimated from the FRET efficiency between AEDANS and DabcyI and by using Förster radius of 37.76 Å. Experiments were performed in triplicate, and the error was calculated as a standard deviation of the mean. A table with the calculated distances is provided ([Figure 4.5C](#)).

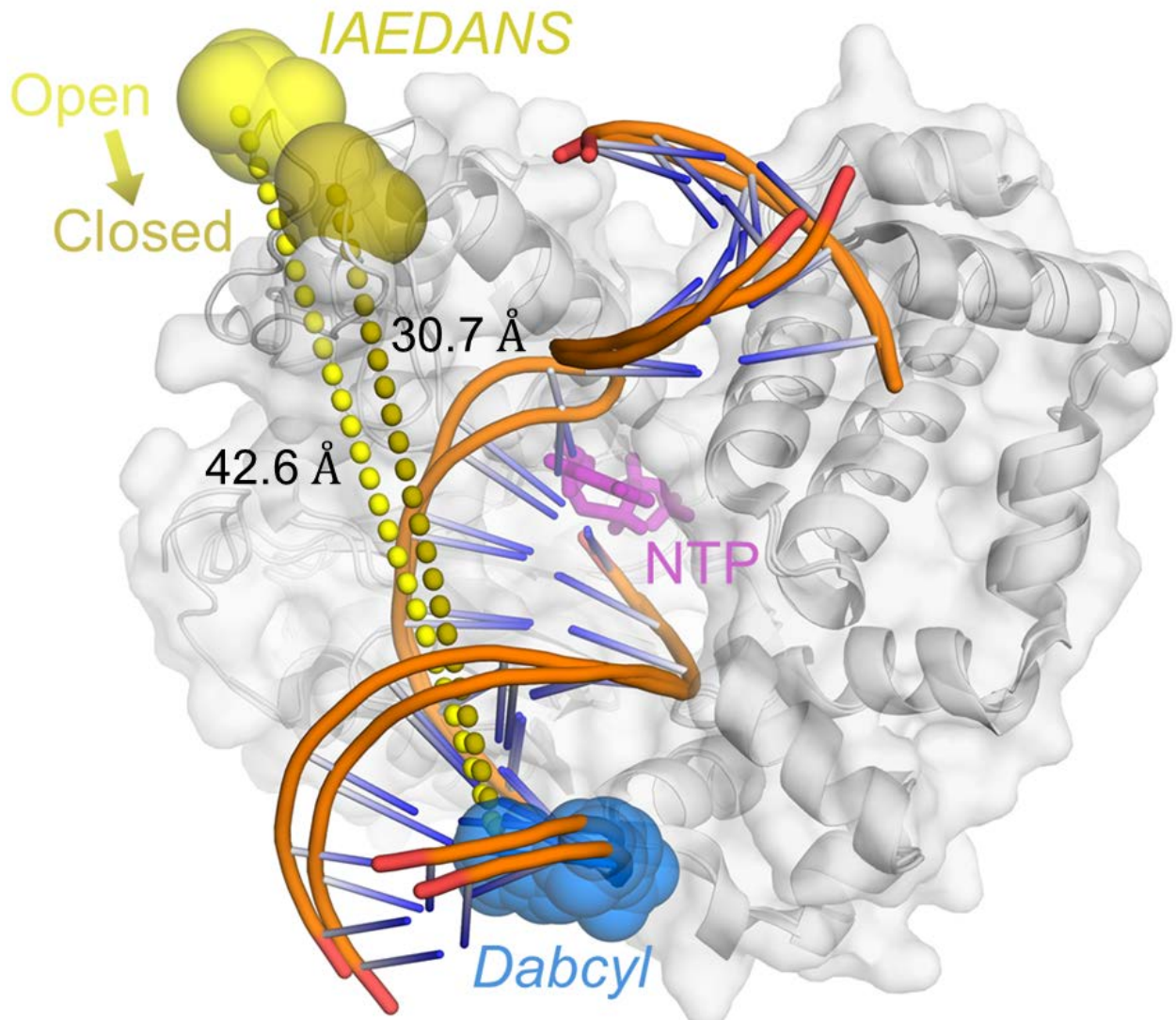
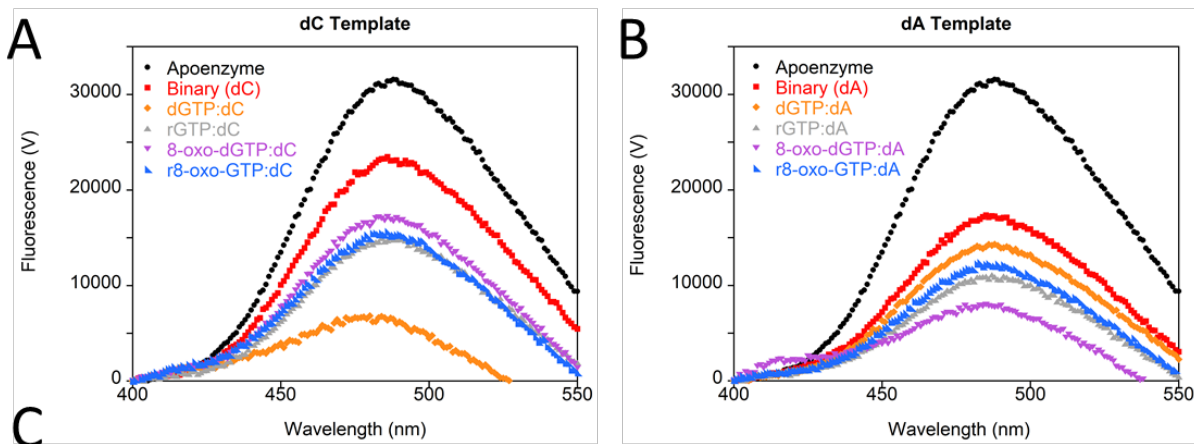


Figure 4.4 Diagram of the polymerase closure FRET system.

The AEDANS label (yellow and dark yellow) is represented by surface representation of residue V303, and the dabcyyl label is highlighted as blue on the T-8 position. The incoming nucleotide (NTP) is shown in stick representation (magenta). Pol β is shown as surface and cartoon representation (grey), and the DNA is shown in cartoon representation (orange/blue). As pol β transitions from an open to a closed conformation, the distance between the AEDANS and the dabcyyl FRET pair decreases. The FRET efficiency after NTP addition for each complex were then calculated as distances. Representative distances are from our FRET data with templating dC (binary and correct complex).



	Distance (Å)					
	Binary	Correct	Incorrect	8-oxo-dGTP	rGTP	r8-oxo-GTP
C-template	42.6±1.3	30.7±0.7 (dGTP)	39.7±0.8 (dTTP)	38.1±0.7	38.1±0.8	37.7±0.9
Δ Distance _{Binary-Ternary}		11.9	2.9	4.5	4.5	4.9
A-template	38.0±0.3	30.9±0.5 (dTTP)	36.0±0.5 (dGTP)	31.8±0.5	35.8±0.4	35.2±0.5
Δ Distance _{Binary-Ternary}		7.1	2	6.2	2.2	2.8

Figure 4.5 Evaluating pol β subdomain closure via steady-state FRET.

A) The fingers domain of pol β undergoes efficient closure upon dGTP (orange) insertion opposite dC, unlike rGTP (gray), 8-oxo-dGTP (purple), and r8-oxo-GTP (blue). Apoenzyme (black) and the binary complex of pol β and DNA (red) are used as a control and for calculating the change in distance upon binding nucleotide, respectively. B) Same scheme as in panel A, but the DNA now contains a templating adenine, whereby only 8-oxo-dGTP (purple) demonstrated an increased efficiency for subdomain closure. C) Table containing the calculated distances and their respective errors for each complex. Additionally, the change in distance between the binary and ternary complexes for each nucleotide is provided. Distances estimated from FRET efficiencies are averaged from three independent experiments for each pol β complex (apo, binary, dGTP, 8-oxo-dGTP, rGTP and r8-oxo-GTP ± the error determined using standard deviation of the mean (S.D.M.).

4.4. Results

4.4.1. *r8-oxo-GTP is a mutagenic substrate for DNA polymerase β*

The efficiency of r8-oxo-GTP and rGTP insertion into a single-nucleotide gap by pol β was measured with both a templating cytosine (dC) and adenine (dA) ([Figure 4.6](#)). To contextualize r8-oxo-GTP insertion, these insertion efficiencies were compared to undamaged deoxyribonucleotide (dGTP) and oxidized deoxyribonucleotide (8-oxo-dGTP) insertion (52,179). Relative to correct dGTP insertion, r8-oxo-GTP insertion efficiency opposite dC and dA is reduced >250,000-fold and 4,000-fold, respectively. The 60-fold preference for insertion of r8-oxo-GTP opposite dA, compared to dC, demonstrates the mutagenicity of r8-oxo-GTP. This is consistent with 8-oxo-dGTP, which is also preferentially inserted opposite dA. However, insertion of r8-oxo-GTP is less efficient than 8-oxo-dGTP by 700 and 4,300-fold opposite dA and dC, respectively. This demonstrates that the ribose O2' hinders insertion of the 8-oxo-G base, but the effect is not strictly additive. For comparison, the O2' of the undamaged base (rGTP) reduces insertion efficiency by 3,500-fold opposite the correct base, dC. Notably, rGTP is extremely difficult to misinsert opposite the wrong base; rGTP insertion opposite dA could not be measured in our assay nor previously (192). Despite the reduced efficiencies imparted by the O2', ribonucleotides are still frequently inserted into DNA (28), and we show that mutagenic r8-oxo-GTP insertion has a similar efficiency to ribonucleotide insertion. To provide molecular insight into the basis of these observations, we turned to a FRET polymerase closure assay and X-ray crystallography.

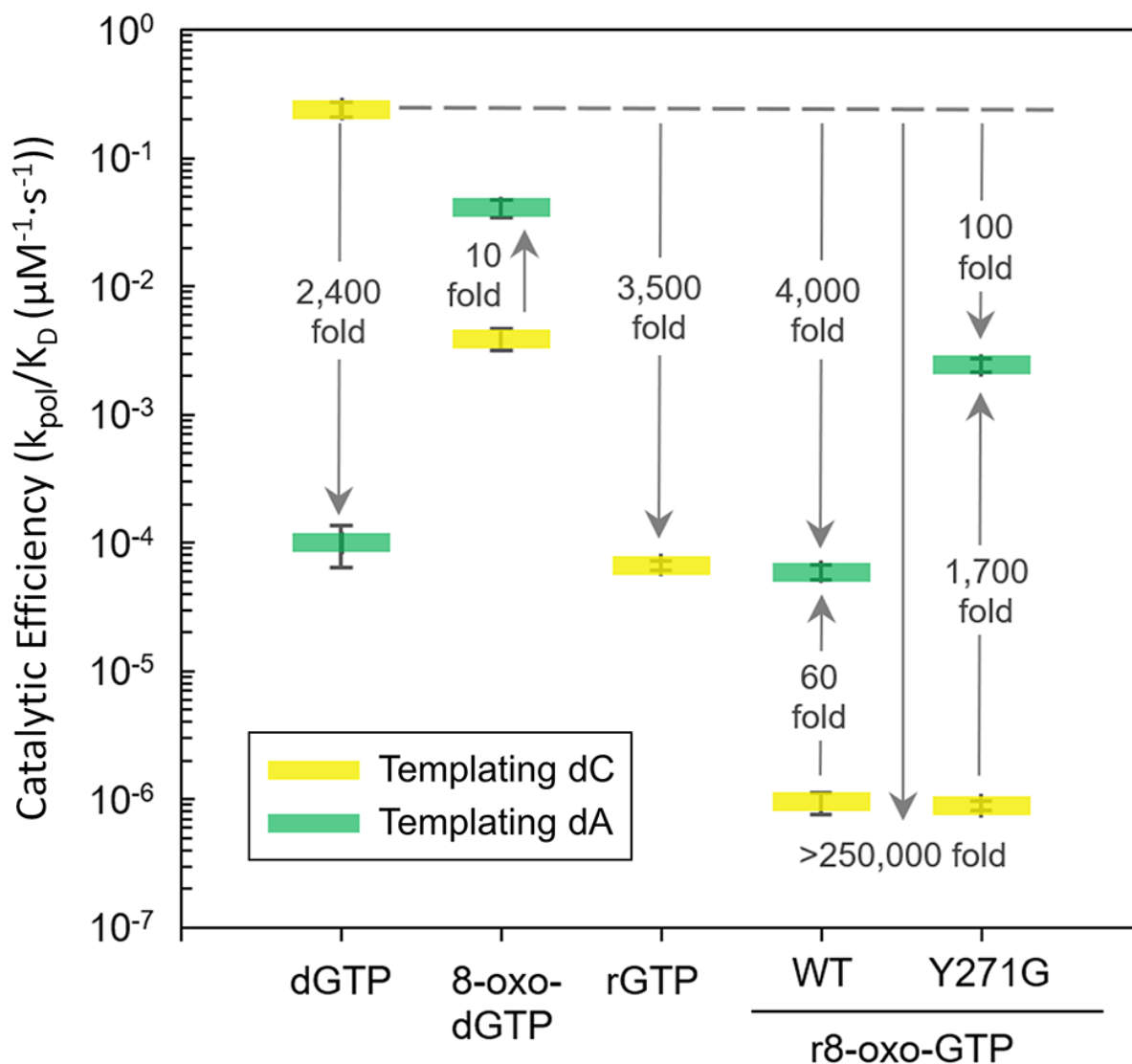


Figure 4.6 Discrimination plot evaluating r8-oxo-GTP insertion.

The catalytic efficiencies (k_{pol}/K_d) for insertion of r8-oxo-GTP opposite dC (yellow) or dA (green) for pol β are shown. The distance between the respective catalytic efficiencies is a measure of discrimination/fidelity. Each horizontal short bar represents the standard deviation of the mean of triplicate independent determinations. The insertion efficiencies for dGTP were reported in (11,12) and 8-oxo-dGTP in (11). The catalytic efficiency values are reported in Figure S1C and are as follows: $2.4 \times 10^{-1} \pm 3.0 \times 10^{-2} \mu\text{M}^{-1}\cdot\text{s}^{-1}$ (dGTP:dC), $1.0 \times 10^{-4} \pm 3.6 \times 10^{-5} \mu\text{M}^{-1}\cdot\text{s}^{-1}$ (dGTP:dA), $3.9 \times 10^{-3} \pm 7.0 \times 10^{-5} \mu\text{M}^{-1}\cdot\text{s}^{-1}$ (8-oxo-dGTP:dC), $4.1 \times 10^{-2} \pm 4.1 \times 10^{-3} \mu\text{M}^{-1}\cdot\text{s}^{-1}$ (8-oxo-dGTP:dA), $6.7 \times 10^{-5} \pm 5.7 \times 10^{-6} \mu\text{M}^{-1}\cdot\text{s}^{-1}$ (rGTP:dC), $9.5 \times 10^{-7} \pm 1.8 \times 10^{-7} \mu\text{M}^{-1}\cdot\text{s}^{-1}$ (r8-oxo-GTP:dC), $5.9 \times 10^{-5} \pm 7.9 \times 10^{-5} \mu\text{M}^{-1}\cdot\text{s}^{-1}$ (r8-oxo-GTP:dA), $8.9 \times 10^{-7} \pm 8.3 \times 10^{-8} \mu\text{M}^{-1}\cdot\text{s}^{-1}$ (Y271G:r8-oxo-GTP:dC), $2.4 \times 10^{-3} \pm 2.9 \times 10^{-4} \mu\text{M}^{-1}\cdot\text{s}^{-1}$ (Y271G:r8-oxo-GTP:dA).

4.4.2. FRET collaboration reveals poor enzyme closure *in vitro*

To evaluate how polymerase subdomain closure might contribute to the decrease in kinetic efficiency for r8-oxo-GTP insertion, we utilized a steady-state FRET-based assay with pol β . Closure of the N-subdomain, triggered by binding of the nucleotide, was measured using FRET between the fluorescent AEDANS label, located at position V303C of the N-subdomain, and the quencher (Dabcyl) located at position -8 relative to the templating base of the DNA substrate ([Figure 4.4](#)). As expected, the correct pairing of dGTP opposite dC results in closure of pol β , indicated by a shift of the N-subdomain ~ 12 Å closer to the DNA compared to the binary open complex ([Figure 4.7](#)). Of note, our calculated distances for the open binary and closed correct ternary associate closely with previous measurements using this assay and those expected from crystallographic data (182). Performing the same experiment with either 8-oxo-dGTP, rGTP, or r8-oxo-GTP insertion opposite dC resulted in a lack of significant N-subdomain closure (shifting only 2.9-4.5 Å). These results indicate that modifications on either the sugar (O2') or the base (O8) inhibit the enzyme from closing and are consistent with the observed reduction in their insertion efficiency opposite dC ([Figure 4.6](#)).

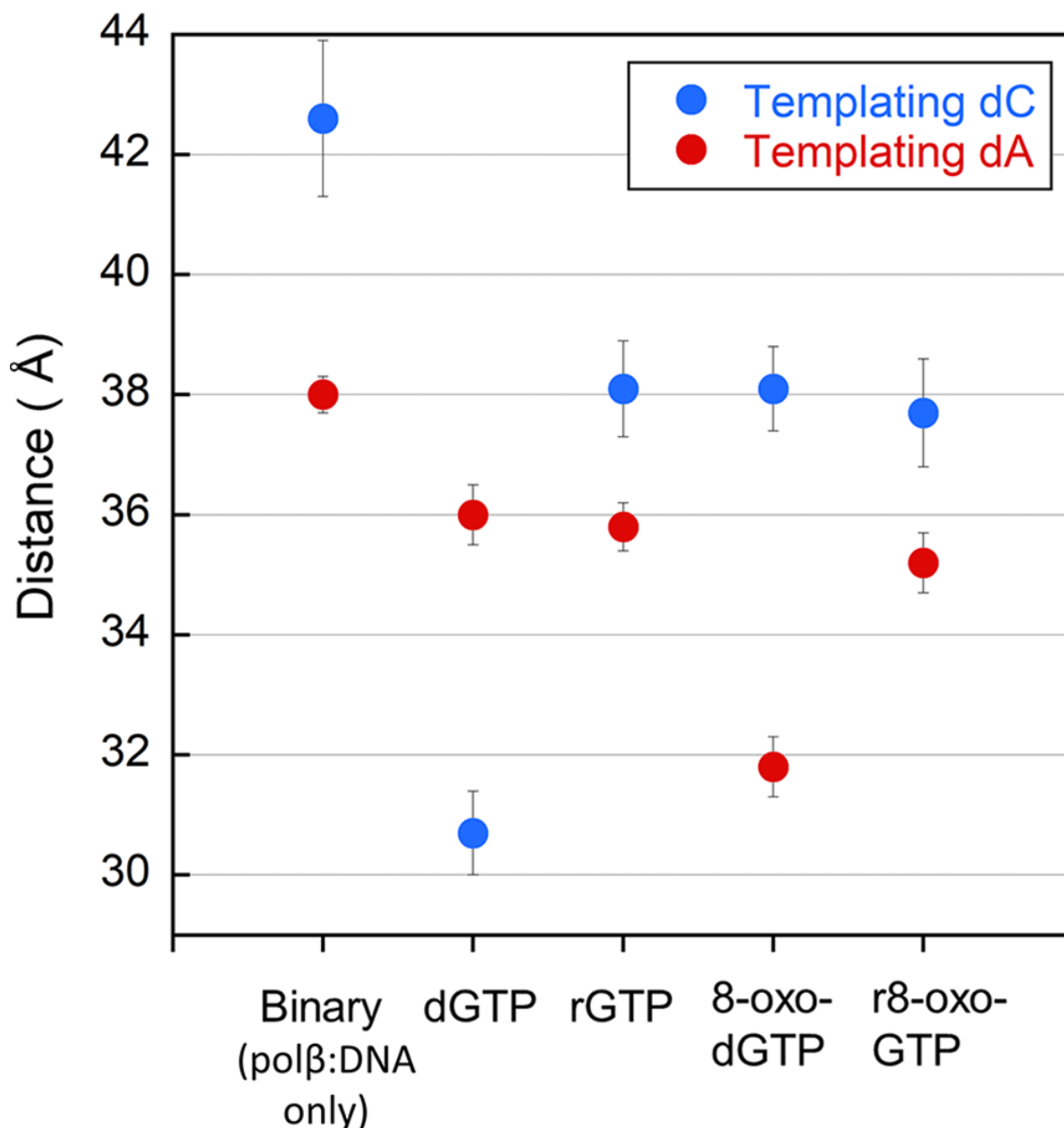


Figure 4.7 Calculated interprobe distances from FRET efficiencies during steady-state FRET experiments.

Efficiencies from triplicate measurements are plotted for the following complexes opposite either a templating cytosine (dark blue) or templating adenine (red): binary, ternary with dGTP, rGTP, or r8-oxo-GTP with error bars (black) calculated using standard deviation of the mean (S.D.M.). Distance values are reported in Figure S3 and are as follows: 42.6 ± 1.3 Å (Binary:dC), 38.0 ± 0.3 Å (Binary:dA), 30.7 ± 0.7 Å (dGTP:dC), 36.0 ± 0.5 Å (dGTP:dA), 38.1 ± 0.8 Å (rGTP:dC), 35.8 ± 0.4 Å (rGTP:dA), 38.1 ± 0.7 Å (8-oxo-dGTP:dC), 31.8 ± 0.5 Å (8-oxo-dGTP:dA), 37.7 ± 0.9 Å (r8-oxo-GTP:dC), 35.2 ± 0.5 Å (r8-oxo-GTP:dA).

The mismatched insertion of dGTP opposite dA results in only a 2.0 Å shift of the N-subdomain from 38.0 Å in the binary complex to 36.0 Å in the ternary and is associated with a significant loss in catalytic efficiency ([Figure 4.6](#) and [Figure 4.7](#)). In contrast, the insertion of 8-oxo-dGTP, the oxidized deoxyribonucleotide, opposite dA leads to a 6.2 Å shift in the N-subdomain from 38.0 Å to 31.8 Å, which is similar to the distance observed in the presence of the correct dTTP:dA pair (30.9 Å) ([Figure 4.5](#) and [Figure 4.7](#)). This ability of pol β to undergo subdomain closure during 8-oxo-dGTP insertion opposite dA correlates with the high catalytic efficiency of this mutagenic deoxyribonucleotide. The lack of closure measured by FRET during rGTP insertion opposite dA provides a potential explanation for the unmeasurable catalytic activity ([Figure 4.6](#) and [Figure 4.7](#)). Lastly, the insertion of r8-oxo-GTP opposite dA resulted in only a 2.8 Å shift in the N-subdomain, which indicates an intermediate, or partially closed state, and correlates with its intermediate insertion efficiency, [Figure 4.7](#).

4.4.3. r8-oxo-GTP base-pair interactions are similar to 8-oxo-dGTP

To investigate the active site geometries and base pairing properties of r8-oxo-GTP, we sought to collect X-ray crystallographic ternary complex structures with wild-type pol β. Unfortunately, we were unable to obtain a wild-type pol β:DNA:r8-oxo-GTP ternary complex, likely as a result of the poor binding between r8-oxo-GTP and pol β. A previous study determined that removal of the Y271 side chain did not appreciably alter insertion of dCTP opposite dG and increased non-damaged ribonucleotide insertion efficiency by 12-fold, in comparison to wild-type pol β (192). Therefore, we utilized a Y271G pol β variant to obtain ternary structures of pol β bound to r8-oxo-GTP. Consistent with this,

Y271G insertion of r8-oxo-GTP showed increased catalytic efficiency opposite dA (2,700-fold) but not opposite dC when compared to wild type ([Figure 4.6](#)). We proceeded to use the Y271G pol β variant to obtain ternary crystal structures of r8-oxo-GTP insertion opposite both dA and dC with MnCl_2 and a dideoxy-terminated primer, which allows for binding of r8-oxo-GTP while preventing catalysis (25,52,193).

The ternary complex, showing Y271G pol β bound to single nucleotide gapped DNA with a templating dC and an incoming r8-oxo-GTP, diffracted to 2.55 Å ([Table 6](#)). The resulting structure contained two pol β complexes in the asymmetric unit with one complex in the open conformation and the other in the closed conformation. The density for r8-oxo-GTP in the open active site of pol β was relatively poor with only clearly defined density for the triphosphate moiety ([Figure 4.8](#)).

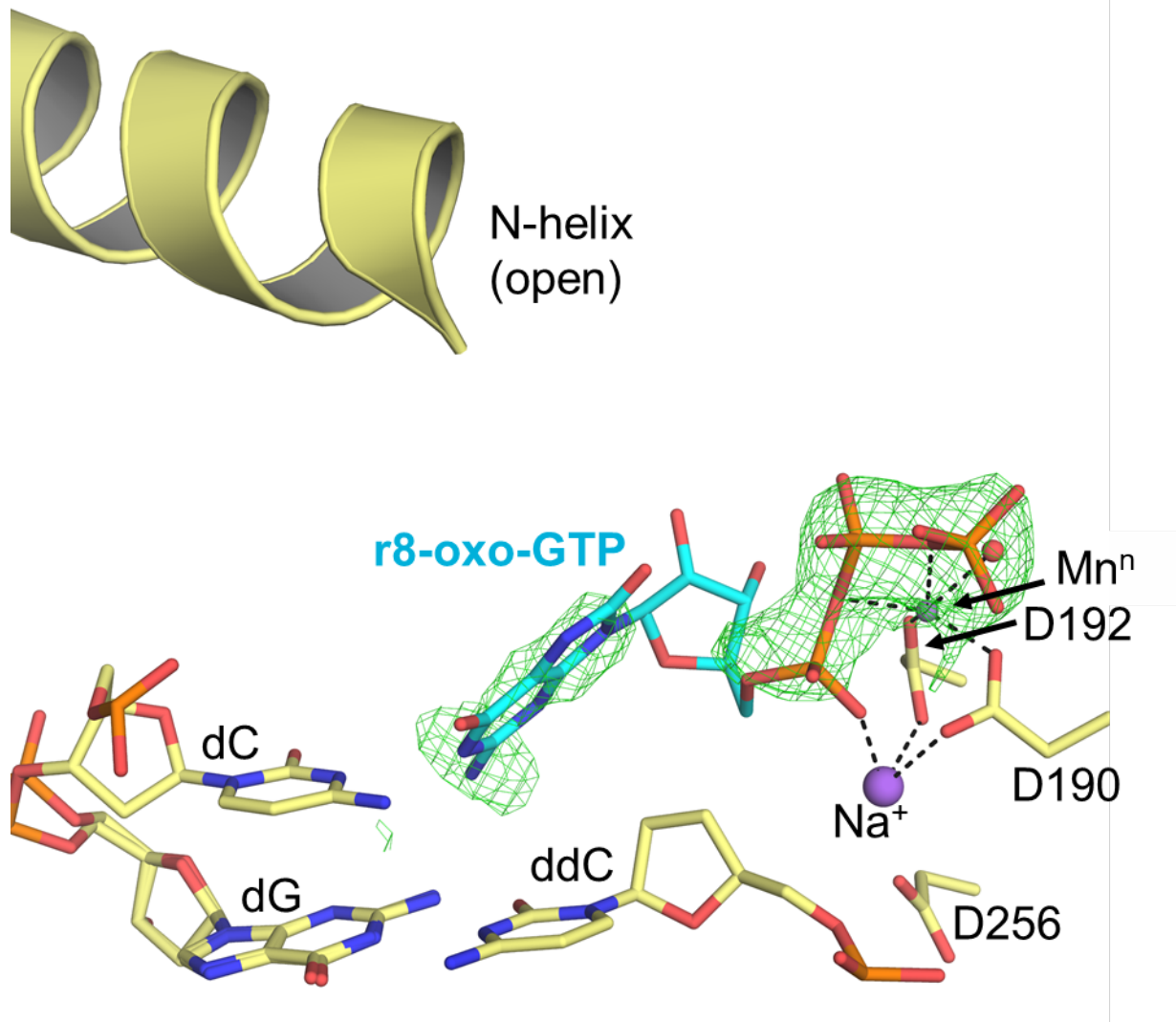


Figure 4.8 Open complex of the pol β :r8-oxo-GTP:dC asymmetric unit.

Pre-catalytic ternary open complex of Y271G pol β (yellow) with r8-oxo-GTP (blue sticks) bound across from dC; Mn²⁺ and Na⁺ ion shown in purple; coordinated H₂O molecule is shown as a red sphere; potential hydrogen bonds are shown as black dashed lines. A polder map (green mesh) contoured at 4.0 σ is shown for the incoming r8-oxo-GTP.

In contrast, the density for r8-oxo-GTP in the closed pol β conformation was more defined and is the focus of our analysis ([Figure 4.9A](#)). In this structure, the r8-oxo-GTP is bound to the pol β active site with a single Mn^{2+} in the nucleotide metal binding site, and the catalytic metal binding site contains a sodium ion. The lack of divalent catalytic metal binding was previously observed for dideoxy-terminated ternary complexes (114). The incoming r8-oxo-GTP resides in the *anti*-conformation opposite a dC template in a closed complex, but the base pairing is not planar. Instead, the angle between base planes in the r8-oxo-GTP:dC nascent pair is 27° , positioning the O8 oxygen in the direction of the N-helix (194). This twist results in the adducted O8 of r8-oxo-GTP sitting 0.5 \AA farther away from the O5' compared to the O8 in a previously solved 8-oxo-dGTP:dC complex (195). In the 8-oxo-dGTP:dC complex, a Ca^{2+} ion interacts with the α -phosphate of the incoming nucleotide to neutralize the close proximity of the O8 and O5'. This metal is not present in the r8-oxo-GTP:dC complex, likely due to the propeller twist accommodating any potential clash between O8 and O5'. The ribose sugar of the incoming nucleotide resides in an O4'-endo-conformation with the O2' pointed towards the backbone carbonyl of Gly271 ([Figure 4.9B](#)). This results in the backbone carbonyl of Gly271 shifting 0.9 \AA , relative to its position in the dGTP:dC complex, to avoid a clash with the O2' ([Figure 4.9B](#)). A stabilizing hydrogen bond between the 3'-OH of the incoming nucleotide and the non-bridging β -phosphate oxygen, observed in the rGTP:dC complex, is not present with r8-oxo-GTP since the 3'-OH is 5 \AA from the non-bridging β -phosphate oxygen of the nucleotide. In a previously obtained Y271A pol β rCTP:dG complex, a rotameric shift of Phe272 and a shift in the primer terminus toward the major groove were observed (25).

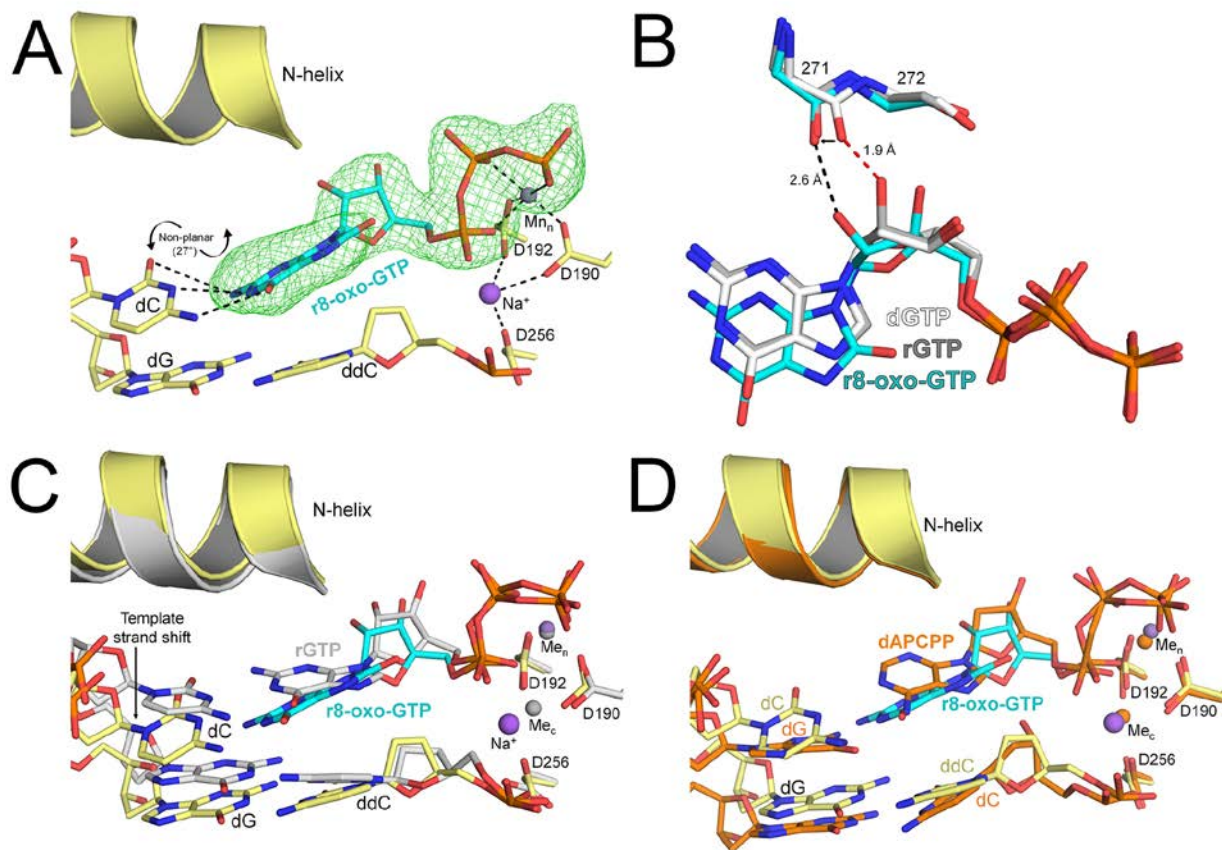


Figure 4.9 X-ray crystallographic structure of Y271G pol β in complex with r8-oxo-GTP opposite dC.

A) Pre-catalytic closed ternary complex of Y271G pol β (yellow) with r8-oxo-GTP (blue sticks) bound across from dC; Mn²⁺ ions are shown in purple; potential hydrogen bonds are shown as black dashed lines. A polder map (green mesh) contoured at 3.0σ is shown for the incoming r8-oxo-GTP. B) An overlay of the incoming nucleotide and steric gating residues for the r8-oxo-GTP:dC complex (blue), the undamaged rGTP:dC complex (gray) (PDBID: 4UB4) highlighting potential clashes with red dashed lines and potential hydrogen bonds as black dashed lines. C) An overlay between the r8-oxo-GTP:dC complex (yellow/blue) and an undamaged rGTP:dC complex (gray). Key residues and DNA are shown as sticks and the N-helix in cartoon. D) An overlay between the r8-oxo-GTP:dC complex (yellow/blue) and a mismatched dAPCPP:dG complex (orange) (PDBID: 3C2M). Key residues and DNA are shown as sticks and the N-helix in cartoon.

These structural features are also present in our r8-oxo-GTP:dC complex as a result of removing the Tyr271 side chain. In the r8-oxo-GTP:dC complex, we also observed a shift of the templating dC along with the 5'-end of the templating strand upstream in comparison to a rGTP:dC complex control ([Figure 4.9C](#)). Ternary mismatches also shift the templating strand upstream, however the r8-oxo-GTP:dC complex does not shift to the same extent ([Figure 4.9D](#)) (52,196). This is likely because of weak interactions between the Watson-Crick faces of r8-oxo-GTP and the templating dC.

8-oxo-dGTP prefers to insert opposite adenine via a rotation of the glycosidic bond and formation of a Hoogsteen base pair with dA. In our solution studies, r8-oxo-GTP similarly prefers to insert opposite adenine ([Figure 4.6](#)). To evaluate whether r8-oxo-GTP uses Hoogsteen base-pairing, we obtained a ternary Y271G pol β structure with an incoming r8-oxo-GTP opposite a templating dA. This complex diffracted to 2.05 Å with only one pol β molecule per asymmetric unit ([Table 6](#)). In the resulting structure, pol β assumed a closed conformation with clear density for r8-oxo-GTP in the nucleotide binding pocket ([Figure 4.10A](#)). r8-oxo-GTP was bound with Mn^{2+} in both the nucleotide and catalytic metal binding sites, indicating a more optimal active site geometry in comparison to r8-oxo-GTP opposite dC ([Figure 4.9A](#)). Similar to 8-oxo-dGTP, r8-oxo-GTP Hoogsteen base pairs opposite dA using the *syn*- conformation. This places the adducted O8 oxygen into the minor groove where it is stabilized by N279, which was also observed with 8-oxo-dGTP ([Figure 4.10B](#)). However, one clear difference between structures with 8-oxo-dGTP and r8-oxo-GTP is that the nucleoside breaks from planarity

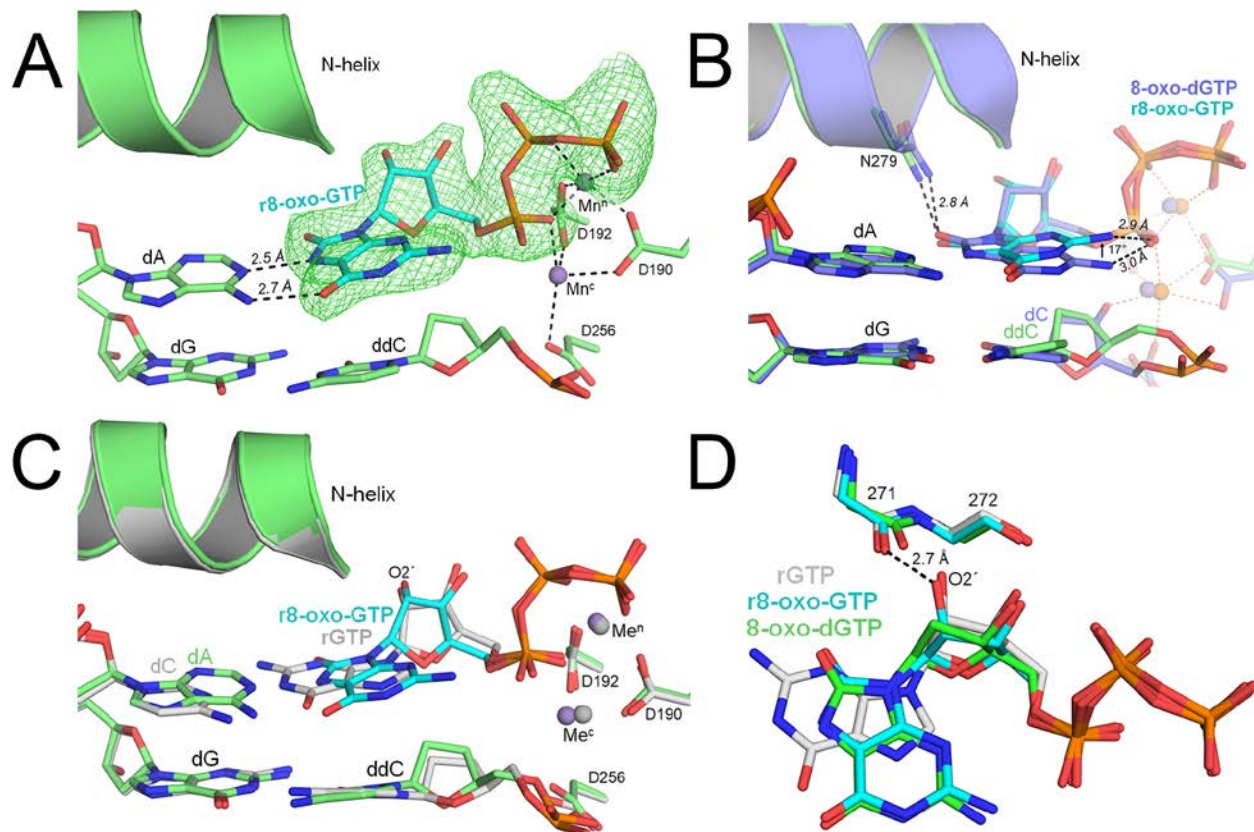


Figure 4.10 X-ray crystallographic structure of Y271G pol β in complex with r8-oxo-GTP opposite dA.

Pre-catalytic closed ternary complex of Y271G pol β (green) with r8-oxo-GTP (blue sticks) bound across from dA; Mn²⁺ ions are shown in purple; potential hydrogen bonds are shown as black dashed lines. A polder map (green mesh) contoured at 3.0 σ is shown for the incoming r8-oxo-GTP. B) An overlay between the r8-oxo-GTP:dA complex (green/blue) and the 8-oxo-dGTP:dA complex (purple). Key residues and DNA are shown as sticks, potential hydrogen bonds are shown as black dashed lines, and the N-helix is in cartoon. C) An overlay between the r8-oxo-GTP:dA complex (green/blue) and a rGTP:dC complex (gray). Key residues and DNA are shown as sticks and the N-helix in cartoon. D) An overlay of the incoming nucleotide and steric gating residues for the r8-oxo-GTP:dA complex (green), the undamaged rGTP:dC complex (gray), and the 8-oxo-dGTP:dA complex (blue) (PDBID: 4UAW). Potential hydrogen bonds are shown as black dashed lines.

by 17° with the ribo form, pointing the N2 away from the α -phosphate and towards the N-helix ([Figure 4.10B](#)) (189).

Despite being non-planar, there was not a significant change to the distance of the hydrogen bond between the N2 and the α -phosphate (2.9 Å) which has been proposed to stabilize the Hoogsteen conformation during 8-oxo-dGTP insertion opposite dA (3.0 Å) ([Figure 4.10B](#)) (195). The overall organization of the active site during r8-oxo-GTP insertion opposite dA aligns well with our rGTP:dC structure and is consistent with respect to their similar kinetic efficiencies ([Figure 4.10C](#)). The ribose O2' was positioned 2.8 Å away from the Gly271 backbone carbonyl similar to rGTP:dC (2.6 Å) ([Figure 4.10D](#)). However, the ribose sugar adopts a C4'-exo conformation as opposed to the more competent C3'-endo in our rGTP:dC complex and other pol β :rNTP structures ([Figure 4.10D](#)). Additionally, the r8-oxo-GTP 3'-OH and its non-bridging β -phosphate oxygen are within hydrogen bonding distance at 3.2 Å.

4.5. Discussion

In this study, we characterized r8-oxo-GTP insertion with DNA polymerase β using single-turnover kinetics, steady-state FRET assay, and X-ray crystallography. Our results show that polymerase subdomain closure opposite both dA and dC is reduced, but differences in active site geometries upon closure lead to the preference for mutagenic (dA) insertion of r8-oxo-GTP ([Figure 4.11](#)). We also showed that mutagenic insertion of r8-oxo-GTP opposite dA occurs at a similar catalytic efficiency to that of a mismatched deoxyribonucleotide or correctly matched undamaged ribonucleotide. Based on the error rate of misinsertion and measured levels of r8-oxo-GTP, together this suggests that r8-

oxo-GTP could be a potential mutagenic substrate for DNA polymerases under oxidizing conditions (12,28). Our findings also demonstrate that the mechanistic barriers that hinder r8-oxo-GTP insertion are manifested by effects arising from the O8 and O2' that closely resemble their independent effects (25,179,192,195).

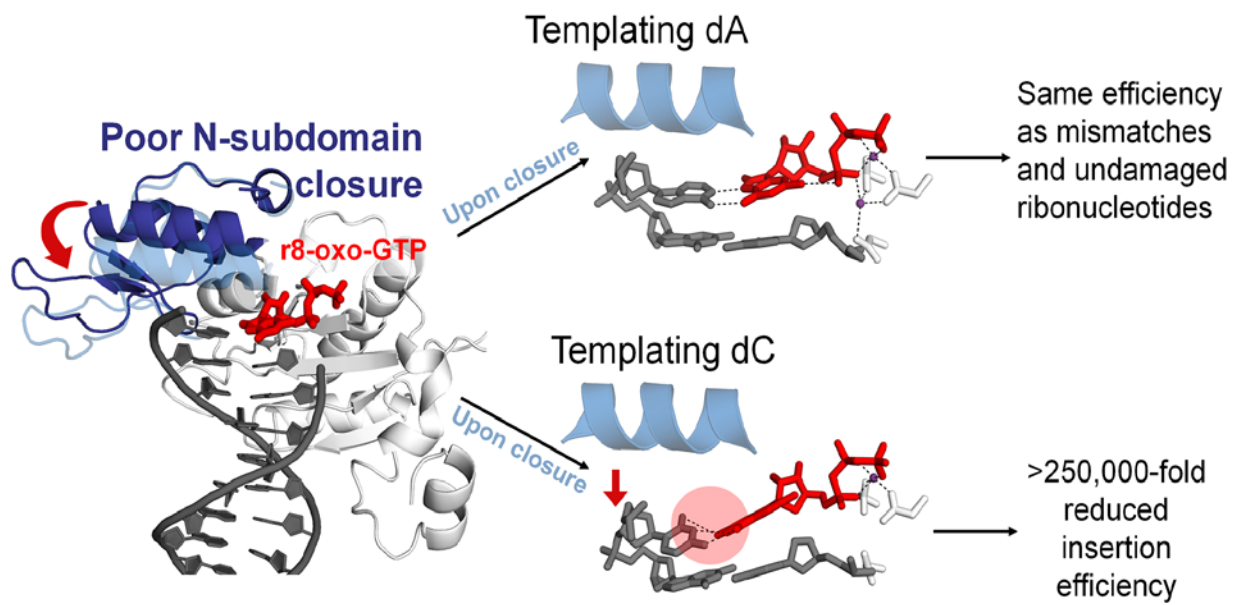


Figure 4.11 Scheme of r8-oxo-GTP processing by human DNA polymerase β .

4.5.1. The adducted O8 promotes mutagenic r8-oxo-GTP insertion by pol β .

It is well characterized that 8-oxo-dGTP is inserted by polymerases across from dA more efficiently than dC, and r8-oxo-GTP continues this trend. 8-oxo-dGTP and r8-oxo-GTP, respectively, have a 10-fold and 60-fold increase in insertion efficiency opposite dA as compared to dC ([Figure 4.6](#)). However, the ribose sugar of r8-oxo-GTP reduces the insertion efficiency as compared to 8-oxo-dGTP. Moreover, when the steric gate residue Tyr271 is mutated, r8-oxo-GTP:dA insertion increases 40-fold, which is only 17-fold less than 8-oxo-dGTP:dA. Mutagenic r8-oxo-GTP insertion by wild-type pol β is only 1.7-fold less than its non-damaged mismatch insertion (dGTP:dA), demonstrating the potential frequency of r8-oxo-GTP given that mismatches are a common replication error. In our FRET experiments, we observed a similar distance between the r8-oxo-GTP:dA and dGTP:dA complexes (35.2 Å and 36.0 Å, respectively) that corroborates the similar catalytic efficiencies ([Figure 4.6](#) and [Figure 4.7](#)). Conversely, ribonucleotide insertion (rGTP:dC), another frequent replication error, is also within 1.3-fold of r8-oxo-GTP:dA but has a more open conformation (38.1 Å), indicating other steps in the enzymatic pathway account for the observed differences in catalytic efficiency.

In our X-ray crystal structures, we see similarities between 8-oxo-dGTP and r8-oxo-GTP insertion. Particularly, the adducted O8 oxygen imparts the same general base pairing properties in the deoxyribo- and ribo-nucleotide forms. When base pairing opposite cytosine, there is a retention of the *anti*-conformation that forms Watson-Crick base pairs. Opposite adenine, both r8-oxo-GTP and 8-oxo-dGTP rotate about their glycosidic bond to a *syn*-conformation and Hoogsteen base pair with dA. Retention of

the base pairing properties between 8-oxo-dGTP and r8-oxo-GTP supports the retained mutagenic behavior of the adducted O8.

4.5.2. r8-oxo-GTP shares attributes from both rNTP and 8-oxodGTP discrimination

The induced-fit model posits that after initial correct dNTP binding, conformational changes of the ternary complex induce catalytic residues to properly align for catalysis (48). The induced-fit model would also assert that mismatch complexes do not properly align the active site for catalysis and instead promote dissociation (48). In a mismatched complex (dG:dAPCPP; PDBID:3C2M), the templating strand is shifted out of coding position, and pol β is positioned in an open conformation (52,54,114,197,198). Similarly, we observed these features in our r8-oxo-GTP:dC complex ([Figure 4.8](#) and [Figure 4.9D](#)) demonstrating a similar method of discrimination between mismatches and r8-oxo-GTP:dC. Furthermore, we observed an open pol β complex within the asymmetric unit with poorly defined density for the nucleoside and only moderately defined triphosphate density ([Figure 4.8](#)). Retention of triphosphate density without nucleobase density is consistent with previous findings that demonstrate triphosphate binding occurs prior to Watson:Crick sampling (158,199). The observance of poor density and reduced occupancy of the r8-oxo-GTP:dC open complex structurally supports our solution experiments showing both a decrease in catalytic efficiency and reduction in pol β closure for this complex.

Another feature of the mismatch complex is the absence of Watson-Crick hydrogen bonds in the nascent pair, which led to the hypothesis that optimal base pairing interactions during nucleotide binding facilitates proper active site assembly (52).

However, we found that r8-oxo-GTP does come within hydrogen bonding distance with the templating dC, despite the template strand shift and propeller twist of the nascent pair. Of note, a similar degree of propeller shift was observed during rCTP:dG insertion with polymerase eta (27°) compared to our r8-oxo-GTP:dC twist (27°) (200). Overall, pol β strongly deters r8-oxo-GTP insertion opposite dC via poor r8-oxo-GTP binding, impaired subdomain closure, and significant active site geometry perturbations should closure occur.

The r8-oxo-GTP lesion is distinctly non-planar opposite both dC and dA. However, the O8 and O2' by themselves do not significantly alter base pair planarity, as observed during 8-oxo-dGTP and rNTP insertion (25,195). This suggests that the combined steric burden of the O2' and O8 prevent the formation of a planar base pair with either the templating dA or dC. In a previous study, non-planarity within the nascent pair was suggested to impair catalytic metal binding (199). Our non-planar r8-oxo-GTP insertion complexes indeed show a reduced catalytic metal binding opposite both dA and dC. The r8-oxo-dGTP:dA complex had a reduced occupancy of the catalytic metal (0.8), and r8-oxo-GTP:dC had no divalent metal binding corresponding with its more severe non-planarity. Therefore, our structures suggest that lack of planarity in the nascent pair impairs proper active site assembly, including catalytic metal binding. Our data also supports the previous suggestion that non-planar geometry in the nascent base pair prohibits DNA stacking interactions within the DNA polymerase active site that are important for nucleotide binding (41). From our fluorescence measurements, pol β adopts a predominantly open position with r8-oxo-GTP that supports inefficient r8-oxo-GTP binding ([Figure 4.6](#)). Inefficient binding can also be inferred by the inability to obtain r8-

oxo-GTP structures with wild-type pol β . Overall, the non-planarity of r8-oxo-GTP contributes to the reduction in catalytic efficiency in addition to poor nucleotide binding, improper organization of the polymerase active site, and inefficient polymerase closure.

4.5.3. Biological consequences of r8-oxo-GTP insertion Our results show that the ribose O2' of r8-oxo-GTP heavily diminishes the rate of insertion opposite adenine and cytosine. Despite this, r8-oxo-GTP can still be mutagenically inserted by pol β at an efficiency similar to undamaged ribonucleotides. If replicative polymerases were to have a similar discrimination for r8-oxo-GTP as pol β , we can speculate on the amount of mutagenic r8-oxo-GTP insertion events during DNA replication. Using replicative DNA polymerase ϵ as an example, the discrimination between rGTP and dGTP is 12-times worse than pol β , indicating r8-oxo-GTP may be inserted more efficiently by pol ϵ than by pol β (201). Altogether, replicative polymerases are estimated to misinsert more than 1 million ribonucleotides (~250,000 rGTP) per round of replication (97), and levels of r8-oxo-GTP have been measured to be between 0.2 - 5% of the rGTP pool during mild oxidative stress (12,202). If 0.2% of the ~250,000 inserted rGTP are oxidized to r8-oxo-GTP, then ~500 r8-oxo-GTP mutagenic insertion events could potentially occur per cell division under mildly oxidative conditions.

The subsequent cellular ramifications of these lesions in duplex DNA are still unclear. Many DNA-damage processing enzymes have been investigated but most are unable to process r8-oxo-GTP or r8-oxo-G including: 8-oxo-dGuanine glycosylase (OGG1), ribonuclease H2 (RNase H2), and ribonucleotide reductase (23,31,203,204). MutT-homolog 1 (MTH1), and AP endonuclease (APE1) only have weak activity on r8-oxo-GTP

and r8-oxo-G processing, making it uncertain if the reduced activities are sufficient to protect the cell from r8-oxo-G(TP) (23,205,206). In cellular extracts subjected to mildly oxidized conditions, r8-oxo-GTP does accumulate (0.3 nmol per 10^6 cells), whereas 8-oxo-dGTP was not detected (12). This suggests that MTH1 is not able to sufficiently remove r8-oxo-GTP from the nucleotide pool, in contrast to its efficient removal of 8-oxo-dGTP. MUTYH was found to have r8-oxo-GMP activity and remove the opposing mutagenic dA. However, the efficiency for inserting the correct base opposite r8-oxo-GMP currently remains unknown to our knowledge.

Chapter 5: Conclusions and Future Directions

This collective work describes our investigation into how DNA polymerase β processes oxidized guanines and enhances our understanding of how errors and mutagenic events are generated. Results showed that each oxidized guanine lesion affected a unique combination of discrimination steps within the pol β mechanism to reduce catalysis. In brief, our data shows: (i) extending from a mutagenic 8-oxo-dGMP:dA base pair is more catalytically efficient than a non-mutagenic 8-oxo-dGMP:dC base pair, (ii) insertion of a Fapy•dGTP analog (β -C-Fapy•dGTP) is not highly mutagenic, and (iii) insertion of r8-oxo-GTP prefers to be inserted mutagenically rather than non-mutagenically but at a lower catalytic efficiency that is similar to non-damaged rGTP. Collectively, these findings contribute to a greater understanding of damaged DNA processing by DNA polymerases and illustrate each lesion's potential mutagenic capacity in the context investigated. In future work, the mutagenicity of the oxidized guanines reported here for human DNA polymerase β should be validated by also characterizing them with other DNA polymerases and nucleic acid enzymes to further evaluate the mutagenic mechanisms in a biological context.

5.1. Patterns of oxidative guanine base-pairing in multiple DNA registries

In this section, the broad patterns of oxidized guanine base pairing are discussed with respect to how the above chapters compare with previously reported findings. Because guanine oxidation largely generates the potential for Hoogsteen base pairing and altered base conformations via the adducted O8, the patterns of conformational selection with varied base pair partners and DNA positions are of particular interest (58).

The 8-oxo-G lesion is a prevalent form of damage and is the most studied form of damaged guanine, **Section 1.3.1** (72). These reports repeatedly demonstrate that 8-oxo-G has the potential to base pair mutagenically with adenine, and the efficiency of this base pair varies depending on the polymerase. For an overview on 8-oxo-G mutagenesis with all the different eukaryotic polymerases, the review by Yudkina et. al. has nicely summarized this information (72). If we instead focus on the properties of 8-oxo-G exclusively in the context of pol β , 8-oxo-G mostly prefers to base pair with a mutagenic adenine rather than the non-mutagenic cytosine, regardless of polymerase registry (16,124,171,179). 8-oxo-dG as a primer terminus (**Chapter 2**), 8-oxo-dGTP as an incoming deoxyribonucleotide (16), and r8-oxo-GTP as an incoming ribonucleotide (**Chapter 4**) show a preference for mutagenic insertion using the *syn*-conformation. However, 8-oxo-dG as a templating base has been shown to have a slight (2-fold) preference for non-mutagenic insertion (124,179). At this low level of discrimination, mutagenic bypass is still likely to occur. Through all the previous studies and data presented in this dissertation, 8-oxo-G consistently maintains the pattern of adopting the *anti*-conformation when base paired to dC and the *syn*-conformation when base paired to dA regardless of the DNA position. Overall, 8-oxo-G has a strong mutagenic propensity that spans all DNA positions and correlates with the extensive mechanisms developed by the cell to mediate the effects of 8-oxo-G, such as MutT homolog 1 (MTH1), 8-oxo-guanine glycosylase (OGG1), MutY homolog (MUTYH) and others (11).

The Fapy•dG lesion (**Section 1.3.2**) has had conflicting reports on its preferred base pairing patterns. One report in particular demonstrated Fapy•dG to adopt a non-

Hoogsteen (*i.e.* *anti*-conformation) mutagenic base pair in the active site of the high-fidelity polymerase I from *Geobacillus stearothermophilus* (*Bst* Pol I). However, there are many inconsistencies observed when measuring Fapy•dG mutagenesis, suggesting that non-Hoogsteen mutagenicity may not be a universal pattern for the Fapy•dG lesion. The varied rates of mutagenicity reported and detail in **Section 1.3.2.** likely stem from the varying systems and assays that have been used. In solution, *Geobacillus stearothermophilus* DNA polymerase I fragment, *Escherichia coli* DNA polymerase I fragment, and *Saccharomyces cerevisiae* DNA polymerase η performed mutagenic Fapy•dG bypass 1.4-fold, 20.8-fold, and >250-fold less efficient than non-mutagenic bypass, respectively (82,83,92). This suggests that Fapy•dG is not preferably mutagenic *in vitro* but has the capability to base pair with adenine.

No study had reported *in vitro* kinetic values for a mammalian polymerase with Fapy•dG until our work presented in **Chapter 3.** We found that the Fapy•dG nucleotide triphosphate analog is not efficiently inserted opposite the correct templating base (dC) and exhibits even lower efficiency when inserted opposite a mutagenic base (dA). After making an active site mutation, Fapy•dG base paired using its Watson-Crick edge (*anti*-) to interact with dC and its Hoogsteen edge (*syn*-) to interact weakly with dA. The observation of a *syn*-Fapy•dG:dA base pair contradicted the earlier suggestion that Fapy•dG utilizes non-Hoogsteen base pairing (82). Of note, one molecular biology study suggests the mutagenic mechanism *in vivo* does not involve direct misinsertions nor template misalignments but instead arises from other contributions, which I speculate could be from the α -anomer (89). Overall, more work is required to accurately determine

the mutagenic potential of Fapy•dG, such as developing better synthesis methods, performing kinetic assays with mammalian polymerases, and further structural studies with the natural Fapy•dG lesion. As better methods for generating high quantities of Fapy•dG-containing DNA are developed, the mechanisms of Fapy•dG-induced mutagenesis will likely follow.

5.2. Mechanisms for nucleotide discrimination by DNA polymerase β

The active sites of high-fidelity DNA polymerases have evolved to match the correct nucleotide with the instructing DNA template. With the high degree of specificity required for a DNA polymerase to select the correct one of four base identities, key structural steps must be satisfied for successful DNA synthesis, [Figure 5.1](#). As a structural and kinetic model for understanding the polymerase nucleotidyl transferase mechanism, DNA polymerase β (pol β), has been the subject of extensive biochemical characterization over the past two decades, [Section 1.2.1](#). The current consensus is that pol β selects correct nucleotides from incorrect nucleotides using an induced fit mechanism, [Section 1.2.2](#). (48,196,207). The induced fit mechanism evaluates the ability of the incoming dNTP to satisfy Watson-Crick hydrogen bonding, base-stacking, and steric constraints that are instructed by the templating base identity and the nucleotide binding pocket in the active site (48,49). When the constraints are satisfied (*i.e.* correct dNTP binding) conformational changes of the N-subdomain and templating DNA strand induce the proper alignment of catalytic residues to promote catalysis (48,50). This mechanism must be able to discriminate between correct and incorrect nucleotides that may only differ by as little as one atom, such as ribonucleotides, oxidized deoxyribonucleotides, and mismatched

deoxyribonucleotides. Mismatched deoxyribonucleotide insertion commonly serves as a reference to compare other non-canonical nucleotide insertions. Structural deviations during mismatch insertion include hindered N-subdomain closure, loss of proper template strand positioning, improper geometries of active site residues, and lack of catalytic metal binding. One or more of these features was observed in each of the above chapters, implying a similar method of discrimination for non-canonical substrates by pol β and a highly complex and orchestrated catalytic mechanism that must be satisfied for efficient catalysis.

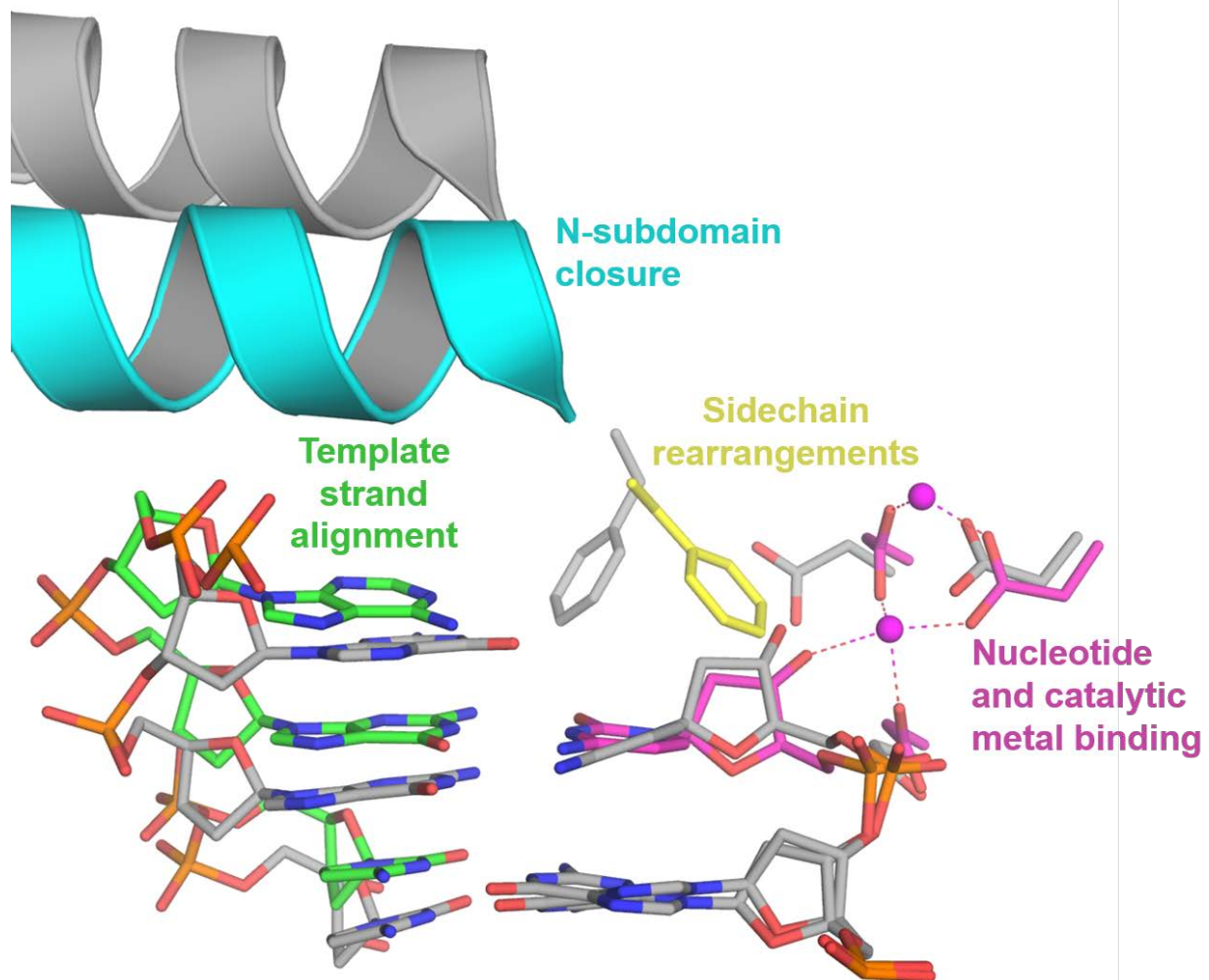


Figure 5.1 Protein and active site changes that facilitate DNA synthesis by DNA polymerase β .

An overlay between pol β prior to nucleotide binding (grey, PDB ID: 3ISB) and pol β poised for catalysis after binding a correct nucleotide triphosphate (colors cyan, green, yellow and magenta, PDB ID: 2FMS). Each differently colored section highlights structural changes that contributes to nucleotide discrimination. Of note, the depiction of sidechain rearrangements is represented by residue Phe272 for the purpose of this figure but is certainly not limited to only this residue during active site assembly.

In **Chapter 2**, we presented results which show that correct dCTP insertion with an 8-oxo-dG in the primer terminal position can impair catalytic metal binding only during mutagenic extension. We also observed the movement of active site residue Arg254 during non-mutagenic extension due to the electronegative clash between the adducted O8 and phosphate backbone in the *anti*- conformation. Movement of Arg254 provided a structural rationale to the reduced insertion efficiency with the 8-oxo-dG:dC primer terminal base pair. We were also able to hypothesize that the canonical position of Arg254 lowers the pKa of catalytic residue Asp256 through a salt bridge interaction that promotes catalysis. This provided further evidence that proton abstraction of the O3' during catalysis is not performed by bulk solvent (a debated point in the nucleotidyl transferase mechanism).

In **Chapter 3**, we described our observations that β -C-Fapy•dGTP, a Fapy•dGTP analog, significantly impaired enzyme closure, catalytic metal binding, and proper template strand positioning. The extensive perturbations incurred during Fapy•dGTP binding were largely alleviated by removing the Asp276 side chain. Previous reports showed that Asp276 is poorly conserved between species, but loss of D276 in an D276A/I277L mutant reduced catalytic efficiency and reduced discrimination (208). Additionally, a glutamic acid mutation (D276E) unexpectedly increased catalytic efficiency and decreased discrimination. This led to the hypothesis that Asp276 may form interactions with residues on neighboring domains that help signal competent nascent pairs during N-subdomain closure (208). However, our study demonstrated that loss of Asp276 (D276G) facilitated polymerase closure during Fapy•dGTP insertion in

comparison to the wild-type enzyme. Of note, the analysis of the contributions of D276 to polymerase closure in our study are also complicated by an interaction between D276 and the O3' of Fapy•dGTP in the wild-type complex. Kinetically, the D276G mutant increased the efficiency of non-mutagenic Fapy•dGTP insertion but decreased the efficiency of mutagenic Fapy•dGTP insertion. This meant that the D276G pol β mutant increased discrimination for the Fapy•dGTP nucleotide (*i.e.* made Fapy•dGTP less mutagenic), which was the opposite effect of D276 mutants studied previously with canonical deoxynucleotides. Therefore, the role of Asp276 during polymerase closure is still not fully understood but is clearly important for fidelity and catalytic efficiency. The inconsistent role of Asp276 during pol β catalysis merits future investigation.

In **Chapter 4**, we presented results which showed that non-mutagenic insertion of r8-oxo-GTP impaired all four aforementioned major structural changes (hindered N-subdomain closure, loss of proper template strand positioning, improper geometries of active site residues, and lack of catalytic metal binding) that occur during correct nucleotide binding. In contrast, mutagenic insertion of r8-oxo-GTP only mildly perturbed N-subdomain closure and catalytic metal binding. Our kinetic data showed a nearly additive decrease to catalytic efficiency between dGTP to rGTP and 8-oxo-dGTP to r8-oxo-GTP, suggesting that ribonucleotide DNA lesions may retain their deoxynucleotide base pairing properties but have a reduced efficiency due to the O2'. This opens up the possibility that this trend may hold for the ribonucleotide versions of other DNA lesions.

Structurally, we observed that r8-oxo-GTP retained the same general placement as the rGTP complex with respect to the proximity between the ribose oxygen (O2') and

the steric gate ([Figure 4.9B](#) and [Figure 4.10D](#)), illustrating an overlying mechanism for discrimination for the O2' ribose oxygen. However, we had to impose a caveat to our structural experiments that increased rNTP binding for complex formation – the removal of the Y271 side chain (the residue in pol β whose backbone carbonyl acts as the steric gate). The inability to observe an rNTP with wild-type pol β demonstrates the presence of additional discrimination steps prior to rNTP binding that cannot be observed with X-ray crystallography. To circumvent these limitations and better understand the structural dynamics occurring prior and during nucleotide binding, we used a FRET-based assay to evaluate polymerase closure via a collaboration with Joann Sweasy and Khadijeh Alnajjar (182). This method has validated the importance of conformational selection on polymerase fidelity and substrate discrimination (49,50,209,210). We found that r8-oxo-GTP impaired polymerase closure to a similar degree as mismatched nucleotides and ribonucleotides, suggesting the presence of common discrimination steps that hinder polymerase closure for all non-canonical nucleotides.

Despite the extensive research to understand the complexities of polymerase discrimination, new data suggests the existence of an unexplained mechanistic step (termed a non-covalent step) which occurs after fingers closing and prior to phosphodiester bond formation in the enzymatic pathway (49,182,183). The current hypothesis is that the non-covalent step may simply be binding of the catalytic metal (183). However, more research and independent experiments are needed to confirm the identity of the non-covalent step. Perhaps some insight on the non-covalent step could be gained with computational studies such as molecular dynamics, quantum mechanical

(QM), and hybrid QM/molecular mechanics (QM/MM) simulations which have been used previously to evaluate the nucleotidyl transferase mechanism (211). As studies continue to reveal to the importance of pre-catalytic conformational steps in selecting the correct nucleotide (49), I predict future research will continue to explore the contributions of individual kinetic checkpoints along the conformational pathway to illuminate all the complexities that govern polymerase fidelity.

References

1. Cadet, J. and Davies, K.J.A. (2017) Oxidative DNA damage & repair: An introduction. *Free Radic Biol Med*, **107**, 2-12.
2. Markkanen, E. (2017) Not breathing is not an option: How to deal with oxidative DNA damage. *DNA Repair*, **59**, 82-105.
3. Tubbs, A. and Nussenzweig, A. (2017) Endogenous DNA Damage as a Source of Genomic Instability in Cancer. *Cell*, **168**, 644-656.
4. Whitaker, A.M., Schaich, M.A., Smith, M.R., Flynn, T.S. and Freudenthal, B.D. (2017) Base excision repair of oxidative DNA damage: from mechanism to disease. *Frontiers in bioscience (Landmark edition)*, **22**, 1493-1522.
5. Gu, H., Marth, J., Orban, P., Mossmann, H. and Rajewsky, K. (1994) Deletion of a DNA polymerase beta gene segment in T cells using cell type-specific gene targeting. *Science (New York, N.Y.)*, **265**, 103-106.
6. Xanthoudakis, S., Smeyne, R.J., Wallace, J.D. and Curran, T. (1996) The redox/DNA repair protein, Ref-1, is essential for early embryonic development in mice. *Proceedings of the National Academy of Sciences of the United States of America*, **93**, 8919-8923.
7. Pogozelski, W.K. and Tullius, T.D. (1998) Oxidative Strand Scission of Nucleic Acids: Routes Initiated by Hydrogen Abstraction from the Sugar Moiety. *Chemical Reviews*, **98**, 1089-1108.
8. Gates, K.S. (2009) An overview of chemical processes that damage cellular DNA: spontaneous hydrolysis, alkylation, and reactions with radicals. *Chemical research in toxicology*, **22**, 1747-1760.
9. Randerath, K., Reddy, R., Danna, T.F., Watson, W.P., Crane, A.E. and Randerath, E. (1992) Formation of ribonucleotides in DNA modified by oxidative damage in vitro and in vivo. Characterization by ³²P-postlabeling. *Mutation research*, **275**, 355-366.
10. Jovanovic, S.V. and Simic, M.G. (1986) One-electron redox potentials of purines and pyrimidines. *The Journal of Physical Chemistry*, **90**, 974-978.
11. Kino, K., Hirao-Suzuki, M., Morikawa, M., Sakaga, A. and Miyazawa, H. (2017) Generation, repair and replication of guanine oxidation products. *Genes and Environment*, **39**, 21.
12. Bolin, C. and Cardozo-Pelaez, F. (2007) Assessing biomarkers of oxidative stress: analysis of guanosine and oxidized guanosine nucleotide triphosphates by high performance liquid

- chromatography with electrochemical detection. *Journal of chromatography. B, Analytical technologies in the biomedical and life sciences*, **856**, 121-130.
13. Rai, P. (2010) Oxidation in the nucleotide pool, the DNA damage response and cellular senescence: Defective bricks build a defective house. *Mutation Research/Genetic Toxicology and Environmental Mutagenesis*, **703**, 71-81.
 14. Nakabeppu, Y., Behmanesh, M., Yamaguchi, H., Yoshimura, D. and Sakumi, K. (2009), pp. 40-53.
 15. Nagy, G.N., Leveles, I. and Vértessy, B.G. (2014) Preventive DNA repair by sanitizing the cellular (deoxy)nucleoside triphosphate pool. *The FEBS Journal*, **281**, 4207-4223.
 16. Freudenthal, B.D., Beard, W.A., Perera, L., Shock, D.D., Kim, T., Schlick, T. and Wilson, S.H. (2015) Uncovering the polymerase-induced cytotoxicity of an oxidized nucleotide. *Nature*, **517**, 635-639.
 17. Hayakawa, H., Taketomi, A., Sakumi, K., Kuwano, M. and Sekiguchi, M. (1995) Generation and Elimination of 8-Oxo-7,8-dihydro-2'-deoxyguanosine 5'-Triphosphate, a Mutagenic Substrate for DNA Synthesis, in Human Cells. *Biochemistry*, **34**, 89-95.
 18. Nakabeppu, Y., Kajitani, K., Sakamoto, K., Yamaguchi, H. and Tsuchimoto, D. (2006) MTH1, an oxidized purine nucleoside triphosphatase, prevents the cytotoxicity and neurotoxicity of oxidized purine nucleotides. *DNA Repair (Amst)*, **5**, 761-772.
 19. Gad, H., Koolmeister, T., Jemth, A.-S., Eshtad, S., Jacques, S.A., Ström, C.E., Svensson, L.M., Schultz, N., Lundbäck, T., Einarsdottir, B.O. *et al.* (2014) MTH1 inhibition eradicates cancer by preventing sanitation of the dNTP pool. *Nature*, **508**, 215.
 20. Warpman Berglund, U., Sanjiv, K., Gad, H., Kalderén, C., Koolmeister, T., Pham, T., Gokturk, C., Jafari, R., Maddalo, G., Seashore-Ludlow, B. *et al.* (2016) Validation and development of MTH1 inhibitors for treatment of cancer. *Annals of Oncology*, **27**, 2275-2283.
 21. Samaranyake, G.J., Huynh, M. and Rai, P. (2017) MTH1 as a Chemotherapeutic Target: The Elephant in the Room. *Cancers (Basel)*, **9**, 47.
 22. Sekiguchi, T., Ito, R., Hayakawa, H. and Sekiguchi, M. (2013) Elimination and Utilization of Oxidized Guanine Nucleotides in the Synthesis of RNA and Its Precursors. *Journal of Biological Chemistry*, **288**, 8128-8135.
 23. Hayakawa, H., Hofer, A., Thelander, L., Kitajima, S., Cai, Y., Oshiro, S., Yakushiji, H., Nakabeppu, Y., Kuwano, M. and Sekiguchi, M. (1999) Metabolic fate of oxidized guanine ribonucleotides in mammalian cells. *Biochemistry*, **38**, 3610-3614.
 24. Tanaka, M., Chock, P.B. and Stadtman, E.R. (2007) Oxidized messenger RNA induces translation errors. *Proceedings of the National Academy of Sciences*, **104**, 66-71.

25. Cavanaugh, N.A., Beard, W.A., Batra, V.K., Perera, L., Pedersen, L.G. and Wilson, S.H. (2011) Molecular insights into DNA polymerase deterrents for ribonucleotide insertion. *The Journal of biological chemistry*, **286**, 31650-31660.
26. Kong, Z., Jia, S., Chabes, A.L., Appelblad, P., Lundmark, R., Moritz, T. and Chabes, A. (2018) Simultaneous determination of ribonucleoside and deoxyribonucleoside triphosphates in biological samples by hydrophilic interaction liquid chromatography coupled with tandem mass spectrometry. *Nucleic acids research*, **46**, e66.
27. Pryor, J.M., Conlin, M.P., Carvajal-Garcia, J., Luedeman, M.E., Luthman, A.J., Small, G.W. and Ramsden, D.A. (2018) Ribonucleotide incorporation enables repair of chromosome breaks by nonhomologous end joining. *Science (New York, N.Y.)*, **361**, 1126-1129.
28. Nick McElhinny, S.A., Watts, B.E., Kumar, D., Watt, D.L., Lundström, E.-B., Burgers, P.M.J., Johansson, E., Chabes, A. and Kunkel, T.A. (2010) Abundant ribonucleotide incorporation into DNA by yeast replicative polymerases. *Proceedings of the National Academy of Sciences of the United States of America*, **107**, 4949-4954.
29. Ordonez, H. and Shuman, S. (2014) Mycobacterium smegmatis DinB2 misincorporates deoxyribonucleotides and ribonucleotides during templated synthesis and lesion bypass. *Nucleic acids research*, **42**, 12722-12734.
30. Sastre-Moreno, G., Sánchez, A., Esteban, V. and Blanco, L. (2014) ATP insertion opposite 8-oxo-deoxyguanosine by Pol4 mediates error-free tolerance in Schizosaccharomyces pombe. *Nucleic acids research*, **42**, 9821-9837.
31. Cilli, P., Minoprio, A., Bossa, C., Bignami, M. and Mazzei, F. (2015) Formation and Repair of Mismatches Containing Ribonucleotides and Oxidized Bases at Repeated DNA Sequences. *The Journal of biological chemistry*, **290**, 26259-26269.
32. Sparks, J.L., Chon, H., Cerritelli, S.M., Kunkel, T.A., Johansson, E., Crouch, R.J. and Burgers, P.M. (2012) RNase H2-initiated ribonucleotide excision repair. *Molecular cell*, **47**, 980-986.
33. Wilson, S.H., Sobol, R.W., Beard, W.A., Horton, J.K., Prasad, R. and Vande Berg, B.J. (2000) DNA polymerase beta and mammalian base excision repair. *Cold Spring Harbor symposia on quantitative biology*, **65**, 143-155.
34. Sobol, R.W., Prasad, R., Evenski, A., Baker, A., Yang, X.P., Horton, J.K. and Wilson, S.H. (2000) The lyase activity of the DNA repair protein beta-polymerase protects from DNA-damage-induced cytotoxicity. *Nature*, **405**, 807-810.
35. Donigan, K.A., Sun, K.W., Nemecek, A.A., Murphy, D.L., Cong, X., Northrup, V., Zelterman, D. and Sweasy, J.B. (2012) Human POLB gene is mutated in high percentage of colorectal tumors. *The Journal of biological chemistry*, **287**, 23830-23839.

36. Ramadan, K., Shevelev, I. and Hubscher, U. (2004) The DNA-polymerase-X family: controllers of DNA quality? *Nature reviews. Molecular cell biology*, **5**, 1038-1043.
37. Hoitsma, N.M., Whitaker, A.M., Schaich, M.A., Smith, M.R., Fairlamb, M.S. and Freudenthal, B.D. (2020) Structure and function relationships in mammalian DNA polymerases. *Cellular and Molecular Life Sciences*, **77**, 35-59.
38. Beard, W.A. and Wilson, S.H. (2014) Structure and Mechanism of DNA Polymerase β . *Biochemistry*, **53**, 2768-2780.
39. Zhong, X., Patel, S.S., Werneburg, B.G. and Tsai, M.-D. (1997) DNA Polymerase β : Multiple Conformational Changes in the Mechanism of Catalysis. *Biochemistry*, **36**, 11891-11900.
40. Aravind, L. and Koonin, E.V. (1999) DNA polymerase β -like nucleotidyltransferase superfamily: Identification of three new families, classification and evolutionary history. *Nucleic acids research*, **27**, 1609-1618.
41. Krahn, J.M., Beard, W.A. and Wilson, S.H. (2004) Structural Insights into DNA Polymerase β Deterrents for Misincorporation Support an Induced-Fit Mechanism for Fidelity. *Structure*, **12**, 1823-1832.
42. Sawaya, M.R., Prasad, R., Wilson, S.H., Kraut, J. and Pelletier, H. (1997) Crystal structures of human DNA polymerase beta complexed with gapped and nicked DNA: evidence for an induced fit mechanism. *Biochemistry*, **36**, 11205-11215.
43. Batra, V.K., Beard, W.A., Pedersen, L.C. and Wilson, S.H. (2016) Structural Analysis of Mispaiored DNA Termini Transitioning to DNA Polymerase Pre-catalytic Complexes Supports an Induced Fit Fidelity Mechanism. *Structure*, **24**, 1863-1875.
44. Yang, L., Arora, K., Beard, W.A., Wilson, S.H. and Schlick, T. (2004) Critical role of magnesium ions in DNA polymerase beta's closing and active site assembly. *J Am Chem Soc*, **126**, 8441-8453.
45. Vashishtha, A.K., Wang, J. and Konigsberg, W.H. (2016) Different Divalent Cations Alter the Kinetics and Fidelity of DNA Polymerases. *Journal of Biological Chemistry*, **291**, 20869-20875.
46. Delagoutte, E. (2012) DNA polymerases: mechanistic insight from biochemical and biophysical studies. *Frontiers in bioscience (Landmark edition)*, **17**, 509-544.
47. Reed, A.J., Vyas, R., Raper, A.T. and Suo, Z. (2017) Structural Insights into the Post-Chemistry Steps of Nucleotide Incorporation Catalyzed by a DNA Polymerase. *Journal of the American Chemical Society*, **139**, 465-471.
48. Johnson, K.A. (2008) Role of induced fit in enzyme specificity: a molecular forward/reverse switch. *The Journal of biological chemistry*, **283**, 26297-26301.

49. Alnajjar, K.S., Krylov, I.S., Negahbani, A., Haratipour, P., Kashemirov, B.A., Huang, J., Mahmoud, M., McKenna, C.E., Goodman, M.F. and Sweasy, J.B. (2019) A pre-catalytic non-covalent step governs DNA polymerase β fidelity. *Nucleic acids research*, **47**, 11839-11849.
50. Joyce, C.M., Potapova, O., DeLucia, A.M., Huang, X., Basu, V.P. and Grindley, N.D.F. (2008) Fingers-Closing and Other Rapid Conformational Changes in DNA Polymerase I (Klenow Fragment) and Their Role in Nucleotide Selectivity. *Biochemistry*, **47**, 6103-6116.
51. Freudenthal, B.D., Beard, W.A., Shock, D.D. and Wilson, S.H. (2013) Observing a DNA polymerase choose right from wrong. *Cell*, **154**, 157-168.
52. Batra, V.K., Beard, W.A., Shock, D.D., Pedersen, L.C. and Wilson, S.H. (2008) Structures of DNA polymerase beta with active-site mismatches suggest a transient abasic site intermediate during misincorporation. *Molecular cell*, **30**, 315-324.
53. Schaich, M.A., Smith, M.R., Cloud, A.S., Holloran, S.M. and Freudenthal, B.D. (2017) Structures of a DNA Polymerase Inserting Therapeutic Nucleotide Analogues. *Chemical Research in Toxicology*, **30**, 1993-2001.
54. Smith, M.R., Shock, D.D., Beard, W.A., Greenberg, M.M., Freudenthal, B.D. and Wilson, S.H. (2019) A guardian residue hinders insertion of a Fapy•dGTP analog by modulating the open-closed DNA polymerase transition. *Nucleic acids research*, **47**, 3197-3207.
55. Batra, V.K., Beard, W.A., Hou, E.W., Pedersen, L.C., Prasad, R. and Wilson, S.H. (2010) Mutagenic conformation of 8-oxo-7,8-dihydro-2'-dGTP in the confines of a DNA polymerase active site. *Nature structural & molecular biology*, **17**, 889-890.
56. Vyas, R., Reed, A.J., Tokarsky, E.J. and Suo, Z. (2015) Viewing Human DNA Polymerase beta Faithfully and Unfaithfully Bypass an Oxidative Lesion by Time-Dependent Crystallography. *J Am Chem Soc*, **137**, 5225-5230.
57. Steenken, S. and Jovanovic, S.V. (1997) How Easily Oxidizable Is DNA? One-Electron Reduction Potentials of Adenosine and Guanosine Radicals in Aqueous Solution. *Journal of the American Chemical Society*, **119**, 617-618.
58. Delaney, S., Jarem, D.A., Volle, C.B. and Yennie, C.J. (2012) Chemical and biological consequences of oxidatively damaged guanine in DNA. *Free radical research*, **46**, 420-441.
59. Valavanidis, A., Vlachogianni, T. and Fiotakis, C. (2009) 8-hydroxy-2' -deoxyguanosine (8-OHdG): A critical biomarker of oxidative stress and carcinogenesis. *J Environ Sci Health C Environ Carcinog Ecotoxicol Rev*, **27**, 120-139.
60. Sentürker, S. and Dizdaroglu, M. (1999) The effect of experimental conditions on the levels of oxidatively modified bases in DNA as measured by gas chromatography-mass

- spectrometry:: How many modified bases are involved? Prepurification or not? *Free Radical Biology and Medicine*, **27**, 370-380.
61. Gedik, C.M. and Collins, A. (2005) Establishing the background level of base oxidation in human lymphocyte DNA: results of an interlaboratory validation study. *FASEB journal : official publication of the Federation of American Societies for Experimental Biology*, **19**, 82-84.
 62. Nakabeppu, Y. (2014) Cellular levels of 8-oxoguanine in either DNA or the nucleotide pool play pivotal roles in carcinogenesis and survival of cancer cells. *International journal of molecular sciences*, **15**, 12543-12557.
 63. Lindahl, T. (1993) Instability and decay of the primary structure of DNA. *Nature*, **362**, 709-715.
 64. Roots, R. and Okada, S. (1975) Estimation of life times and diffusion distances of radicals involved in x-ray-induced DNA strand breaks of killing of mammalian cells. *Radiat Res*, **64**, 306-320.
 65. Radak, Z. and Boldogh, I. (2010) 8-Oxo-7,8-dihydroguanine: links to gene expression, aging, and defense against oxidative stress. *Free Radic Biol Med*, **49**, 587-596.
 66. Koizume, S., Inoue, H., Kamiya, H. and Ohtsuka, E. (1998) Neighboring base damage induced by permanganate oxidation of 8-oxoguanine in DNA. *Nucleic acids research*, **26**, 3599-3607.
 67. Cheng, X., Kelso, C., Hornak, V., de los Santos, C., Grollman, A.P. and Simmerling, C. (2005) Dynamic behavior of DNA base pairs containing 8-oxoguanine. *J Am Chem Soc*, **127**, 13906-13918.
 68. Uesugi, S. and Ikehara, M. (1977) Carbon-13 magnetic resonance spectra of 8-substituted purine nucleosides. Characteristic shifts for the syn conformation. *J Am Chem Soc*, **99**, 3250-3253.
 69. Cho, B.P. and Evans, F.E. (1991) Structure of oxidatively damaged nucleic acid adducts. 3. Tautomerism, ionization and protonation of 8-hydroxyadenosine studied by ¹⁵N NMR spectroscopy. *Nucleic acids research*, **19**, 1041-1047.
 70. Hoogsteen, K. (1963) The crystal and molecular structure of a hydrogen-bonded complex between 1-methylthymine and 9-methyladenine. *Acta Crystallographica*, **16**, 907-916.
 71. Batra, V.K., Shock, D.D., Beard, W.A., McKenna, C.E. and Wilson, S.H. (2012) Binary complex crystal structure of DNA polymerase beta reveals multiple conformations of the templating 8-oxoguanine lesion. *Proceedings of the National Academy of Sciences of the United States of America*, **109**, 113-118.

72. Yudkina, A.V.S., Evgeniy S.; Endutkin, Anton V.; Makarova, Alena V.; Zharkov, Dmitry O. . (2019) Reading and Misreading 8-oxoguanine, a Paradigmatic Ambiguous Nucleobase. *Crystals*, **9**, 31.
73. Shibutani, S., Takeshita, M. and Grollman, A.P. (1991) Insertion of specific bases during DNA synthesis past the oxidation-damaged base 8-oxodG. *Nature*, **349**, 431-434.
74. Rodriguez, G.P., Song, J.B. and Crouse, G.F. (2013) In vivo bypass of 8-oxodG. *PLoS genetics*, **9**, e1003682-e1003682.
75. Pouget, J.P., Douki, T., Richard, M.J. and Cadet, J. (2000) DNA damage induced in cells by gamma and UVA radiation as measured by HPLC/GC-MS and HPLC-EC and Comet assay. *Chemical research in toxicology*, **13**, 541-549.
76. Gajewski, E., Rao, G., Nackerdien, Z. and Dizdaroglu, M. (1990) Modification of DNA bases in mammalian chromatin by radiation-generated free radicals. *Biochemistry*, **29**, 7876-7882.
77. Xue, L. and Greenberg, M.M. (2007) Facile quantification of lesions derived from 2'-deoxyguanosine in DNA. *J Am Chem Soc*, **129**, 7010-7011.
78. Pouget, J.P., Frelon, S., Ravanat, J.L., Testard, I., Odin, F. and Cadet, J. (2002) Formation of modified DNA bases in cells exposed either to gamma radiation or to high-LET particles. *Radiat Res*, **157**, 589-595.
79. Kalam, M.A., Haraguchi, K., Chandani, S., Loechler, E.L., Moriya, M., Greenberg, M.M. and Basu, A.K. (2006) Genetic effects of oxidative DNA damages: comparative mutagenesis of the imidazole ring-opened formamidopyrimidines (Fapy lesions) and 8-oxo-purines in simian kidney cells. *Nucleic acids research*, **34**, 2305-2315.
80. Pande, P., Haraguchi, K., Jiang, Y.L., Greenberg, M.M. and Basu, A.K. (2015) Unlike catalyzing error-free bypass of 8-oxodGuo, DNA polymerase lambda is responsible for a significant part of Fapy.dG-induced G --> T mutations in human cells. *Biochemistry*, **54**, 1859-1862.
81. Imoto, S., Patro, J.N., Jiang, Y.L., Oka, N. and Greenberg, M.M. (2006) Synthesis, DNA Polymerase Incorporation, and Enzymatic Phosphate Hydrolysis of Formamidopyrimidine Nucleoside Triphosphates. *Journal of the American Chemical Society*, **128**, 14606-14611.
82. Gehrke, T.H., Lischke, U., Gasteiger, K.L., Schneider, S., Arnold, S., Muller, H.C., Stephenson, D.S., Zipse, H. and Carell, T. (2013) Unexpected non-Hoogsteen-based mutagenicity mechanism of FaPy-DNA lesions. *Nature chemical biology*, **9**, 455-461.
83. Ober, M., Müller, H., Pieck, C., Gierlich, J. and Carell, T. (2005) Base Pairing and Replicative Processing of the Formamidopyrimidine-dG DNA Lesion. *Journal of the American Chemical Society*, **127**, 18143-18149.

84. Tudek, B. (2003) Imidazole ring-opened DNA purines and their biological significance. *Journal of biochemistry and molecular biology*, **36**, 12-19.
85. Dizdaroglu, M., Kirkali, G. and Jaruga, P. (2008) Formamidopyrimidines in DNA: Mechanisms of formation, repair, and biological effects. *Free Radical Biology and Medicine*, **45**, 1610-1621.
86. Patro, J.N., Haraguchi, K., Delaney, M.O. and Greenberg, M.M. (2004) Probing the configurations of formamidopyrimidine lesions Fapy.dA and Fapy.dG in DNA using endonuclease IV. *Biochemistry*, **43**, 13397-13403.
87. Busch, F., Pieck, J.C., Ober, M., Gierlich, J., Hsu, G.W., Beese, L.S. and Carell, T. (2008) Dissecting the differences between the alpha and beta anomers of the oxidative DNA lesion FaPydG. *Chemistry*, **14**, 2125-2132.
88. Lukin, M., Minetti, C.A., Remeta, D.P., Attaluri, S., Johnson, F., Breslauer, K.J. and de Los Santos, C. (2011) Novel post-synthetic generation, isomeric resolution, and characterization of Fapy-dG within oligodeoxynucleotides: differential anomeric impacts on DNA duplex properties. *Nucleic acids research*, **39**, 5776-5789.
89. Sha, Y., Minko, I.G., Malik, C.K., Rizzo, C.J. and Lloyd, R.S. (2017) Error-prone replication bypass of the imidazole ring-opened formamidopyrimidine deoxyguanosine adduct. *Environmental and molecular mutagenesis*, **58**, 182-189.
90. Basu, A.K., Pande, P. and Bose, A. (2017) Translesion Synthesis of 2'-Deoxyguanosine Lesions by Eukaryotic DNA Polymerases. *Chemical research in toxicology*, **30**, 61-72.
91. Patro, J.N., Wiederholt, C.J., Jiang, Y.L., Delaney, J.C., Essigmann, J.M. and Greenberg, M.M. (2007) Studies on the Replication of the Ring Opened Formamidopyrimidine, Fapy·dG in Escherichia coli. *Biochemistry*, **46**, 10202-10212.
92. Wiederholt, C.J. and Greenberg, M.M. (2002) Fapy·dG Instructs Klenow Exo- to Misincorporate Deoxyadenosine. *Journal of the American Chemical Society*, **124**, 7278-7279.
93. Lukin, M., Zaliznyak, T., Attaluri, S., Johnson, F. and de Los Santos, C. (2012) Solution structure of duplex DNA containing a beta-carba-Fapy-dG lesion. *Chemical research in toxicology*, **25**, 2423-2431.
94. Wiederholt, C.J., Delaney, M.O., Pope, M.A., David, S.S. and Greenberg, M.M. (2003) Repair of DNA containing Fapy.dG and its beta-C-nucleoside analogue by formamidopyrimidine DNA glycosylase and MutY. *Biochemistry*, **42**, 9755-9760.
95. Hofer, T., Badouard, C., Bajak, E., Ravanat, J.L., Mattsson, A. and Cotgreave, I.A. (2005) Hydrogen peroxide causes greater oxidation in cellular RNA than in DNA. *Biol Chem*, **386**, 333-337.

96. Hofer, T., Seo, A.Y., Prudencio, M. and Leeuwenburgh, C. (2006) A method to determine RNA and DNA oxidation simultaneously by HPLC-ECD: greater RNA than DNA oxidation in rat liver after doxorubicin administration. *Biol Chem*, **387**, 103-111.
97. Reijns, M.A., Rabe, B., Rigby, R.E., Mill, P., Astell, K.R., Lettice, L.A., Boyle, S., Leitch, A., Keighren, M., Kilanowski, F. *et al.* (2012) Enzymatic removal of ribonucleotides from DNA is essential for mammalian genome integrity and development. *Cell*, **149**, 1008-1022.
98. Clausen, A.R., Zhang, S., Burgers, P.M., Lee, M.Y. and Kunkel, T.A. (2013) Ribonucleotide incorporation, proofreading and bypass by human DNA polymerase δ . *DNA repair*, **12**, 121-127.
99. Ames, B.N. and Gold, L.S. (1991) Endogenous mutagens and the causes of aging and cancer. *Mutation research*, **250**, 3-16.
100. Topal, M.D. and Baker, M.S. (1982) DNA precursor pool: a significant target for N-methyl-N-nitrosourea in C3H/10T1/2 clone 8 cells. *Proceedings of the National Academy of Sciences of the United States of America*, **79**, 2211-2215.
101. Kamiya, H. and Kasai, H. (1995) Formation of 2-hydroxydeoxyadenosine triphosphate, an oxidatively damaged nucleotide, and its incorporation by DNA polymerases. Steady-state kinetics of the incorporation. *The Journal of biological chemistry*, **270**, 19446-19450.
102. Tsuzuki, T., Egashira, A., Igarashi, H., Iwakuma, T., Nakatsuru, Y., Tominaga, Y., Kawate, H., Nakao, K., Nakamura, K., Ide, F. *et al.* (2001) Spontaneous tumorigenesis in mice defective in the MTH1 gene encoding 8-oxo-dGTPase. *Proceedings of the National Academy of Sciences of the United States of America*, **98**, 11456-11461.
103. Caglayan, M., Horton, J.K., Dai, D.P., Stefanick, D.F. and Wilson, S.H. (2017) Oxidized nucleotide insertion by pol beta confounds ligation during base excision repair. *Nat Commun*, **8**, 14045.
104. Hsu, G.W., Ober, M., Carell, T. and Beese, L.S. (2004) Error-prone replication of oxidatively damaged DNA by a high-fidelity DNA polymerase. *Nature*, **431**, 217-221.
105. Sakumi, K., Furuichi, M., Tsuzuki, T., Kakuma, T., Kawabata, S., Maki, H. and Sekiguchi, M. (1993) Cloning and expression of cDNA for a human enzyme that hydrolyzes 8-oxo-dGTP, a mutagenic substrate for DNA synthesis. *The Journal of biological chemistry*, **268**, 23524-23530.
106. Huber, K.V., Salah, E., Radic, B., Gridling, M., Elkins, J.M., Stukalov, A., Jemth, A.S., Gokturk, C., Sanjiv, K., Stromberg, K. *et al.* (2014) Stereospecific targeting of MTH1 by (S)-crizotinib as an anticancer strategy. *Nature*, **508**, 222-227.
107. De Bont, R. and van Larebeke, N. (2004) Endogenous DNA damage in humans: a review of quantitative data. *Mutagenesis*, **19**, 169-185.

108. Fraga, C.G., Shigenaga, M.K., Park, J.W., Degan, P. and Ames, B.N. (1990) Oxidative damage to DNA during aging: 8-hydroxy-2'-deoxyguanosine in rat organ DNA and urine. *Proceedings of the National Academy of Sciences of the United States of America*, **87**, 4533-4537.
109. Culp, S.J., Cho, B.P., Kadlubar, F.F. and Evans, F.E. (1989) Structural and conformational analyses of 8-hydroxy-2'-deoxyguanosine. *Chemical research in toxicology*, **2**, 416-422.
110. Oda, Y., Uesugi, S., Ikehara, M., Nishimura, S., Kawase, Y., Ishikawa, H., Inoue, H. and Ohtsuka, E. (1991) NMR studies of a DNA containing 8-hydroxydeoxyguanosine. *Nucleic acids research*, **19**, 1407-1412.
111. Grollman, A.P. and Moriya, M. (1993) Mutagenesis by 8-oxoguanine: an enemy within. *Trends in genetics : TIG*, **9**, 246-249.
112. Freudenthal, B.D., Beard, W.A. and Wilson, S.H. (2015) New structural snapshots provide molecular insights into the mechanism of high fidelity DNA synthesis. *DNA Repair (Amst)*, **32**, 3-9.
113. Beard, W.A. and Wilson, S.H. (1995), *Methods in enzymology*. Academic Press, Vol. 262, pp. 98-107.
114. Batra, V.K., Beard, W.A., Shock, D.D., Krahn, J.M., Pedersen, L.C. and Wilson, S.H. (2006) Magnesium-Induced Assembly of a Complete DNA Polymerase Catalytic Complex. *Structure*, **14**, 757-766.
115. Otwinowski, Z. and Minor, W. (1997) Processing of X-ray diffraction data collected in oscillation mode. *Methods in enzymology*, **276**, 307-326.
116. Adams, P.D., Afonine, P.V., Bunkoczi, G., Chen, V.B., Davis, I.W., Echols, N., Headd, J.J., Hung, L.W., Kapral, G.J., Grosse-Kunstleve, R.W. *et al.* (2010) PHENIX: a comprehensive Python-based system for macromolecular structure solution. *Acta crystallographica. Section D, Biological crystallography*, **66**, 213-221.
117. Emsley, P. and Cowtan, K. (2004) Coot: model-building tools for molecular graphics. *Acta crystallographica. Section D, Biological crystallography*, **60**, 2126-2132.
118. Beard, W.A., Shock, D.D. and Wilson, S.H. (2004) Influence of DNA structure on DNA polymerase beta active site function: extension of mutagenic DNA intermediates. *The Journal of biological chemistry*, **279**, 31921-31929.
119. Batra, V.K., Beard, W.A., Pedersen, L.C. and Wilson, S.H. (2016) Structures of DNA Polymerase Mispaiored DNA Termini Transitioning to Pre-catalytic Complexes Support an Induced-Fit Fidelity Mechanism. *Structure*, **24**, 1863-1875.
120. Batra, V.K., Perera, L., Lin, P., Shock, D.D., Beard, W.A., Pedersen, L.C., Pedersen, L.G. and Wilson, S.H. (2013) Amino acid substitution in the active site of DNA polymerase

- beta explains the energy barrier of the nucleotidyl transfer reaction. *J Am Chem Soc*, **135**, 8078-8088.
121. Nakamura, T., Zhao, Y., Yamagata, Y., Hua, Y.J. and Yang, W. (2012) Watching DNA polymerase beta make a phosphodiester bond. *Nature*, **487**, 196-201.
 122. Cavanaugh, N.A., Beard, W.A. and Wilson, S.H. (2010) DNA polymerase beta ribonucleotide discrimination: insertion, misinsertion, extension, and coding. *J Biol Chem*, **285**, 24457-24465.
 123. Jha, V. and Ling, H. (2017) Structural basis of accurate replication beyond a bulky major benzo[a]pyrene adduct by human DNA polymerase kappa. *DNA Repair (Amst)*, **49**, 43-50.
 124. Freudenthal, B.D., Beard, W.A. and Wilson, S.H. (2013) DNA polymerase minor groove interactions modulate mutagenic bypass of a templating 8-oxoguanine lesion. *Nucleic acids research*, **41**, 1848-1858.
 125. Klvana, M., Bren, U. and Florian, J. (2016) Uniform Free-Energy Profiles of the P-O Bond Formation and Cleavage Reactions Catalyzed by DNA Polymerases beta and lambda. *The journal of physical chemistry. B*, **120**, 13017-13030.
 126. Matute, R.A., Yoon, H. and Warshel, A. (2016) Exploring the mechanism of DNA polymerases by analyzing the effect of mutations of active site acidic groups in Polymerase beta. *Proteins*, **84**, 1644-1657.
 127. Lin, P., Pedersen, L.C., Batra, V.K., Beard, W.A., Wilson, S.H. and Pedersen, L.G. (2006) Energy analysis of chemistry for correct insertion by DNA polymerase beta. *Proceedings of the National Academy of Sciences of the United States of America*, **103**, 13294-13299.
 128. Menge, K.L., Hostomsky, Z., Nodes, B.R., Hudson, G.O., Rahmati, S., Moomaw, E.W., Almassy, R.J. and Hostomska, Z. (1995) Structure-function analysis of the mammalian DNA polymerase beta. active site: role of aspartic acid 256, arginine 254, and arginine 258 in nucleotidyl transfer. *Biochemistry*, **34**, 15934-15942.
 129. Bienstock, R.J., Beard, W.A. and Wilson, S.H. (2014) Phylogenetic analysis and evolutionary origins of DNA polymerase X-family members. *DNA Repair (Amst)*, **22**, 77-88.
 130. Cisneros, G.A., Perera, L., Garcia-Diaz, M., Bebenek, K., Kunkel, T.A. and Pedersen, L.G. (2008) Catalytic mechanism of human DNA polymerase lambda with Mg²⁺ and Mn²⁺ from ab initio quantum mechanical/molecular mechanical studies. *DNA Repair (Amst)*, **7**, 1824-1834.
 131. Fouquerel, E., Lormand, J., Bose, A., Lee, H.T., Kim, G.S., Li, J., Sobol, R.W., Freudenthal, B.D., Myong, S. and Opresko, P.L. (2016) Oxidative guanine base damage regulates human telomerase activity. *Nature structural & molecular biology*, **23**, 1092-1100.

132. Ziech, D., Franco, R., Pappa, A. and Panayiotidis, M.I. (2011) Reactive oxygen species (ROS)--induced genetic and epigenetic alterations in human carcinogenesis. *Mutation research*, **711**, 167-173.
133. Perez-Campo, R., Lopez-Torres, M., Cadenas, S., Rojas, C. and Barja, G. (1998) The rate of free radical production as a determinant of the rate of aging: evidence from the comparative approach. *Journal of comparative physiology. B, Biochemical, systemic, and environmental physiology*, **168**, 149-158.
134. Ellermann, M., Eheim, A., Rahm, F., Viklund, J., Guenther, J., Andersson, M., Ericsson, U., Forsblom, R., Ginman, T., Lindstrom, J. *et al.* (2017) Novel Class of Potent and Cellularly Active Inhibitors Devalidates MTH1 as Broad-Spectrum Cancer Target. *ACS Chem Biol*, **12**, 1986-1992.
135. Aristizabal Prada, E.T., Orth, M., Nolting, S., Spottl, G., Maurer, J. and Auernhammer, C. (2017) The MTH1 inhibitor TH588 demonstrates anti-tumoral effects alone and in combination with everolimus, 5-FU and gamma-irradiation in neuroendocrine tumor cells. *PLoS One*, **12**, e0178375.
136. Gavande, N.S., VanderVere-Carozza, P.S., Hinshaw, H.D., Jalal, S.I., Sears, C.R., Pawelczak, K.S. and Turchi, J.J. (2016) DNA repair targeted therapy: The past or future of cancer treatment? *Pharmacology & Therapeutics*, **160**, 65-83.
137. Ewald, B., Sampath, D. and Plunkett, W. (2008) Nucleoside analogs: molecular mechanisms signaling cell death. *Oncogene*, **27**, 6522.
138. Huber, K.V., Salah, E., Radic, B., Gridling, M., Elkins, J.M., Stukalov, A., Jemth, A.S., Gokturk, C., Sanjiv, K., Stromberg, K. *et al.* (2014) Stereospecific targeting of MTH1 by (S)-crizotinib as an anticancer strategy. *Nature*.
139. Pouget, J.P., Frelon, S., Ravanat, J.L., Testard, I., Odin, F. and Cadet, J. (2002) Formation of Modified DNA Bases in Cells Exposed Either to Gamma Radiation or to High-LET Particles. *Radiation Research*, **157**, 589-595.
140. Dizdaroglu, M. and Jaruga, P. (2012) Mechanisms of free radical-induced damage to DNA. *Free radical research*, **46**, 382-419.
141. Beard, W.A., Batra, V.K. and Wilson, S.H. (2010) DNA polymerase structure-based insight on the mutagenic properties of 8-oxoguanine. *Mutation research*, **703**, 18-23.
142. Greenberg, M.M., Hantosi, Z., Wiederholt, C.J. and Rithner, C.D. (2001) Studies on N4-(2-Deoxy-d-pentofuranosyl)-4,6-diamino-5-formamidopyrimidine (Fapy•dA) and N6-(2-Deoxy-d-pentofuranosyl)- 6-diamino-5-formamido-4-hydroxypyrimidine (Fapy•dG). *Biochemistry*, **40**, 15856-15861.

143. Weledji, Y.N., Wiederholt, C.J., Delaney, M.O. and Greenberg, M.M. (2008) DNA polymerase bypass in vitro and in *E. coli* of a C-nucleotide analogue of Fapy•dG. *Bioorganic & medicinal chemistry*, **16**, 4029-4034.
144. Kamiya, H., Cadena-Amaro, C., Dugue, L., Yakushiji, H., Minakawa, N., Matsuda, A., Pochet, S., Nakabeppu, Y. and Harashima, H. (2006) Recognition of nucleotide analogs containing the 7,8-dihydro-8-oxo structure by the human MTH1 protein. *J Biochem*, **140**, 843-849.
145. Fujikawa, K., Kamiya, H., Yakushiji, H., Fujii, Y., Nakabeppu, Y. and Kasai, H. (1999) The oxidized forms of dATP are substrates for the human MutT homologue, the hMTH1 protein. *The Journal of biological chemistry*, **274**, 18201-18205.
146. Beard, W.A. and Wilson, S.H. (1995), *Methods in enzymology*. Academic Press, Vol. 262, pp. 98-107.
147. Batra, V.K., Beard, W.A., Shock, D.D., Krahn, J.M., Pedersen, L.C. and Wilson, S.H. (2006) Magnesium induced assembly of a complete DNA polymerase catalytic complex. *Structure (Camb)*, **14**, 757-766.
148. Otwinowski, Z. and Minor, W. (1997) [20] Processing of X-ray diffraction data collected in oscillation mode. *Methods in enzymology*, **276**, 307-326.
149. Liebschner, D., Afonine, P.V., Moriarty, N.W., Poon, B.K., Sobolev, O.V., Terwilliger, T.C. and Adams, P.D. (2017) Polder maps: improving OMIT maps by excluding bulk solvent. *Acta crystallographica. Section D, Structural biology*, **73**, 148-157.
150. Schrödinger, L.L.C. (2010).
151. Freudenthal, B.D., Beard, W.A., Shock, D.D. and Wilson, S.H. (2013) Observing a DNA Polymerase Choose Right from Wrong. *Cell*, **154**, 157-168.
152. Tsai, Y.C. and Johnson, K.A. (2006) A new paradigm for DNA polymerase specificity. *Biochemistry*, **45**, 9675-9687.
153. Freudenthal, B.D., Beard, W.A. and Wilson, S.H. (2012) Structures of dNTP intermediate states during DNA polymerase active site assembly. *Structure*, **20**, 1829-1837.
154. Bailey, S., Wing, R.A. and Steitz, T.A. (2006) The structure of *T. aquaticus* DNA polymerase III is distinct from eukaryotic replicative DNA polymerases. *Cell*, **126**, 893-904.
155. Lamers, M.H., Georgescu, R.E., Lee, S.G., O'Donnell, M. and Kuriyan, J. (2006) Crystal structure of the catalytic alpha subunit of *E. coli* replicative DNA polymerase III. *Cell*, **126**, 881-892.

156. Wu, S., Beard, W.A., Pedersen, L.G. and Wilson, S.H. (2014) Structural comparison of DNA polymerase architecture suggests a nucleotide gateway to the polymerase active site. *Chemical reviews*, **114**, 2759-2774.
157. Schaich, M.A., Smith, M.R., Cloud, A.S., Holloran, S.M. and Freudenthal, B.D. (2017) Structures of a DNA Polymerase Inserting Therapeutic Nucleotide Analogues. *Chemical research in toxicology*.
158. Eckenroth, B.E., Towle-Weicksel, J.B., Sweasy, J.B. and Doublet, S. (2013) The E295K cancer variant of human polymerase beta favors the mismatch conformational pathway during nucleotide selection. *The Journal of biological chemistry*, **288**, 34850-34860.
159. Vande Berg, B.J., Beard, W.A. and Wilson, S.H. (2001) DNA structure and aspartate 276 influence nucleotide binding to human DNA polymerase beta. Implication for the identity of the rate-limiting conformational change. *The Journal of biological chemistry*, **276**, 3408-3416.
160. Pelletier, H., Sawaya, M.R., Wolfle, W., Wilson, S.H. and Kraut, J. (1996) Crystal Structures of Human DNA Polymerase β Complexed with DNA: Implications for Catalytic Mechanism, Processivity, and Fidelity. *Biochemistry*, **35**, 12742-12761.
161. Yang, L., Beard, W.A., Wilson, S.H., Broyde, S. and Schlick, T. (2004) Highly organized but pliant active site of DNA polymerase beta: compensatory mechanisms in mutant enzymes revealed by dynamics simulations and energy analyses. *Biophys J*, **86**, 3392-3408.
162. Beard, W.A., Shock, D.D., Batra, V.K., Prasad, R. and Wilson, S.H. (2014) Substrate-induced DNA polymerase beta activation. *The Journal of biological chemistry*, **289**, 31411-31422.
163. Oda, Y., Uesugi, S., Ikehara, M., Nishimura, S., Kawase, Y., Ishikawa, H., Inoue, H. and Ohtsuka, E. (1991) NMR studies of a DNA containing 8-hydroxydeoxyguanosine. *Nucleic Acids Research*, **19**, 1407-1412.
164. Batra, V.K., Shock, D.D., Beard, W.A., McKenna, C.E. and Wilson, S.H. (2012) Binary complex crystal structure of DNA polymerase β reveals multiple conformations of the templating 8-oxoguanine lesion. *Proceedings of the National Academy of Sciences*, **109**, 113-118.
165. Nakamura, J. and Swenberg, J.A. (1999) Endogenous apurinic/apyrimidinic sites in genomic DNA of mammalian tissues. *Cancer research*, **59**, 2522-2526.
166. Braithwaite, E.K., Kedar, P.S., Lan, L., Polosina, Y.Y., Asagoshi, K., Poltoratsky, V.P., Horton, J.K., Miller, H., Teebor, G.W., Yasui, A. *et al.* (2005) DNA polymerase lambda protects mouse fibroblasts against oxidative DNA damage and is recruited to sites of DNA damage/repair. *The Journal of biological chemistry*, **280**, 31641-31647.

167. Braithwaite, E.K., Kedar, P.S., Stumpo, D.J., Bertocci, B., Freedman, J.H., Samson, L.D. and Wilson, S.H. (2010) DNA polymerases beta and lambda mediate overlapping and independent roles in base excision repair in mouse embryonic fibroblasts. *PLoS one*, **5**, e12229.
168. Garcia-Diaz, M., Bebenek, K., Krahn, J.M., Kunkel, T.A. and Pedersen, L.C. (2005) A closed conformation for the Pol lambda catalytic cycle. *Nature structural & molecular biology*, **12**, 97-98.
169. Lavrik, O.I., Prasad, R., Beard, W.A., Safronov, I.V., Dobrikov, M.I., Srivastava, D.K., Shishkin, G.V., Wood, T.G. and Wilson, S.H. (1996) dNTP binding to HIV-1 reverse transcriptase and mammalian DNA polymerase beta as revealed by affinity labeling with a photoreactive dNTP analog. *The Journal of biological chemistry*, **271**, 21891-21897.
170. Freudenthal, B.D., Beard, W.A. and Wilson, S.H. (2015) New Structural Snapshots Provide Molecular Insights into the Mechanism of High Fidelity DNA Synthesis. *DNA repair*, **32**, 3-9.
171. Whitaker, A.M., Smith, M.R., Schaich, M.A. and Freudenthal, B.D. (2017) Capturing a mammalian DNA polymerase extending from an oxidized nucleotide. *Nucleic acids research*, **45**, 6934-6944.
172. Cadet, J. and Wagner, J.R. (2013) DNA base damage by reactive oxygen species, oxidizing agents, and UV radiation. *Cold Spring Harbor perspectives in biology*, **5**.
173. Jena, N.R. (2012) DNA damage by reactive species: Mechanisms, mutation and repair. *Journal of biosciences*, **37**, 503-517.
174. Cerchiaro, G., Bolin, C. and Cardozo-Pelaez, F. (2009) Hydroxyl radical oxidation of guanosine 5'-triphosphate (GTP): requirement for a GTP-Cu(II) complex. *Redox Report*, **14**, 82-92.
175. Haghdoost, S., Sjölander, L., Czene, S. and Harms-Ringdahl, M. (2006) The nucleotide pool is a significant target for oxidative stress. *Free Radical Biology and Medicine*, **41**, 620-626.
176. Beard, W.A., Batra, V.K. and Wilson, S.H. (2010) DNA polymerase structure-based insight on the mutagenic properties of 8-oxoguanine. *Mutation Research/Genetic Toxicology and Environmental Mutagenesis*, **703**, 18-23.
177. Kulkarni, A. and Wilson, D.M. (2008) The Involvement of DNA-Damage and -Repair Defects in Neurological Dysfunction. *The American Journal of Human Genetics*, **82**, 539-566.
178. Nakabeppu, Y. (2014) Cellular levels of 8-oxoguanine in either DNA or the nucleotide pool play pivotal roles in carcinogenesis and survival of cancer cells. *International journal of molecular sciences*, **15**, 12543-12557.

179. Brown, J.A., Duym, W.W., Fowler, J.D. and Suo, Z. (2007) Single-turnover Kinetic Analysis of the Mutagenic Potential of 8-Oxo-7,8-dihydro-2'-deoxyguanosine during Gap-filling Synthesis Catalyzed by Human DNA Polymerases λ and β . *Journal of Molecular Biology*, **367**, 1258-1269.
180. Beard, W.A., Osheroff, W.P., Prasad, R., Sawaya, M.R., Jaju, M., Wood, T.G., Kraut, J., Kunkel, T.A. and Wilson, S.H. (1996) Enzyme-DNA interactions required for efficient nucleotide incorporation and discrimination in human DNA polymerase beta. *The Journal of biological chemistry*, **271**, 12141-12144.
181. Genna, V., Vidossich, P., Ippoliti, E., Carloni, P. and De Vivo, M. (2016) A Self-Activated Mechanism for Nucleic Acid Polymerization Catalyzed by DNA/RNA Polymerases. *Journal of the American Chemical Society*, **138**, 14592-14598.
182. Towle-Weicksel, J.B., Dalal, S., Sohl, C.D., Doublet, S., Anderson, K.S. and Sweasy, J.B. (2014) Fluorescence resonance energy transfer studies of DNA polymerase beta: the critical role of fingers domain movements and a novel non-covalent step during nucleotide selection. *The Journal of biological chemistry*, **289**, 16541-16550.
183. Huang, J., Alnajjar, K.S., Mahmoud, M.M., Eckenroth, B., Doublet, S. and Sweasy, J.B. (2018) The nature of the DNA substrate influences pre-catalytic conformational changes of DNA polymerase beta. *The Journal of biological chemistry*, **293**, 15084-15094.
184. Werneburg, B.G., Ahn, J., Zhong, X., Hondal, R.J., Kraynov, V.S. and Tsai, M.D. (1996) DNA polymerase beta: pre-steady-state kinetic analysis and roles of arginine-283 in catalysis and fidelity. *Biochemistry*, **35**, 7041-7050.
185. Brown, J.A., Fiala, K.A., Fowler, J.D., Sherrer, S.M., Newmister, S.A., Duym, W.W. and Suo, Z. (2010) A novel mechanism of sugar selection utilized by a human X-family DNA polymerase. *Journal of molecular biology*, **395**, 282-290.
186. Potenski, C.J. and Klein, H.L. (2014) How the misincorporation of ribonucleotides into genomic DNA can be both harmful and helpful to cells. *Nucleic acids research*, **42**, 10226-10234.
187. Flood, C.L., Rodriguez, G.P., Bao, G., Shockley, A.H., Kow, Y.W. and Crouse, G.F. (2015) Replicative DNA polymerase delta but not epsilon proofreads errors in Cis and in Trans. *PLoS genetics*, **11**, e1005049.
188. Beard, W.A. and Wilson, S.H. (1995) Purification and domain-mapping of mammalian DNA polymerase beta. *Methods in enzymology*, **262**, 98-107.
189. Lu, X.-J. and Olson, W.K. (2008) 3DNA: a versatile, integrated software system for the analysis, rebuilding and visualization of three-dimensional nucleic-acid structures. *Nature Protocols*, **3**, 1213.

190. Schneider, C.A., Rasband, W.S. and Eliceiri, K.W. (2012) NIH Image to ImageJ: 25 years of image analysis. *Nature Methods*, **9**, 671.
191. Kirsch, P.D. and Ekerdt, J.G. (2000) KaleidaGraph: Graphing and Data Analysis. Version 3.5 for Windows Synergy Software, 2457 Perkiomen Ave., Reading, PA 19606-2049. www.Synergy.com. \$155.00. *Journal of the American Chemical Society*, **122**, 11755-11755.
192. Cavanaugh, N.A., Beard, W.A. and Wilson, S.H. (2010) DNA polymerase beta ribonucleotide discrimination: insertion, misinsertion, extension, and coding. *The Journal of biological chemistry*, **285**, 24457-24465.
193. Yang, L., Beard, W.A., Wilson, S.H., Broyde, S. and Schlick, T. (2004) Highly organized but pliant active site of DNA polymerase beta: compensatory mechanisms in mutant enzymes revealed by dynamics simulations and energy analyses. *Biophys J*, **86**, 3392-3408.
194. Lu, X.-J. and Olson, W.K. (2003) 3DNA: a software package for the analysis, rebuilding and visualization of three-dimensional nucleic acid structures. *Nucleic acids research*, **31**, 5108-5121.
195. Freudenthal, B.D., Beard, W.A., Perera, L., Shock, D.D., Kim, T., Schlick, T. and Wilson, S.H. (2014) Uncovering the polymerase-induced cytotoxicity of an oxidized nucleotide. *Nature*, **517**, 635.
196. Krahn, J.M., Beard, W.A. and Wilson, S.H. (2004) Structural insights into DNA polymerase beta deterrents for misincorporation support an induced-fit mechanism for fidelity. *Structure*, **12**, 1823-1832.
197. Koag, M.C. and Lee, S. (2018) Insights into the effect of minor groove interactions and metal cofactors on mutagenic replication by human DNA polymerase beta. *The Biochemical journal*, **475**, 571-585.
198. Batra, V.K., Beard, W.A., Shock, D.D., Pedersen, L.C. and Wilson, S.H. (2005) Nucleotide-Induced DNA Polymerase Active Site Motions Accommodating a Mutagenic DNA Intermediate. *Structure*, **13**, 1225-1233.
199. Freudenthal, B.D., Beard, W.A. and Wilson, S.H. (2012) Structures of dNTP intermediate states during DNA polymerase active site assembly. *Structure*, **20**, 1829-1837.
200. Su, Y., Egli, M. and Guengerich, F.P. (2016) Mechanism of Ribonucleotide Incorporation by Human DNA Polymerase η . *The Journal of biological chemistry*, **291**, 3747-3756.
201. Goksenin, A.Y., Zahurancik, W., LeCompte, K.G., Taggart, D.J., Suo, Z. and Pursell, Z.F. (2012) Human DNA polymerase epsilon is able to efficiently extend from multiple consecutive ribonucleotides. *The Journal of biological chemistry*, **287**, 42675-42684.

202. Bolin, C. and Cardozo-Pelaez, F. (2009) Characterization of oxidized guanosine 5'-triphosphate as a viable inhibitor of soluble guanylyl cyclase. *Free Radic Biol Med*, **46**, 828-835.
203. Ishibashi, T., Hayakawa, H., Ito, R., Miyazawa, M., Yamagata, Y. and Sekiguchi, M. (2005) Mammalian enzymes for preventing transcriptional errors caused by oxidative damage. *Nucleic acids research*, **33**, 3779-3784.
204. Sassa, A., Yasui, M. and Honma, M. (2019) Current perspectives on mechanisms of ribonucleotide incorporation and processing in mammalian DNA. *Genes and Environment*, **41**, 3.
205. Malfatti, M.C., Balachander, S., Antoniali, G., Koh, K.D., Saint-Pierre, C., Gasparutto, D., Chon, H., Crouch, R.J., Storici, F. and Tell, G. (2017) Abasic and oxidized ribonucleotides embedded in DNA are processed by human APE1 and not by RNase H2. *Nucleic acids research*, **45**, 11193-11212.
206. Carreras-Puigvert, J., Zitnik, M., Jemth, A.-S., Carter, M., Unterlass, J.E., Hallström, B., Loseva, O., Karem, Z., Calderón-Montaño, J.M., Lindskog, C. *et al.* (2017) A comprehensive structural, biochemical and biological profiling of the human NUDIX hydrolase family. *Nature Communications*, **8**, 1541.
207. Washington, M.T. (2016) DNA Polymerase Fidelity: Beyond Right and Wrong. *Structure*, **24**, 1855-1856.
208. Skandalis, A. and Loeb, L.A. (2001) Enzymatic properties of rat DNA polymerase beta mutants obtained by randomized mutagenesis. *Nucleic acids research*, **29**, 2418-2426.
209. Santoso, Y., Joyce, C.M., Potapova, O., Le Reste, L., Hohlbein, J., Torella, J.P., Grindley, N.D. and Kapanidis, A.N. (2010) Conformational transitions in DNA polymerase I revealed by single-molecule FRET. *Proceedings of the National Academy of Sciences of the United States of America*, **107**, 715-720.
210. Maxwell, B.A. and Suo, Z. (2013) Single-molecule investigation of substrate binding kinetics and protein conformational dynamics of a B-family replicative DNA polymerase. *The Journal of biological chemistry*, **288**, 11590-11600.
211. Walker, A.R. and Cisneros, G.A. (2017) Computational Simulations of DNA Polymerases: Detailed Insights on Structure/Function/Mechanism from Native Proteins to Cancer Variants. *Chemical research in toxicology*, **30**, 1922-1935.